# GABAERGIC INHIBITION AS A DYNAMIC ORGANIZER OF CORTICAL ACTIVITY

**EDRIS REZAEI**

**Master of Science, National Institute of Genetic Engineering and Biotechnology, 2018**

A thesis submitted

in partial fulfillment of the requirements for the degree of

**DOCTOR OF PHILOSOPHY**

in

**Neuroscience**

Department of Neuroscience

University of Lethbridge

LETHBRIDGE, ALBERTA, CANADA

**GABAERGIC INHIBITION AS A DYNAMIC ORGANIZER OF CORTICAL ACTIVITY**

Edris Rezaei

Date of defense: 01/13/2026

| | | |
|---|---|---|
| Ian Q. Whishaw<br>Supervisor | Professor | Ph.D. |
| Robert Sutherland<br>Thesis Examination<br>Committee Member | Professor | Ph.D. |
| Artur Luczak<br>Thesis Examination<br>Committee Member | Professor | Ph.D. |
| Dustin Hines<br>External Examiner<br>University of Nevada, Las Vegas | Associate Professor | Ph.D. |
| Robbin Gibb<br>Chair, Thesis Examination<br>Committee | Professor | Ph.D. |

**Dedication**

To my parents, for their unwavering support and sacrifices; to my wife, for her patience and love throughout this journey; and to my daughter, Lena, for bringing hope and happiness into my life.

**Abstract**

Most studies of cortical function have focused on excitatory neurons and their circuit dynamics, while inhibitory GABAergic dynamics has been examined primarily at the level of local microcircuits. As a result, GABAergic dynamics at the mesoscale and large-scale network level remain poorly understood. To close this gap, mesoscale wide-field imaging employing the genetically encoded GABA sensor iGABASnFR2 was employed to resolve cortical inhibitory dynamics during sensory processing and hippocampal–cortical interactions.

During sensory stimulation, GABA release was evoked across multiple modalities, including whisker, forelimb, hindlimb, and visual inputs. Inhibitory responses were spatially specific and localized to the appropriate primary sensory cortices, with stronger activation in the contralateral hemisphere. Inhibitory dynamics appeared to differ with brain state, with quiet wakefulness associated with faster, stronger, and more widespread GABA responses than anesthesia, while the spatial organization of sensory maps was preserved. Increasing extracellular GABA with tiagabine was accompanied by a loss of detectable sensory-evoked GABA responses and changes in large-scale cortical connectivity.

Examining cortical GABA dynamics around hippocampal sharp-wave ripples (SWRs) revealed large-scale, coordinated inhibitory activation across the cortex. During NREM sleep, GABA activation emerged earlier and propagated from medial to lateral cortical regions, whereas during wakefulness, activation followed the ripple and propagated from lateral to medial cortex. In both states, a global increase in inhibitory tone was observed, but with distinct spatiotemporal organization. The spatial distribution and timing of these components differed between wakefulness and NREM sleep, indicating that hippocampal ripples recruit distinct inhibitory network depending on behavioral state. These results identified cortical GABA signaling as a large-scale network process involved in sensory processing and hippocampal–cortical communication.

## Preface

This dissertation is original, and all methods and interventions were approved by the University of Lethbridge's Animal Care Committee. The work presented in Chapters 2 and 3 was conducted in Dr. Mohajerani's laboratory at the Canadian Centre for Behavioural Neuroscience. The research in Chapter 2 of this dissertation has been published in *Neurophotonics* under the title:

**"Characterization of iGABASnFR2 for in vivo mesoscale imaging of intracortical GABA dynamics"**
(DOI: 10.1117/1.NPh.12.3.035006)

Authors

Edris Rezaei[1], Setare Tohidi[1], Mojtaba Nazari[1], Javad Karimi Abadchi[2]

[1] University of Lethbridge (Canada)
[2] McGill University (Canada)

Author Contributions

E. R. conceptualized the study, designed and conducted the main experiments, prepared all figures, and wrote and revised the paper. M. N. contributed to the additional experimental procedures. J. K. A. implemented the strobing imaging system. E. R. and S. T. analyzed the data.

Chapter 3, titled **"Cortical GABAergic inhibition dynamics around hippocampal sharp-wave ripples"**, has received comments from reviewers (October 2025), and the revision is ready for submission to *Nature Communications Biology*. A preprint of this work is available on bioRxiv (DOI: 10.1101/2025.08.17.670701).

Authors

Edris Rezaei[1], Setare Tohidi[1]

[1] University of Lethbridge (Canada)

Author Contributions

E. R. conceptualized the study, designed and conducted the main experiments, prepared all figures, and wrote and revised the paper. E. R. and S. T. analyzed the data.

Chapter 4, titled **“GABAergic inhibition as a dynamic organizer of cortical activity”**, **will be submitted.**

Authors

Edris Rezaei[1]

[1] University of Lethbridge (Canada)

Author Contributions

E. R. conceptualized the study, prepared all figures, and wrote the manuscript.

## Ethics

Work described in this thesis received research ethics approval from the University of Lethbridge Research Ethics Board under protocol 2209, Project Name “Project Area I: In vivo assessment of subcortical-cortical interactions”.

**AI Generative**

I would like to acknowledge the use of Grammarly, which provided suggestions for rephrasing, restructuring sentences, and enhancing paragraphs by recommending additional words or alternative expressions.

**Acknowledgment**

I would like to sincerely thank the members of my thesis examination committee for their time, expertise, and valuable feedback: **Dr. Robert James Sutherland** and **Dr. Artur Luczak** as Thesis Examination Committee Members, **Dr. Dustin Hines** as the External Examiner from the University of Nevada, Las Vegas, and **Dr. Robbin Gibb** as Chair of the Thesis Examination Committee. My deepest thanks go to my supervisor, **Dr. Ian Whishaw**, for his unwavering guidance, encouragement, and mentorship, and for helping me grow into a true scientist.

**Table of contents**

**List of figures**

**List of abbreviations**

| | |
|---|---|
| GABA | Gamma-Aminobutyric Acid |
| NREM | Non-Rapid Eye Movement |
| REM | Rapid Eye Movement |
| GAT-1 | GABA Transporter Type 1 |
| LED | Light Emitting Diode |
| AAV | Adeno-Associated Virus |
| GCs | Genome Copies |
| EMG | Electromyography |
| LFP | Local Field Potential |
| ROI | Region of Interest |
| TTL | Transistor–Transistor Logic |
| CCD | Charge-Coupled Device |
| ΔF/F | Delta F over F |
| RSC | Retrosplenial Cortex |
| VISp | Primary Visual Cortex |
| VISa | Anterior Visual Area |
| BC | Barrel Cortex |
| M1 | Primary Motor Cortex |
| SST | Somatostatin interneuron |
| PV | Parvalbumin interneuron |
| cpSFGFP | Circularly Permuted Super folder GFP |
| VSD | Voltage-Sensitive Dye |

| | |
|---|---|
| BOLD | Blood-Oxygen-Level Dependent |
| ANOVA | Analysis of Variance |

# Chapter 1

## 1. General Introduction

Inhibition regulates excitatory activity in cortical circuits and determines when, where, and how neurons fire. Inhibitory neurons, which release GABA, consist of special and diverse populations that affect excitatory neurons through feedforward and feedback inhibition, refining the timing, precision, and strength of neuron responses. Cortical GABAergic inhibition is the basis for information processing, such as stimulus selectivity, gain modulation, normalization, and the generation of synchronous oscillations coordinating activity between distributed brain areas.

This chapter starts with a brief historical perspective of the inhibition concept. I then explore its molecular mechanisms with respect to inhibitory neurotransmitters like GABA, glycine, and serotonin, and their receptor subtypes. I conclude by discussing how GABAergic inhibition shapes cortical function prior to presenting the conceptual background and experimental hypotheses for the rest of this thesis.

### 1.1. The concept of inhibition

The concept of inhibition comes from Plato and Aristotle, who believed moral Behaviour depended on reason controlling emotion. In the early 1800s, Franz Gall advanced a similar hierarchical model in the context of brain function. He argued that mental abilities (higher faculties)—like reasoning, judgment, and self-control—should guide or regulate more basic impulses or instincts (lower faculties), such as desire, or hunger. Gall didn't talk about inhibition as we do today. The German philosopher-psychologist Herbart (1776–1841), unlike Gall, did not use the term *inhibition* in a hierarchy of faculties. Instead, he believed inhibition was what stopped unrelated or conflicting ideas from entering our conscious awareness all at once, allowing only compatible thoughts to stay in focus. He used the term *associative inhibition* to describe how some memories or pieces of information can block or interfere with others. Today, we call this *proactive inhibition* (old memories interfere with new ones) and *retroactive inhibition* (new memories interfere with old ones).

Later, psychiatrists used inhibition to explain symptoms of mental illnesses. The German psychiatrist Griesinger believed that thoughts turn into actions unless they are stopped by a person's willpower or self-control. He described how in depression there's too much inhibition (people are blocked or slowed down), and in mania/excitement there's too little inhibition (people

do things without control). In this model, inhibition = willpower, and the symptoms of mental illness were viewed as a physiological issue. Consciousness and willpower were linked to inhibition in early theories, but neurophysiological theories subsequently went in another direction, with more emphasis on how the brain itself regulates inhibition, not on concepts such as will or consciousness (Bari & Robbins, 2013).

### 1.2. The physiological discovery of inhibition

Sir Charles Bell was among the first to notice that nerve signals can reduce or stop activity, not just cause it, while studying eye muscles. In his book *On the Motions of the Eye*, Sir Charles Bell investigated the distinct roles of the recti and oblique muscles in controlling eye movement, proposing that the recti muscles govern voluntary, directional motion while the oblique muscles perform involuntary, protective functions such as rolling the eye upward. When he described the nerves, he found that the fourth cranial nerve, which controls the superior oblique, might not always function by stimulating the muscle to contract; instead, it might sometimes act by allowing the muscle to relax. He wrote, **"We have seen that the effect of dividing the superior oblique was to cause the eye to roll more forcibly upwards; and if we suppose that the influence of the fourth nerve is, on certain occasions, to cause a relaxation of the muscle to which it goes, the eyeball must be then rolled upwards."** (Charles, 1824)

After Volkmann's work on frogs—where he suggested that the brain could block or reduce nerve activity, even though he didn't use the term inhibition—scientists came to agree that the discovery that stimulating the vagus nerve slows the heart was key to forming the first real theories about how nerve signals can inhibit or reduce activity .Later, Weber and Weber in 1845 observed the same thing and were the first to actually call it "inhibition" whereas Lister was the first to talk about an "inhibitory system" in physiology (Bari & Robbins, 2013).

Although previous research addressed peripheral inhibition, genuine understanding of central mechanisms started with Sechenov's experiments in 1863. Sechenov used frogs to show that brainstem stimulation had the effect of inhibiting reflex responses (Stuart, 2014). Following Sechenov's research, subsequent researchers started examining inhibition not merely as a physiological phenomenon, but as a fundamental principle in the operation of the nervous system. In 1906, Charles Sherrington, who was working on reflex physiology, defined the mechanisms of inhibition. He introduced the synapse theory and advanced the idea of reciprocal inhibition—

showing that activating one group of muscles is accompanied by the inhibition of its antagonistic counterpart (Breathnach, 2004).

### 1.3. Inhibition in Behaviour, learning and brain

The concept of inhibition was also used in theories of Behaviour and learning. Ivan Pavlov argued that all Behaviours can be learned through a process known as conditioning. He introduced two main types of inhibition in classical conditioning: *external inhibition* and *internal inhibition*. External inhibition is when an irrelevant stimulus interrupts a conditioned response while internal inhibition is a process where a new conditioned response interferes with an existing one. As the concept of inhibition became more clearly defined through both Behavioural and physiological studies, attention gradually shifted toward understanding *where* in the nervous system inhibition occurs. Physiologists and neuroscientists early on looked for an inhibition neural "locus"—an area accountable for dampening activity.

Inhibitory control in the brain was first envisioned as acting between higher and lower nerve centers, but later perspectives highlighted its ubiquitous nature throughout the brain. Rather than being tied to specific locations, inhibition came to be seen as a general function of higher brain regions influencing lower ones. Early theories proposed cellular mechanisms for inhibition and later linked it to attention, where the mind filters out irrelevant information to focus. Research eventually connected inhibitory control to areas involved in emotion and Behaviour regulation, such as the frontal lobes. Damage to these areas was discovered to disrupt self-control, impulse control, and attention. The same effects were seen with damage of other brain regions, indicating that inhibition is generated by a distributed network and not by a single brain center. In addition to lesion research, researchers employed electrical stimulation to investigate how brain areas such as the cortex, hypothalamus, and reticular formation regulate inhibition. These studies helped map out the brain's inhibitory pathways and showed that multiple regions work together to regulate movement and Behaviour (Bari & Robbins, 2013).

### 1.4 Experimental description of neural inhibition

The mid-20th century provided physiological evidence of inhibitory mechanisms at the neural level, with Renshaw's work being a key example. He investigated the effects of antidromic motor volleys—electrical impulses traveling backward along motor neuron axons—on spinal cord activity. The investigation was prompted by the earlier findings of Müller and collaborators that stimulation of the central end of a transected ventral root failed to produce muscular contractions or to activate other motor neurons. Renshaw sought to investigate the inhibitory mechanism underlying these observations. He performed his experiments on decerebrate or lightly anesthetized rabbits and cats, taking great pains to isolate motor pathways by cutting the dorsal roots to eliminate all sensory feedback.

Electrical stimuli were then applied to the ventral root to induce antidromic volleys, and fine microelectrodes were inserted into the ventral horn of the spinal cord to record the electrical responses of nearby interneurons. He discovered interneurons in the ventral horn responded to a single antidromic volley with brief, high-frequency bursts of action potentials. These discharges were consistent in shape and timing, localized to individual cells, and reliably evoked only in specific regions of the spinal cord. He proposed that the interneurons were likely activated by *recurrent collaterals* of motor neurons (Renshaw, 1946).

Following up on Renshaw's discovery, Eccles and his co-workers examined the mechanism by which antidromic volleys in motor axons produce inhibitory actions on spinal motoneurons. They used cats as their experimental animals and applied electrophysiological methods—both intracellular and extracellular recordings—on the lumbar spinal cord. They aimed to find out if impulses in the motor axon collaterals activate the ventral horn interneurons, already described by Renshaw, and if these interneurons, in turn, have an inhibitory action on motoneurons. They established that antidromic stimulation caused prolonged discharges in the interneurons and simultaneous inhibitory post-synaptic potentials (IPSPs) in the motoneurons. Pharmacological experiments revealed that cholinergic antagonists such as dihydro-β-erythroidine inhibited the interneuron discharges and anticholinesterases such as eserine prolonged them. They also showed that acetylcholine could evoke similar interneuron activity. From these findings, they concluded

that motor axon collaterals excite these interneurons via cholinergic synapses, and the interneurons inhibit motor neurons through a direct synaptic pathway (Eccles et al., 1954).

Building on spinal models of recurrent inhibition, researchers soon turned their attention to cortical structures like the hippocampus to determine whether similar inhibitory mechanisms existed in higher brain areas. Andersen and colleagues investigated recurrent inhibition in the hippocampus, aiming to identify the inhibitory cell responsible and describe its synapses. They focused on the hippocampal pyramidal cells and their responses to stimulation from three input pathways: commissural, septal, and local. The study was conducted using anesthetized cats, in which the neocortex was removed to expose the hippocampus. Using intracellular microelectrodes filled with potassium citrate, potassium chloride, or sodium acetate, they recorded from CA3 pyramidal cells while stimulating the input pathways. They found that virtually all successfully penetrated cells produced large inhibitory postsynaptic potentials (IPSPs) of long duration in response to each of the three inputs.

The authors observed that the inhibitory effect appeared at the soma of the pyramidal cells, based on the distribution of extracellular potentials and latency measurements. They proposed that the inhibition was mediated by a specific type of interneuron. Based on physiological and anatomical features, they suggested that the basket cell matched the expected properties: its axon ramifies extensively, contacts the soma of many pyramidal cells, and can be activated by all three inputs. The study concludes that basket cells are probably the inhibitory neurons that are accountable for recurrent inhibition in the hippocampus (Andersen et al., 1963).

Whereas Andersen and colleagues were concerned with the cellular origin of recurrent inhibition in the hippocampus, Kandel et al. took this line of research further by making a comparison between the electrophysiological characteristics of hippocampal pyramidal cells and spinal motoneurons. Employing adult cats anesthetized with Evipal, they exposed the hippocampus through suction decortication and made intracellular recordings using 2M potassium citrate-filled microelectrodes. Stimulation was applied to the fornix, fimbria, alveus, and subiculum. In some experiments, the fornix and commissure were cut. They found that pyramidal cells could be identified by antidromic activation and showed sequential spike invasion. Subiculum

stimulation produced excitatory postsynaptic potentials, while fimbria stimulation evoked inhibitory potentials (Kandel et al., 1961).

### 1.5 Investigating inhibition through Hippocampal lesions

Building on physiological insights into hippocampal inhibition, researchers also turned to lesion studies to understand the behavioural role of this brain region. An example is the work of Robert J. Douglas, who examined how hippocampal damage affects the ability of animals to inhibit dominant responses. From evidence on behavioural tasks—maze learning, avoidance learning, discrimination, and sequential tasks—Douglas observed that animals with hippocampal lesions do worse when inhibition is required but, where it is not, they perform better. He also compared the findings to lesions in other parts of the brain and established that the pattern is specific to the hippocampus. He elaborated on the Douglas-Pribram model, which views the hippocampus as a regulator of attention by inhibitory gating of sensory input. This model is substantiated in behavioural data and fits into Pavlov's description of internal inhibition. He proposed that the hippocampus acts to screen out irrelevant information to protect memory and regulate behavioural accordingly (Douglas, 1967).

Continuing to elucidate the role of the hippocampus in the regulation of behavioural ,Daniel P. Kimble investigated whether the structure plays a role in internal inhibition, as initially formulated in Pavlovian learning theory. Using rats as subjects, Kimble compared three groups: normal rats, rats with bilateral hippocampal lesions, and rats with lesions to the neocortex above the hippocampus. All rats were trained on a brightness discrimination task in a Y-maze, followed by discrimination reversal, overtraining (50 repeated trials), and extinction (removal of the reward). The results showed that all groups learned the initial task equally well, but the hippocampal-lesioned rats were impaired in reversal learning. Under overtraining, normal rats and rats with cortical lesions ceased to respond after a period of approximately 25 trials, but rats with hippocampal lesions persisted in responding throughout all 50 trials. In extinction, the hippocampal group also exhibited a more gradual decrement in responding. Kimble interpreted that hippocampal damage disrupts internal inhibition and results in more rigid and perseverative behavioural (Kimble, 1968).

### 1.6. GABA neurotransmitter

Although GABA was detected in biological tissues as early as 1910, it wasn't until the 1950s that it was identified in mammalian brain tissue. In 1950, Eugene Roberts (Roberts & Frankel, 1950) and Awapara (Awapara, 1950) independently reported the discovery of γ-aminobutyric acid (GABA) as a naturally occurring compound in brain tissue. Bazemore and colleagues discovered an inhibitory substance found in brain extracts, known as Factor I. This substance had shown the ability to block nerve signals in the crayfish stretch receptor neuron, and the team wanted to isolate and identify it. They extracted and purified the active compound from beef brain using chemical processes and bioassays on crayfish neurons. The final crystals were confirmed to be γ-aminobutyric acid (GABA) through various chemical tests. They also showed that synthetic GABA had identical effects, and concluded that Factor I is GABA, at least in the crayfish nervous system (Bazemore et al., 1957).

Then, Florey and McLennan (1959) investigated if GABA could explain all the effects of Factor I, not just in neurons but in smooth muscle tissues. They tested both Factor I and synthetic GABA on guineapig and rabbit ileum, as well as on the oesophagus of sea-urchins, using different stimulant drugs like acetylcholine and nicotine to trigger contractions. They observed that GABA and Factor I showed similar effects, but GABA couldn't fully explain Factor I's actions, suggesting that Factor I may include other active components. Therefore, they suggested that GABA might be a natural inhibitory neurotransmitter (Florey & McLennan, 1959). In the 1950s and 60s, GABA's role as a neurotransmitter was questioned due to unclear inactivation mechanisms and conflicting data. However, invertebrate studies supported its inhibitory function, and key findings in 1967 by Krnjevic and Schwartz confirmed GABA's action on **cerebral cortical neurons** (Bari & Robbins, 2013).

#### 1.6.1 GABA receptors

##### 1.6.1.1 GABA_A receptor

GABA_A receptor is an ionotropic ligand-gated chloride channel that facilitates fast inhibitory neurotransmission. When GABA acts on these receptors, the channel opens and $Cl^-$ ions enter the

neuron, resulting in membrane hyperpolarization. In certain situations, however, GABA can be excitatory. When the intracellular concentration of $Cl^-$ is higher than the outside, $Cl^-$ flows out and depolarizes the neuron. This naturally happens in neonatal neurons, where the $Cl^-$ gradient is reversed. Thus, the action of GABA relies on the $Cl^-$ electrochemical gradient and the developmental stage (Ben-Ari et al., 2007). Structurally, the GABA_A receptors are pentameric, formed by different combinations of subunits (e.g., α, β, γ, δ, ε, and π), which dictate their functional and pharmacological characteristics. The diversity of subunits is the reason the receptor can respond differently to modulators such as benzodiazepines, barbiturates, neurosteroids, and zinc. Their distinct subunit distribution and sophisticated regulation highlight the fundamental role of GABA_A receptors in the maintenance of inhibitory control in the central nervous system (Bormann, 2000).

#### 1.6.1.2 GABA_B receptor

The GABA_B receptors are metabotropic (G-protein-coupled) receptors that allow for slow and sustained inhibition. Presynaptically, activation of the GABA_B receptor suppresses the release of neurotransmitters—GABA itself, glutamate, dopamine, and serotonin—by inhibition of voltage-gated calcium channel activity and thus calcium influx. Postsynaptically, the receptors open potassium channels (GIRKs), causing membrane hyperpolarization. Structurally, the functional receptor is a heterodimer of two subunits: GABA_B R1 (with splice variants like R1a and R1b) and GABA_B R2, which have differential patterns of expression in neuronal populations (Bettler et al., 2004).

#### 1.6.1.3 GABA_C receptors

GABA_C receptors are also chloride ion channels, as are GABA_A receptors, and consist of ρ (rho) subunits. In spite of their structural similarity to GABA_A receptors, they possess different functional characteristics, such as greater sensitivity to GABA, lower current responses, and an absence of desensitization. These ionotropic receptors are found primarily in the retina, where they mediate long-term inhibitory responses that are necessary for the processing of visual information (Bormann, 2000).

## 1.7 How inhibition shape cortical activity

In the cortex, excitatory and inhibitory signals work together. When a neuron is stimulated by sensory stimulation or spontaneous activity, a wave of inhibition follows a latency. This dynamic balance is flexible and adaptive, adjusting to the specific needs of each neuron, stimulus, and moment, ensuring the brain remains in balance. As excitation becomes too intense, inhibition comes into play to modulate it. When too little excitation threatens to result in silence, inhibition reduces. The result is a system that is both stable and responsive, capable of precision as well as adaptability. Inhibition, then, is not merely a suppressive force; instead, it is a chief architect of neural computation (Isaacson & Scanziani, 2011).

The architects of cortical inhibition are a diverse class of GABA-releasing interneurons, making up about 20% of cortical neurons (Markram et al., 2004). There is a strong classification system in place that incorporates molecular markers to divide cortical interneurons into three main and distinct classes: those expressing parvalbumin (PV), those expressing somatostatin (SST), and those expressing vasoactive intestinal peptide (VIP) (Rudy et al., 2011). These classes correlate with specific morphological, electrophysiological, and functional properties and hence make separate contributions to network computations and behavioural control. Interneurons form local networks through feedback and feed-forward inhibition. In feedback inhibition, they receive input from excitatory neurons and send inhibition back. In feed-forward inhibition, long-range excitatory signals activate inhibitory cells first, allowing early and strong inhibition to follow. Moreover, GABAergic interneurons inhibit one another, fine-tuning the timing, strength, and spatial distribution of inhibition across cortical circuits.

### 1.7.1 Inhibition shapes tuning

Cortical neurons are tuned to features of stimuli—a particular tone, orientation, or whisker deflection. A key player in the generation and refinement of this tuning is inhibition. For example, pharmacological blockade of GABA_A receptors causes neurons to fire more, losing their selective response. Early models proposed that tuning was sharpened by lateral inhibition, whereby neurons inhibit the activity of surrounding cells tuned to a different feature, similar to mechanisms

in the retina. Yet in most rodent cortical regions where spatial maps of stimulus features do not exist, such a model cannot apply. Instead, inhibition tends to be co-tuned with excitation, i.e., inhibitory and excitatory inputs are maximal in response to the same preferred stimuli (Isaacson & Scanziani, 2011). Inhibition regulates neural activity through multiple mechanisms. The "iceberg effect" occurs when inhibition reduces the resting membrane potential, silencing subthreshold excitatory inputs and allowing only the strongest inputs to generate spikes. Inhibiting responses to less preferred stimuli, since inhibition tends to be more widely tuned than excitation. Reducing the time window for firing by tracking excitation only a few milliseconds later. Collectively, these mechanisms demonstrate that inhibition does not simply counteract excitation, determining when and how neurons fire, ultimately increasing the fidelity and specificity of cortical sensory processing (Isaacson & Scanziani, 2011).

### 1.7.2 Inhibition and gain control

In addition, inhibition is essential in controlling the gain of a neuron, or its sensitivity to incremental inputs. Like how altering the volume of a speaker amplifies sound without altering the song, gain control scales the amplitude of neural responses without altering their selectivity. Such a process is essential for processes such as attention, where the brain amplifies relevant signals. In the brain's dynamic environment, inhibition that is coincident with excitation is important in controlling the size of neuronal responses without affecting their targets, an effect known as multiplicative gain modulation. Inhibition also maintains the fidelity of sensory representations even as their amplitude changes. Inhibition also extends the dynamic range of the brain. If not for inhibition, minor increments in excitatory input may cause unconstrained recruitment of huge neural populations, which would decrease the brain's power to separate subtle differences. Nevertheless, as inhibition strengthens together with excitation, neural activation turns out to be more gradual and constrained. Such coordination enables the brain to depict a wider, more subtle extent of inputs with high accuracy (Isaacson & Scanziani, 2011).

### 1.7.3 Inhibition and oscillations

Inhibition also creates rhythmic cortical activity, particularly in the beta (20–30 Hz) and gamma (30–80 Hz) frequency ranges. Such oscillations allow for temporal coordination, information

binding, and communication between cortical areas. Parvalbumin-positive interneurons play a key role in this process, synchronizing with high precision due to their mutual connection. Two main models explain rhythm generation: PING (excitatory-inhibitory loops) and ING (interneuron-driven inhibition). In both scenarios, inhibition does more than regulate—it organizes. By setting precise timing and synchrony, it allows distributed neurons to function as a unified, pulsing network (Isaacson & Scanziani, 2011).

### 1.8. Glycine

Glycine is the simplest in structure and its journey to recognition as a major inhibitory neurotransmitter in the spinal cord and brainstem has been detailed. The first suggestion that glycine acts as a neurotransmitter came nearly 60 years ago, when Aprison and Werman (1965) observed that glycine concentrations in the spinal cord were significantly higher than in other parts of the brain (Aprison & Werman, 1965). Using techniques developed by Curtis and Watkins, subsequent studies showed that application of glycine to spinal neurons consistently decreased their firing rates, furnishing physiological proof of its inhibitory role (Curtis & Watkins, 1960).

The glycine receptor (GlyR) usually acts as an inhibitory receptor because it allows chloride ions ($Cl^-$) to flow in and bring the neuron's membrane potential closer to the $Cl^-$ equilibrium, which is typically negative. This either keeps the neuron stable or makes it less likely to fire (hyperpolarization). Even small changes that don’t reach firing threshold can still suppress neuron activity through a process called shunting inhibition. However, in developing (embryonic) neurons, the situation is different. These cells have high internal chloride levels, so when GlyR opens, $Cl^-$ flows outward, causing a strong depolarization that can actually excite the neuron and trigger important developmental events, like calcium influx and formation of glycinergic synapses. As the nervous system develops, the neuron starts to express KCC2, a transporter that reduces internal $Cl^-$ concentrations. This change renders GlyR's action inhibitory once again, representing a fundamental switch from developmental excitation to mature inhibition in the nervous system (Dutertre et al., 2012).

### 1.8.1 Glycine receptors

Researchers, including Betz and colleagues, first purified glycine receptors (GlyRs) from the rat spinal cord using affinity chromatography with aminostrychnine. Glycine receptors (GlyRs) are found in both homomeric and heteromeric forms, composed of α (α1–α4) and β subunits. During development, homomeric α2 GlyRs dominate in embryonic neurons but are replaced by heteromeric α1β GlyRs after birth, which are the main inhibitory receptors in the adult spinal cord and brainstem. Homomeric α1 and α3 GlyRs are rare in adults and likely extrasynaptic, while α4 is a pseudogene in humans and functionally irrelevant. Heteromeric α2β GlyRs persist in some adult retinal neurons, and α3β GlyRs are found in pain pathways, where they are regulated by inflammation. Overall, eight GlyR types are identified: four homomeric (α1–α4) and four heteromeric (α1β–α4β), with α1β being the most functionally important in adults (Dutertre et al., 2012).

## 1.9 Other Neurotransmitters and Neuromodulators with Inhibitory Effects

Although GABA is the principal inhibitory neurotransmitter**,** inhibitory control of neuronal excitability is implemented through a broad network of neuromodulators that act alongside GABAergic transmission. Several endogenous molecules exert powerful inhibitory regulation by suppressing synaptic release, hyperpolarizing neurons, and stabilizing network activity. Taurine (Wu & Prentice, 2010) and β-alanine (Wu et al., 1993) act as inhibitory neuromodulators through activation of GABA_A and glycine receptors, contributing to neuroprotection and control of excitability, particularly in brainstem and spinal circuits. Opioid peptides such as enkephalins and dynorphins produce strong inhibition by activating Gi/o-coupled opioid receptors that suppress presynaptic calcium entry and enhance potassium conductance, thereby reducing neurotransmitter release and neuronal firing (Rysztak & Jutkiewicz, 2022). The neuropeptide galanin exerts widespread inhibitory effects in hippocampal, hypothalamic, and cortical networks by dampening excitatory transmission and regulating arousal, memory, and metabolic homeostasis (Lang et al., 2015). Adenosine serves as a global homeostatic inhibitor of brain activity, accumulating during prolonged wakefulness and suppressing synaptic transmission via A1 receptors to promote sleep pressure and network stabilization (Huang et al., 2024). Also, classical monoamines including

dopamine (Beaulieu & Gainetdinov, 2011), serotonin (Albert & Ansari, 2019), and norepinephrine (Jones & Cohen, 2005) exert potent inhibitory modulation through specific receptor subtypes which suppress neuronal firing and transmitter release across basal ganglia, cortical, and brainstem circuits .

## 1.10 Conceptual framework and research hypotheses

These findings provide the foundation for the present GABAergic inhibition theory, which proposes that GABA is the primary regulator of neuronal excitability and network stability across brain systems. Therefore, I build my study around the proposed GABAergic inhibition theory.

### The GABAergic inhibition theory

This theory proposes that GABA exerts an inhibitory effect on neuronal activity throughout the nervous system.

### Hypothesis 1

Therefore, GABAergic neurons play a role in regulating cortical responses to both external and internal stimuli.

### Hypothesis 2

Furthermore, cortical responses to other brain signals, such as hippocampal sharp-wave ripples (SWRs), are expected to involve inhibitory GABAergic mechanisms.

## Chapter 2

## Characterization of iGABASnFR2 for in vivo mesoscale imaging of intracortical GABA dynamics


### Abstract

Although genetically encoded sensors have advanced the study of cortical excitation, tools for large-scale imaging of inhibition remain limited. Visualizing extracellular gamma-aminobutyric acid (GABA) dynamics in vivo is essential for understanding how inhibitory networks shape brain activity across sensory, behavioural, and pharmacological states. My goal is to validate and apply the genetically encoded sensor iGABASnFR2 for wide-field imaging of extracellular GABA and to characterize how cortical inhibition reorganizes across brain states, sensory modalities, and after GABA transporter blockade. I performed mesoscale imaging in head-fixed C57BL/6 mice systemically expressing iGABASnFR2. Recordings were conducted under isoflurane anesthesia, during quiet wakefulness, natural sleep [non-rapid eye movement (NREM) and rapid eye movement], and after administration of the GAT-1 inhibitor tiagabine. I analyzed both sensory-evoked and spontaneous GABA signals using timeseries, spectral, and seed-pixel correlation analyses. iGABASnFR2 demonstrated strong and modality-specific GABAergic responses to sensory stimulation, with faster and stronger activation in the contralateral cortex. Although the general spatial patterns of sensory-evoked GABA responses were consistent across anesthesia and quiet wakefulness, the amplitude, timing, and spread of these responses were significantly greater during wakefulness. During spontaneous activity, cortical GABA levels and connectivity modulated by brain state: GABA amplitude and interhemispheric synchrony, were highest during quiet wakefulness but reduced during NREM sleep. Tiagabine elevated baseline GABA levels, abolished stimulus-evoked responses, and enhanced local and long-range inhibitory synchrony. iGABASnFR2 enables reliable, high-resolution imaging of cortical GABA dynamics in vivo. These results demonstrate that inhibitory signaling is dynamically structured across brain states and can be pharmacologically modulated. This tool offers opportunities to explore the role of inhibition in health and disease at the mesoscale level.

## 2.1 Introduction

The nervous system is composed of two basic cell types: neurons and glial cells. Neurons can be categorized into excitatory and inhibitory types. Excitatory neurons primarily release glutamate which is the major neurotransmitter in the nervous system to facilitate communication among neurons across different brain regions (Zhou & Danbolt, 2014),whereas inhibitory neurons mainly release gamma-aminobutyric acid (GABA) to stabilize neural networks by balancing excitatory activity and preventing excessive neuronal firing (Froemke, 2015). Maintaining this precise balance between excitation and inhibition is essential for sensory processing, memory formation, and motor control (Tatti et al., 2017; Yuste, 2005). Through temporally and spatially precise modulation of neuronal activity, inhibitory signaling contributes to a wide range of brain functions, including sensory processing, circuit refinement, and the regulation of oscillatory dynamics (Ferguson & Gao, 2018; Kepecs & Fishell, 2014; Markram et al., 2004; Tremblay et al., 2016; Urban-Ciecko & Barth, 2016).

Disruptions in GABAergic signaling underlie a variety of neurological and psychiatric disorders, including epilepsy, schizophrenia, and autism spectrum disorders, highlighting the clinical importance of understanding GABAergic modulation in both health and disease (Curley & Lewis, 2012; de Lanerolle et al., 1989; Gonzalez-Burgos & Lewis, 2008; Lewis & Moghaddam, 2006; Marín, 2012; Rubenstein & Merzenich, 2003). Despite the importance of GABA in regulating cortical activity, direct, real-time visualization of GABA dynamics in vivo remains unknown. The development of genetically encoded neurotransmitter sensors has significantly expanded the ability to monitor neural activity across spatial and temporal scales (Marvin et al., 2013). For instance, the glutamate sensor iGluSnFR enabled high-resolution, real-time imaging of excitatory neurons, providing insights into cortical connectivity and sensory-evoked activity in awake and anesthetized animals (Xie et al., 2016).Building on advances in sensor engineering, the genetically encoded fluorescent sensor iGABASnFR2 was developed to detect extracellular GABA dynamics (Marvin et al., 2019) This sensor permits real-time, in vivo monitoring of extracellular GABA, providing a powerful tool for visualizing GABA's spatial and temporal dynamics across large-scale cortical regions. Wide-field imaging with iGABASnFR2 enables comprehensive mapping of inhibitory circuits. However, a detailed characterization of

iGABASnFR2 functionality across different brain states, sensory modalities, and pharmacological conditions is still needed.

In this study, I characterized spontaneous and sensory-evoked GABAergic activity across the dorsal cortex using wide-field imaging of iGABASnFR2 sensor in natural sleep, awake mice, and under 1% isoflurane anesthesia. In addition, I assess the effects of tiagabine, a GABA reuptake inhibitor, to further characterize sensor performance and demonstrate its sensitivity to pharmacological manipulation of cortical GABA levels. These results not only validate the robustness and sensitivity of iGABASnFR2 as a practical tool for monitoring GABAergic neurotransmission in vivo but also lay a solid foundation for future studies into inhibitory dynamics in health and disease, including conditions such as epilepsy, schizophrenia, and autism spectrum disorders.

## 2.2 Material and Methods

### 2.2.1 Animal Subjects

The University of Lethbridge animal care committee approved all procedures, which adhered to the guidelines set forth by the Canadian Council on Animal Care and Use. I used 20 young adult (6 weeks old) C57BL/6 mice (12 males and 8 females). Mice were accommodated in transparent plastic cages within a 12-h light–dark cycle, with lights turning on at 7:30 AM, and provided unrestricted food and water access. Room temperature was maintained at 24°C, and relative humidity was kept between 40% and 50%.

### 2.2.2 Viral Constructs

The viral constructs originated from the Viral Vector Core of the Canadian Neurophotonics Platform (RRID: SCR_016477). Plasmids encoding iGABASnFR2 and cpSFGFP were obtained from Addgene, and AAV2/PHP.N-CAG-iGABASnFR2 and AAV2/PHP.N-CAG-cpSFGFP viral vectors were subsequently designed, packaged, and purified by the CNP Viral Vector Core at a final concentration of 1.5 $X10^{13}$ genome copies (GCs)/mL.

### 2.2.3 Retro-Orbital Injection

For retro-orbital viral injections (Yardeni et al., 2011), 4- to 6-week-old C57BL/6 mice were anesthetized with 3% isoflurane and maintained at 2% to 2.5% during the procedure. Metacam (5 mg/kg, subcutaneous) was administered for analgesia, and body temperature was maintained using a heating blanket. Topical anesthesia (0.5% proparacaine hydrochloride) was applied to the eye, followed by gentle pressure to induce mild eye protrusion. A 30-G needle was then inserted through the medial canthus at a 30-deg angle into the retro-orbital sinus. Mice received 1.4 X $10^{11}$ GCs of either AAV2/ PHP.N-CAG-iGABASnFR2 or AAV2/PHP.N-CAG-cpSFGFP, using the PHP.N capsid for widespread CNS expression, as originally described by Ref. (Chan et al., 2017). iGABASnFR2 has a secretion signal (IgG kappa) and a transmembrane domain (from PDGFR). Combined those two sits target it to the plasma membrane, facing out. Without those, it will be expressed in the cytosol, and in theory could be used to detect cytosolic GABA. In addition to neuronal synaptic release, astrocytes are known to contribute to extracellular GABA via non-vesicular release mechanisms that generate tonic inhibition. Therefore, the iGABASnFR2 signal likely reflects the combined contribution of neuronal and glial sources of extracellular GABA.

### 2.2.4 Drug Administration

Tiagabine hydrochloride (Cat #SML0035, Sigma-Aldrich Canada, Oakville, Canada) was purchased from Sigma-Aldrich. Tiagabine was dissolved in sterile saline to achieve a concentration of 5 mg/ml. For intraperitoneal injection, mice received tiagabine at a dosage of 10 mg/kg body weight. Control animals were administered an equivalent volume of sterile saline.

### 2.2.5 Surgical Procedure and Post-Operative Care

C57BL/6 mice received buprenorphine (0.05 to 0.1 mg/kg, subcutaneously) ~30 min before surgery, followed by anesthesia with isoflurane (1% to 2% in oxygen) delivered via a nose cone. After shaving and sterilizing the scalp, lidocaine (0.5%, 5 mg/mL, subcutaneously) was administered at the incision site for local anesthesia (0.04 to 0.08 mL for mice weighing 25 to 55 g). A midline incision was made to expose the skull, and the overlying skin was carefully removed to avoid damaging the underlying bone. A custom-designed head plate was affixed to the skull

using C&B Metabond Quick Base (Parkell, Brentwood, New York, United States) mixed with C&B Metabond Clear L-Powder (3 g, Product Code S399, Parkell, Tokyo, Japan). A sterile 12-mm circular glass coverslip (Carolina Biological Supply, Cat. No. 633005, Burlington, North Carolina, United States) was placed on the skull surface and sealed in place with the same adhesive. For hippocampal recordings, a bipolar electrode made of two twisted 50-μm Tefloncoated stainless-steel wires (A-M Systems, Sequim, Washington, United States) was slowly inserted through a craniotomy at a 57-deg angle relative to vertical. Electrode placement was guided by continuous monitoring of signal quality using both visual and auditory feedback. The electrode was secured to the skull using Krazy Glue, followed by dental cement. An electromyography (EMG) electrode was also implanted into the neck muscles to monitor muscle activity. Following surgery, animals were housed individually in temperature-controlled recovery cages and received subcutaneous injections of Baytril (enrofloxacin, 10 mg/kg), meloxicam (5 mg/kg), and 1 mL of warm sterile saline. These injections were administered once every 24 h for 3 days postoperatively, in accordance with institutional guidelines. After this recovery period, animals were monitored twice daily for the remainder of the experiment.

### 2.2.6 iGABASnFR2 Imaging Under Anesthesia

Following, the animals were anesthetized with isoflurane (2.5% for induction, followed by 1% for maintenance). The depth of anesthesia was confirmed by assessing reflexes. Once adequately anesthetized, each mouse was positioned in a head-stage, and the head was securely head-fixed. A homeothermic blanket was utilized to maintain their body temperature, and isoflurane was administered via a nosepiece. The isoflurane concentration was adjusted to 1% to initiate the imaging procedure. Images were acquired using a microscope consisting of a front-to-front pair of video lenses with a field of view measuring 8.6 X 8.6 mm. The camera's focal plane was positioned 0.5 to 1 mm (~0.04) below the cortical surface. A 12-bit charge-coupled device (CCD) camera (1M60 Pantera Dalsa, Waterloo, Ontario, Canada) and an EPIX E8 frame grabber with XCAP 3.8 imaging software (EPIX, Inc., Buffalo Grove, Illinois, United States) were used to capture images at a frame rate of 80 Hz. These imaging parameters have been employed in previous studies (Mohajerani et al., 2013; Silasi et al., 2016; Vanni & Murphy, 2014). Carefully designed data collection protocols support the robustness of our findings. Sequential illumination was achieved

using alternating blue and green light-emitting diodes (LEDs) (Xiao et al., 2021). The timing of LED alternation is illustrated in Fig. S1 in the Supplementary Material. Blue light (473 nm, filtered through a 467- to 499-nm bandpass) was used to excite the iGABASnFR2 indicator, and green light (530 nm, filtered through a 527/42-nm bandpass) was

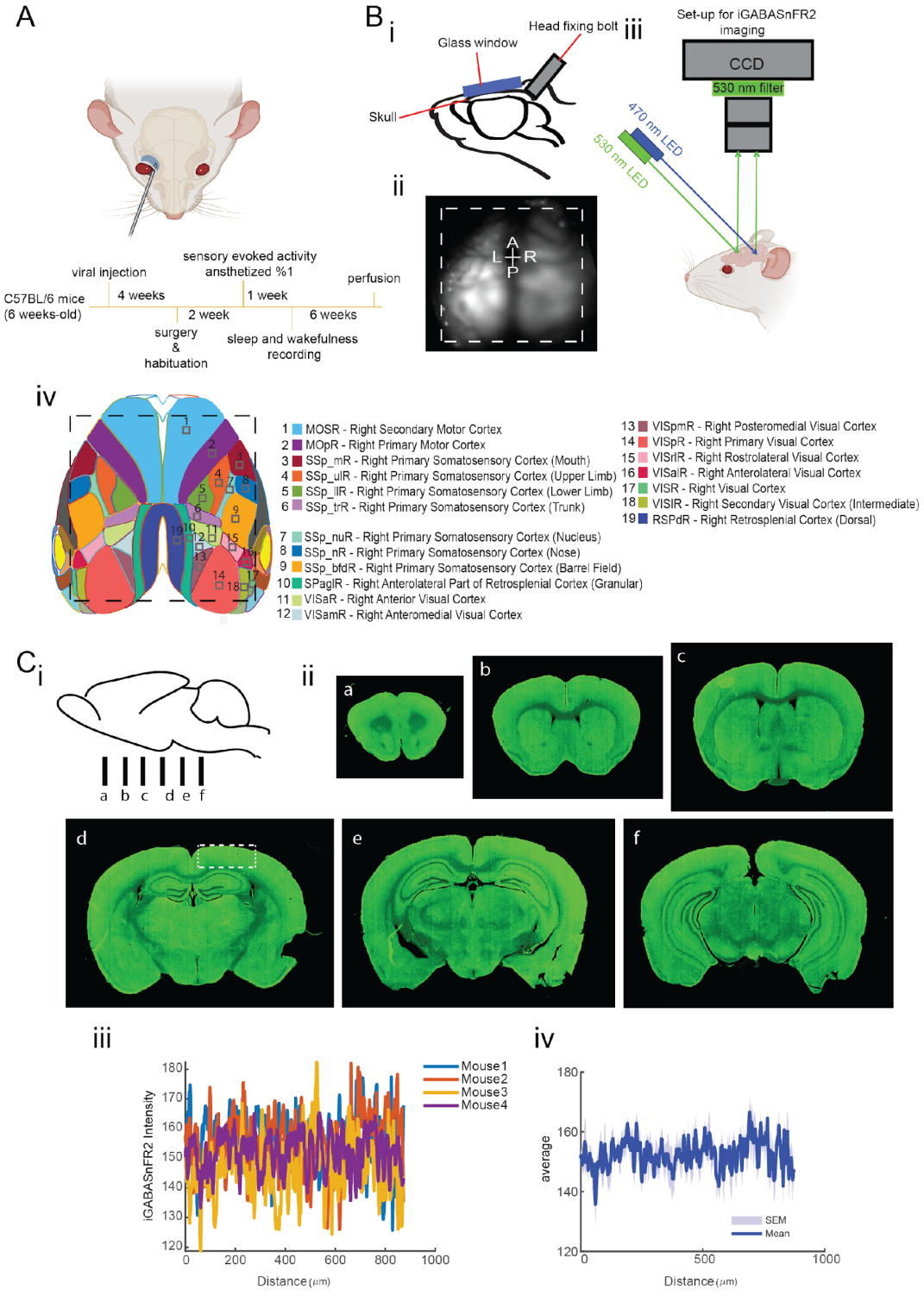


**Fig. 1 Schematic of experimental workflow, imaging setup, and expression of iGABASnFR2. (A) Experimental timeline.** AAV2/PHP.N-CAG-iGABASnFR2 or the control virus AAV2/PHP.N-CAGcpSFGFP was systemically administered via retro-orbital injection into 6-week-old C57BL/6 mice. Four weeks after viral injection, the animals underwent cranial window

surgery. Following a 7-day recovery period, animals gradually habituated to the head-fixation setup over the course of another week. Sensory-evoked imaging was then conducted under 1% isoflurane anesthesia. After this session, longitudinal recordings during quiet wakefulness and natural sleep were carried out for up to 6 weeks. Mice were subsequently euthanized, and the brains were perfused for histological analysis. (B) Imaging setup. (i) Illustration of the cranial window implantation over the skull following scalp removal. (ii) Representative image showing the cortical imaging area, indicated by the dashed white line. (iii) Schematic of the wide-field imaging setup: a blue LED (470 nm) was used for excitation, and signals were captured using a CCD camera at 530 nm emission. (iv) Map of the bilateral craniotomy showing the targeted cortical regions based on the Allen Mouse Brain Atlas. (C) Expression of iGABASnFR2. (i) Schematic of coronal sectioning locations (a–f) along the anterior–posterior axis. (ii) Coronal sections (a–f) show strong iGABASnFR2 expression in the cortex and hippocampus. (iii) The region marked by a white dashed rectangle in panel C(iid) was used to extract fluorescence profiles across animals (n . 4), highlighting the unique expression and inter-animal expression consistency. (iv) The average profile with SEM as a shaded region.

used for intrinsic signal imaging of blood volume. A bandpass emission filter (shown in Fig. 1) was positioned in front of the CCD camera to enable selective detection of either fluorescence or reflectance signals. Blue and green LEDs were synchronized and alternated on a frame-by-frame basis using transistor-transistor logic (TTL) triggering, resulting in interleaved acquisition of fluorescence and reflectance images at 40 Hz per channel. In addition, images of reflectance, crucial for blood artifact corrections, were evaluated within the current pipeline (Kramer & Pearlstein, 1979; Ma et al., 2016; Scott et al., 2018). Anesthetized iGABASnFR2 imaging of spontaneous activity was conducted without sensory stimulation for 15-min sessions.

### 2.2.7 Sensory Stimulation

I captured the iGABASnFR2 signal in response to varied peripheral simulations while utilizing urethane anesthesia, following the methodology outlined in previous studies. Sensory stimuli were employed to map the functional areas of the hindlimb somatosensory, forelimb somatosensory, auditory, visual, and barrel cortices (Mohajerani et al., 2013). Sensory stimuli were applied to map the cortical regions corresponding to forelimb, hindlimb, whisker, visual, and auditory modalities. For forelimb and hindlimb stimulation, a piezoelectric bending actuator delivered a single 300-ms tap via a square pulse directly to the skin of one forelimb or hindlimb. Whisker stimulation targeted the whisker, which was attached to a piezoelectric actuator (Q220-A4-203YB, Piezo Systems, Inc., Woburn, Massachusetts, United States) and deflected using a single 300-ms square pulse. Visual stimuli consisted of a single 20-ms pulse of 435-nm light (LED), delivered at a fixed distance and

height relative to the right eye. For each sensory modality, 40 stimulus presentations were delivered with a 10-s interstimulus interval to calculate the average cortical responses. The timing of stimulus delivery is illustrated in Fig. S1 in the Supplementary Material.

### 2.2.8 Habituation

After the 7-day recovery period from surgery, mice gradually habituated to the head restraint in the recording environment. Initially, each mouse was placed individually on the recording platform along with Cheerios cereal, allowing them to explore freely and become comfortable. Mice were progressively acclimated to eating the cereal while head-fixed, beginning with 5-min sessions and increasing by 5 min each day until reaching 60 min.

### 2.2.9 iGABASnFR2 Imaging During Wakefulness

Following habituation, wakefulness recordings began. Each animal underwent recording sessions every 3 days, completing three to four sessions per mouse. Recordings were consistently performed at the same time of the day to reduce variability and stress. Among sessions, mice were returned to their home cages for rest and recovery before the next recording. After finishing all wakefulness sessions, mice proceeded to the sleep recording phase.

### 2.2.10 iGABASnFR2 Imaging During Sleep

To optimize conditions for natural sleep under head restraint, mice were transferred from their colony housing to a separate room at noon the day before recording. Sleep was restricted for 6 h by gentle stimulation (using a cotton-tip stick) whenever signs of drowsiness were observed. Following 6 h of sleep deprivation, mice were placed overnight in large, enriched cages containing a running wheel, Cheerios, and a water container to promote exploration and natural sleep. The next morning (~9:00 AM), animals were transferred to the imaging platform for sleep recordings. Afterward, they were returned to their home cages for at least 3 days of recovery before any further recordings. This sleep deprivation protocol is commonly used to induce moderate but physiologically meaningful sleep pressure (Vyazovskiy et al., 2008), which is known to trigger a homeostatic increase in slow-wave activity during subsequent non-rapid eye movement (NREM) sleep.

### 2.2.11 Preprocessing

Image stacks were first de-interleaved to separate the GABA-sensitive fluorescence signal (blue channel) and the hemodynamic reflectance (green channel) signal. The correct channel assignment was verified by computing pixel-wise correlations between the first frame of each stack and reference images corresponding to each illumination wavelength. To quantify extracellular GABA dynamics, the relative fluorescence change (ΔF/F) was calculated on a per-pixel basis using a 2-second pre-stimulus window to define baseline fluorescence ($F_0$). The ΔF/F signal was defined as:

$$\Delta F/F(t) = (F(t) - F_0) / F_0$$

where F(t) is the fluorescence intensity at time t, and $F_0$ is the baseline fluorescence. To correct for hemodynamic artifacts (Kramer & Pearlstein, 1979; Ma et al., 2016; Scott et al., 2018) , a pixel-wise linear regression was applied, in which a scaled version of the reflectance signal R(t) was subtracted from the fluorescence trace:

$$F_{corrected}(t) = F(t) - \alpha \cdot R(t)$$

The corrected fluorescence signal was then normalized to the baseline (ΔF/F) and bandpass filtered to remove low-frequency drift and high-frequency noise. Trial-averaged ΔF/F responses were generated to assess sensory-evoked activity. All preprocessed data—including corrected ΔF/F, raw fluorescence, and reflectance signals—were saved in float32 format.

### 2.2.12 ROI-based Fluorescence Analysis

Following preprocessing, imaging data from specific regions of interest (ROIs)—defined as 3×3-pixel areas (~40,401 μm²) centered around anatomical coordinates corresponding to stimulation sites)— were extracted. Baseline correction was conducted by subtracting the mean fluorescence signals calculated from a 1-second pre-stimulus period from the post-stimulus fluorescence signals. The signals were further filtered to eliminate slow baseline drifts using a

high-pass filter (>0.1 Hz) and to reduce high-frequency noise using a low-pass filter (<5 Hz). From the filtered signals, several key parameters were derived, including peak amplitude (maximum $\Delta F/F_0$ within a 1-second post-stimulus interval), time-to-peak, and decay time (duration for the fluorescence to fall to 50% of peak amplitude). For visualization, the corrected $\Delta F/F_0$ signals were plotted with indicators marking peak and decay times, facilitating clear interpretation of response dynamics. Mean responses across trials were computed separately for each sensory modality, with variability assessed by plotting the standard error of the mean (SEM) as shaded regions surrounding the mean trace.

### 2.2.13 Motion Detection and Exclusion

Motion artifacts were identified and excluded from analyses using electromyography (EMG) signals recorded simultaneously with imaging data. EMG recordings were smoothed using a median filter and squared to enhance the detection of muscle activity periods. An activity threshold was established at the 95th percentile of the processed EMG signal to identify movement onset and offset events. These EMG-detected motion periods were temporally aligned with imaging frames via synchronized camera clock signals. Frames coinciding with detected movements were subsequently removed from analysis, ensuring the seed pixel correlation analysis reflected only stationary periods free of motion-related artifacts.

### 2.2.14 Seed-pixel Correlation Analysis

Seed pixel correlation analysis was performed to evaluate functional connectivity based on spontaneous GABA activity from sleep and anesthetized mice. preprocessed data were spatially registered to the Allen Brain Atlas, enabling anatomical alignment and inter-subject comparisons. Regions of interest (ROIs)—specifically the barrel cortex (BC), visual cortex (VC), hindlimb (HL), and forelimb (FL)—were defined using anatomical coordinates derived from the atlas. Within each ROI, seed pixels were selected to serve as reference points for correlation-based connectivity analysis.

### 2.2.15 Motion Signal Extraction, Alignment, and Sleep Scoring

Behavioural videos were used to monitor animal movement during imaging. Motion signals were extracted using FaceMap (Syeda et al., 2024), which computes frame-to-frame pixel intensity changes in user-defined regions of interest (ROIs). Five ROIs—nose, whisker pad, ear, shoulder, and trunk—were selected to capture both facial and body movements. To synchronize video with neural data, camera frame pulses were recorded on analog channels during acquisition. These were used to align motion traces with electrophysiological recordings (LFP and EMG, sampled at 2 kHz). Traces were interpolated or trimmed as needed, z-scored, and averaged across ROIs to generate composite facial and body motion signals. This enabled detection of both gross movement and small twitches, such as those occurring during REM sleep, which may not be captured by EMG alone. With motion aligned, vigilance states were classified as wakefulness, NREM, or REM sleep using combined behavioural and physiological features. Wakefulness was marked by visible movement and high EMG activity. NREM sleep was defined by low EMG, a low hippocampal theta-to-delta power ratio, and the presence of Large Irregular Activity (LIA) in the LFP. REM sleep was characterized by minimal EMG activity, a high theta-to-delta ratio, and continuous hippocampal theta. In head-fixed recordings, pupil constriction served as an additional marker of sleep onset (Karimi Abadchi et al., 2020; Yüzgeç et al., 2018). This multimodal approach enabled robust, accurate classification of sleep stages across different experimental conditions.

### 2.2.16 Effect of Isoflurane Anesthesia on Extracellular GABA Dynamics

At concentrations around 1%, isoflurane induces a slow-wave cortical state characterized by synchronized network activity and enhanced inhibitory tone. Isoflurane potentiates synaptic GABA_A receptor–mediated currents (Topf et al., 2003), enhances tonic inhibition via extrasynaptic GABA_A receptors that are sensitive to ambient extracellular GABA (Jia et al., 2008), and can directly activate GABA_A receptor channels at higher concentrations (Neumahr et al., 2000). In addition, isoflurane preferentially suppresses pyramidal neuron excitability relative to parvalbumin interneurons, biasing cortical circuits toward inhibition (Qiu et al., 2023). Under these slow-wave conditions, the iGABASnFR2 sensor reports physiologically meaningful

extracellular GABA dynamics within an inhibition-dominated network regime (Neumahr et al., 2000; Topf et al., 2003; Jia et al., 2008; Qiu et al., 2023)

### 2.2.17 Statistical Analysis

All data processing and analyses were performed using custom scripts written in MATLAB R2024a.

## 2.3 Results

### 2.3.1 Experimental Workflow, Imaging Setup, and Cortical Expression of iGABASnFR2

To characterize extracellular GABA dynamics, I first injected AAV2/PHP.N-CAGiGABASnFR2 and AAV2/PHP.N-CAG-csGFP systemically via retro-orbital injection [Fig. 1(a)]. Imaging was performed under isoflurane anesthesia, during quiet wakefulness, NREM, and REM sleep. The imaging setup [Fig. 1(b)] utilized a bilateral cranial window and a CCD-based wide-field microscope that captured fluorescence across an 8.6 Å~ 8.6 mm field of view. Sequential blue (470 nm) and green (530 nm) LED illumination enabled alternating frame acquisition and hemodynamic correction (Kramer and Levitan, 1979; Ma et al., 2016; Scott et al., 2018). To validate sensor expression, I conducted a histological analysis [Fig. 1(c)]. A robust expression of iGABASnFR2 was revealed in cortical and hippocampal regions. The coronal brain sections [Fig. 1(c)ii] demonstrated consistent expression across animals. To assess inter-animal variability and regional expression strength, fluorescence intensity profiles were extracted using ImageJ from defined cortical areas [Fig. 1(c)iii], and to further quantify and visualize overall trends, these profiles were averaged across animals, with the mean±SEM shown [Fig. 1(c)iv] confirming uniform sensor expression suitable for quantitative cortical imaging.

### 2.3.2 iGABASnFR2 Reveals Modality- and Hemisphere-Specific Cortical Inhibition Under Anesthesia

Previous studies on sensory processing have primarily focused on excitatory neuronal responses, often using calcium or glutamate indicators to map stimulus-evoked activity across the cortex (Xie et al., 2016; Mohajerani et al., 2013; Chen et al., 2012). However, much less is known about how sensory stimuli engage inhibitory networks, particularly at the mesoscale. Inhibitory interneurons play a crucial role in shaping sensory responses, modulating cortical excitability, and controlling the timing and precision of neural coding (Atallah et al., 2012; Wilson et al., 2012).To examine the spatiotemporal dynamics of GABA activity across the cortex, I delivered contralateral whisker, hindlimb, forelimb, and visual stimulation under 1% isoflurane anesthesia and recorded GABA activity using the iGABASnFR2 sensor. As shown in Fig. 2(a), each sensory modality shows a localized increase in GABAergic fluorescence within the corresponding primary sensory cortex, with response onsets occurring ∼75 to 150 ms after stimulus. All sensory modalities elicited more robust and spatially localized GABAergic activity. Temporal response profiles [Fig. 2(b)] demonstrated stronger GABAergic activation in the contralateral hemisphere relative to the ipsilateral side across all sensory modalities.

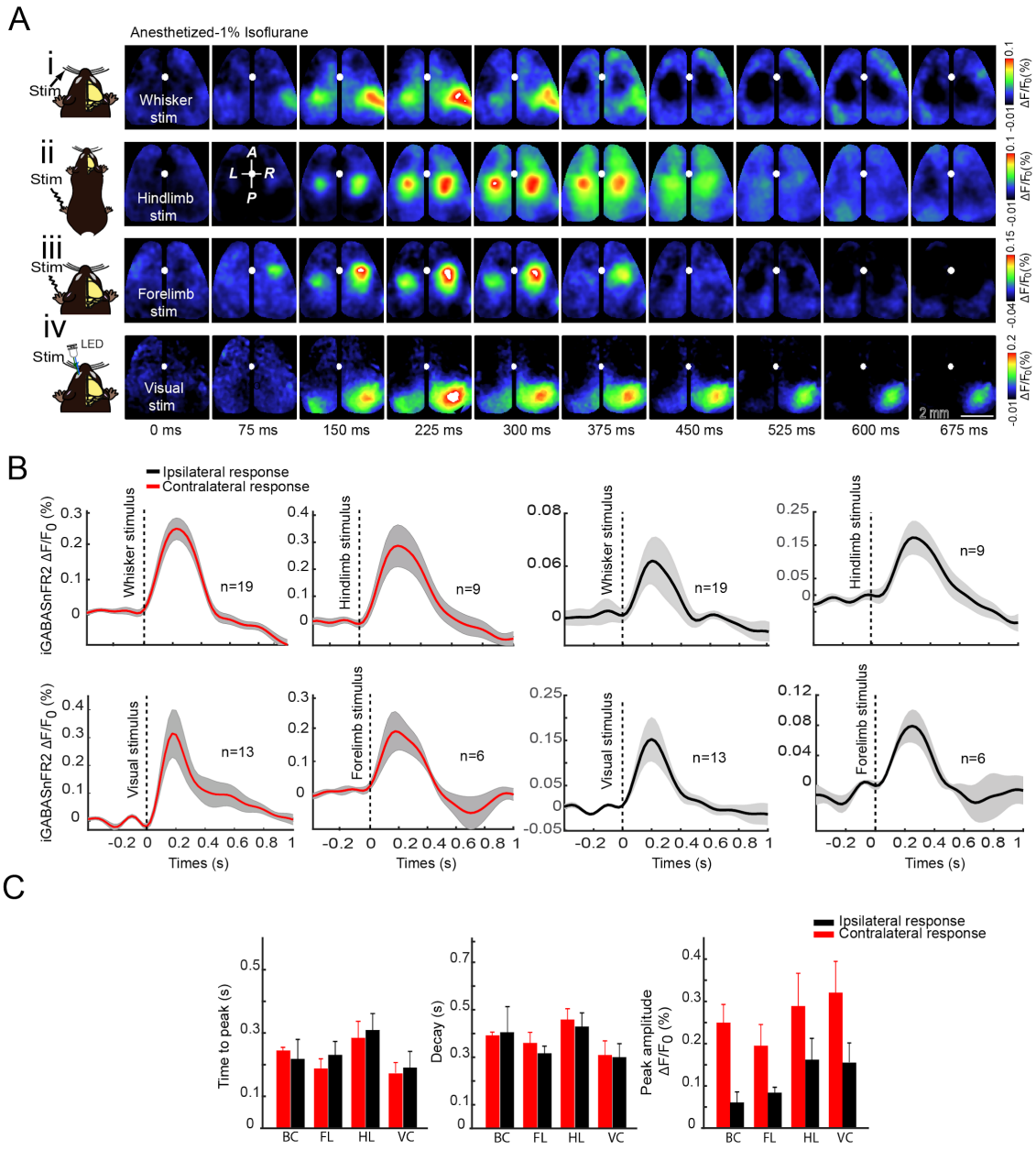


**Fig. 2 Sensory-evoked GABAergic responses in the neocortex measured by iGABASnFR2 imaging.** (a) Montages of the wide bilateral craniotomy, with bregma marked by a white circle. Cortical GABAergic activation patterns are shown in a mouse anesthetized with isoflurane (1%) following (i) whisker stimulation (300 ms), (ii) hindlimb stimulation (300 ms), (iii) forelimb stimulation (300 ms), and (iv) visual stimulation (20 ms) of the eye using an LED. Sensory-evoked extracellular GABA signals were detected using the iGABASnFR2 sensor. Activation is observed within 50- to 375-ms post-primary sensory cortex activation. Responses represent an average of 40 trials. The second image in the second row indicates anterior (A), posterior (P), medial (M), and lateral (L) directions. (b) Time series of sensory-evoked GABA responses. The time series of GABA responses for each sensory stimulation was measured from the respective primary sensory regions. Contralateral responses are shown in red, and ipsilateral responses are shown in black.

Data are presented as mean ± SEM, with responses extracted from 3 X 3-pixel ROI (~40; 401 μm2), n = number of animals. (c) Summary of sensory-evoked GABA response features. Decay time (ms), peak amplitude (ΔF⁄F), and time to peak (ms) for contralateral and ipsilateral responses. Data are shown as mean ± SEM, with contralateral responses in red and ipsilateral responses in black.
A significant region X laterality interaction was found for time to peak (p = 0.0055), indicating lateralization effects vary across sensory regions (Video 1, avi, 12.7 MB [URL: https://doi.org/10.1117/1.NPH.XX.XX.XXXXXX.s1];Video 2, avi, 12.9 MB [URL: https://doi.org/10.1117/1.NPH.XX.XX.XXXXXX.s2];Video 3, avi, 13.3 MB [URL: https://doi.org/10.1117/1.NPH.XX.XX.XXXXXX.s3];Video 4, avi,13.6 MB [URL: https://doi.org/10.1117/1.NPH.XX.XX.XXXXXX.s4]).

Specifically, the contralateral visual cortex exhibited the highest peak amplitude, followed by hindlimb, whisker, and forelimb cortices, whereas ipsilateral responses were generally weaker and slower. To quantify these differences, I extracted response features including decay time, time to peak, and peak amplitude across all sensory regions [Fig. 2(c)]. A two-way analysis of variance (ANOVA) revealed significant main effects of sensory region on all three measures of inhibitory response dynamics. Time to peak (p= 0.0092), decay time (p= 0.0006), and peak amplitude (p= 0.0011) all varied significantly across sensory regions, indicating region-specific characteristics of GABAergic inhibition. Laterality (ipsilateral versus contralateral) had a significant main effect only on peak amplitude ($p < 0.0001$), with contralateral responses consistently showing higher amplitudes. No significant effects of laterality were observed for time to peak (p= 0.35) or decay time (p= 0.77). Furthermore, there were no significant interactions between region and laterality for any of the three metrics (time to peak: p= 0.22, decay: p=0.83, and peak amplitude: p=0.78), suggesting that hemispheric differences in GABAergic inhibition were consistent across modalities and not dependent on specific sensory regions.

To confirm that these delayed signals were specific to GABAergic dynamics and not artifacts of hemodynamics or sensor excitation, I used cpSFGFP-expressing mice under identical imaging conditions as a negative control. As shown in Fig. S2 in the Supplementary Material, cpSFGFP mice showed no significant sensory-evoked or spontaneous fluorescence changes, confirming that the iGABASnFR2 signals reflect GABAergic activity. Auditory stimulation under anesthesia evoked clear iGABASnFR2 responses in the auditory cortex (Fig. S3 in the Supplementary Material), further validating sensor specificity. To assess cortical coordination during sensory processing, I performed seed-pixel correlation analysis across 10 anatomically defined cortical regions.

This revealed structured and modality-specific inhibitory networks, with the strongest intrahemispheric connectivity observed contralateral to the stimulus (Fig. S4 in the Supplementary Material). Across sensory modalities—including whisker (Video 1), hindlimb (Video 2), forelimb (Video 3), and visual (Video 4) stimulation—sensory input activates thalamocortical projections targeting layer 4 of the primary sensory cortices, leading to early excitatory responses (Petersen, 2007; Ridder and Nusinowitz, 2006).These are primarily mediated by excitatory neurons and refined by fast feedforward inhibition from parvalbumin (PV)-expressing interneurons (Gabernet et al., 2005 ; Isaacson and Scanziani, 2011).Subsequently, a delayed GABAergic response emerges, largely driven by somatostatin (SST)-expressing interneurons providing feedback inhibition to modulate dendritic activity and maintain cortical stability (Urban-Ciecko and Barth, 2016; Muñoz et al., 2017; Gentet et al., 2012). This response is consistently stronger and earlier in the contralateral hemisphere, which receives direct thalamic input, whereas the ipsilateral hemisphere exhibits a weaker and more delayed GABAergic response, likely due to slower callosal transmission and reduced excitatory drive (Ferezou et al., 2007; Minamisawa et al., 2018).Together, these results demonstrate that sensory-evoked GABA dynamics follow a consistent temporal structure across modalities and hemispheres and confirm that iGABASnFR2 reliably detects extracellular GABA responses with spatiotemporal precision across cortical regions, establishing its utility for mesoscale mapping of inhibitory dynamics.

### 2.3.3 Sensory-Evoked and Spontaneous GABA Activity in Quiet Wakefulness Resembles Anesthesia-Induced Patterns

Cortical brain states vary across behavioural conditions, shaping spontaneous activity and sensory processing. During active behaviour, such as locomotion or whisking, cortical activity becomes desynchronized, and inhibition is modulated to refine sensory gain (Pakan et al., 2016; Gentet et al., 2010; Keller and Mrsic-Flogel, 2018).In contrast, during quiet wakefulness and under light anesthesia, neuronal activity is dominated by slow, synchronized fluctuations that reflect reduced arousal and a shift toward global inhibitory tone (Muñoz et al., 2017; McGinley et al., 2015) .Although previous studies have shown that GABAergic interneurons contribute significantly to these state dependent dynamics, (Chen et al., 2012; Pfeffer et al., 2013) it remains unclear whether the spatiotemporal profile of extracellular GABA during quiet wakefulness

resembles that observed under anesthesia. To examine whether GABAergic responses to sensory stimulation and spontaneous activity in quiet awake mice exhibit spatiotemporal dynamics like those observed under anesthesia, I performed wide-field imaging of the cortex using the iGABASnFR2 sensor. Head-fixed mice were imaged in both quiet wakefulness and anesthetized states, the latter induced by 1% isoflurane. EMG recordings from a neck muscle electrode, along with video monitoring of body and whisker movement, were used to classify behavioural state [Fig. 3(a)]. Power spectral analysis of EMG signals confirmed a reduction in muscle tone under anesthesia compared with the quiet awake state.

I recorded cortical GABA signals evoked by contralateral visual or whisker stimulation, averaging responses across 40 trials for each condition [Fig. 3(b)]. Both anesthetized and quiet awake states showed robust stimulus-evoked increases in extracellular GABA in primary sensory areas, including the primary visual cortex (VISp), anterior visual area (VISa), BC, and primary motor cortex (M1). In Fig. 3(b)i, which shows cortical GABA responses to visual stimulation, the quiet awake state is characterized by an earlier onset and more widespread GABA release across the visual cortex. In contrast, under anesthesia, the GABA signal appears later and is more spatially restricted. Similarly, in Fig. 3(b)ii, following whisker stimulation, the quiet awake state shows strong and broad activation of the contralateral BC and associated motor areas (M1). This response is both faster and more spatially extensive than in the anesthetized state. To assess how GABAergic responses vary across brain states, I analyzed their temporal dynamics during visual and whisker stimulation [Fig. 3(c)]. Responses were stronger and more spatially distinct during quiet wakefulness than under anesthesia—VISp > VISa for visual input and BC > M1 for whisker input. Quantitative analysis [Fig. 3(d)] confirmed significantly higher peak amplitudes and longer decay times in the awake state. Time to peak was generally shorter in the awake state, suggesting faster inhibitory onset, though most differences were not statistically significant. However, BC in wakefulness responded significantly faster than M1 under anesthesia. Decay times were longer under anesthesia, especially in BC, suggesting more prolonged inhibition when cortical activity is suppressed. These results highlight the influence of both brain state and region on the strength and timing of GABAergic responses.

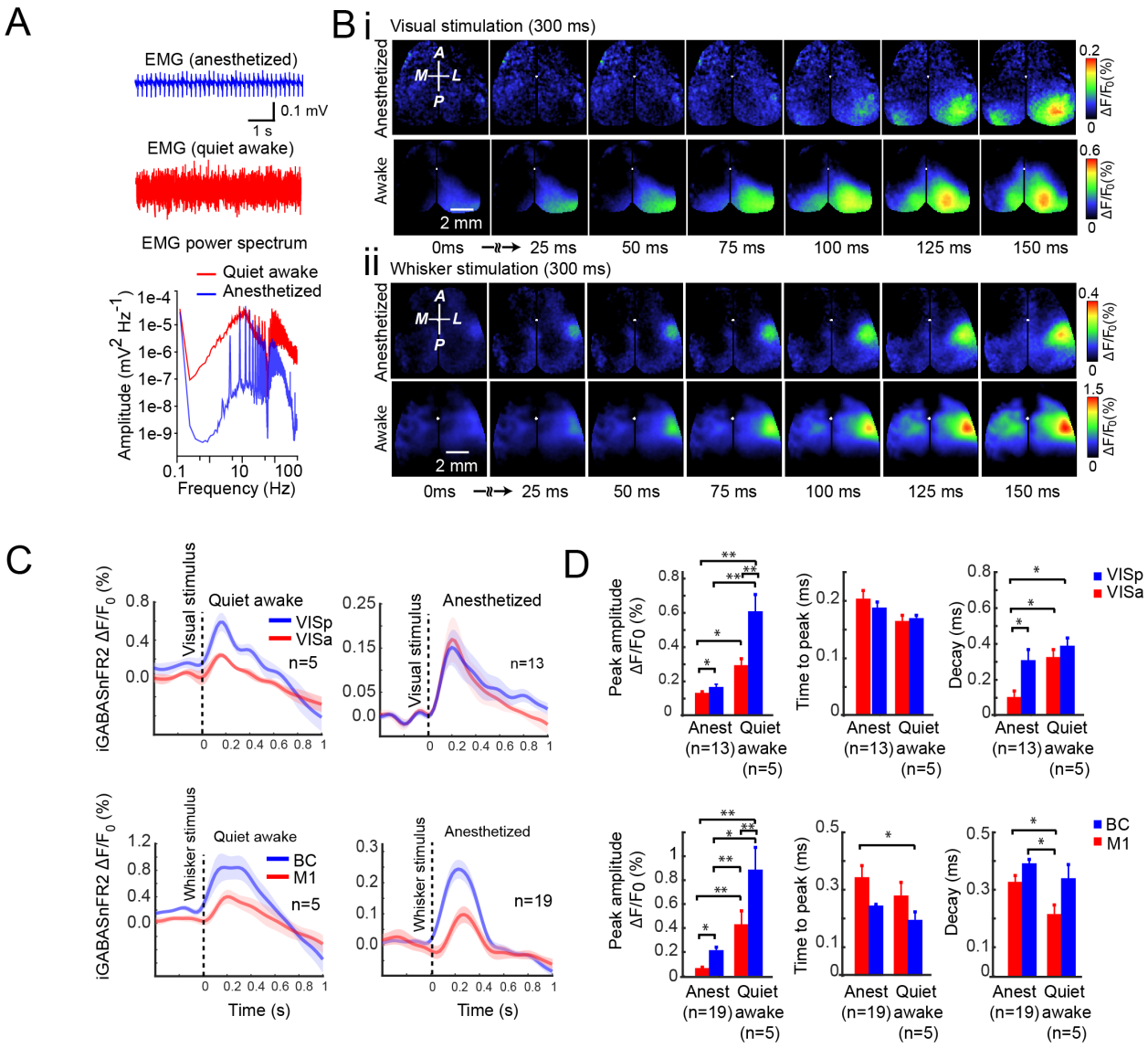


**Fig. 3 Sensory-evoked and spontaneous GABA activity in quiet wakefulness resembles patterns observed under anesthesia.** (a) Individual example of neck muscle EMG (>1 Hz) from a head restrained mouse under isoflurane (1%) anesthesia (top trace) and quite awake (bottom trace). The power spectra of the EMG signals differ between states of anesthesia (blue) and wakefulness (red). (b) Representative cortical GABA signals are taken from the iGABASnFR2 sensor in response to contralateral visual or whisker stimulation during anesthesia or in quiet awake states. The images represent an average of 40 trials of stimulation. (c) Quantification of GABA signals in response to sensory stimulation under anesthesia and quiet wakefulness. Plots show averaged responses from 3 X 3-pixel ROIs (~0.04 mm2) within VISp (blue) and VISa (red) for visual stimulation and BC (blue) and M1 (red) for whisker stimulation (Ciii and Civ). Shaded areas represent SEM. (d) Statistical comparison of peak amplitude, time to peak, and decay time of GABA responses across states. $P < 0.05$, $P < 0.01$, one-way ANOVA. Error bars indicate SEM.

### 2.3.4 Mesoscale Imaging of Cortical GABA Dynamics During Natural Sleep and Wakefulness

Although many studies have explored cortical dynamics across sleep and wake states using electrophysiological methods and excitatory activity sensors (Dash et al., 2009; Nazari et al., 2023; Karimi Abadchi et al., 2023), the ability to track inhibitory signaling at mesoscale resolution across natural brain states remains limited. To further assess iGABASnFR2 performance across different brain states, I examined cortical GABA dynamics during quiet wakefulness, NREM sleep, and REM sleep. Mesoscale iGABASnFR2 imaging was combined with simultaneous hippocampal LFP and EMG recordings in head-fixed mice. Animals were allowed to transition naturally among vigilance states while cortical GABA levels were monitored [Figs. 4(a)–4(c)]. GABA signals were highest during wakefulness and reduced during NREM sleep [Fig. 4(d)]. Spectral analysis showed a reduction in low-frequency GABA fluctuations during REM compared with both wakefulness and NREM [Fig. 4(e)], suggesting diminished slow GABA oscillations during REM sleep.

To further assess the spatial coordination of cortical GABA activity, I computed pairwise correlation maps across the cortex during each brain state over multiple days. As shown in [Fig. 4(f)], cortical GABA signals exhibited strong bilateral synchrony during quiet wakefulness, which was markedly reduced during NREM sleep and only moderately diminished during REM. This pattern is evident in interhemispheric correlation heatmaps [Fig. 4(f)], where NREM shows the most substantial decrease in bilateral synchrony, whereas REM correlations remain relatively higher. Quantitative analysis confirmed that the mean interhemispheric correlation values were lower during NREM sleep compared with both wakefulness and REM [Fig. 4(g)]. During transitions from REM to wakefulness, I observed a sharp increase in cortical GABA levels [Fig. 4(h)]. This transition was accompanied by a broad re-engagement of cortical GABAergic activity across multiple regions [Fig. 4(i)], suggesting rapid reinstatement of the GABA response upon arousal from REM sleep. A detailed overview of the motion-based and electrophysiological features used for behavioural state classification is provided in Fig. S5 in the Supplementary Material, which illustrates the temporal alignment of whisker pad and nose motion, EMG power, body motion, theta-to-delta ratio, and hippocampal LFP signals across NREM and REM sleep transitions. Together, these findings demonstrate that iGABASnFR2 reliably captures spontaneous, brain state-dependent fluctuations in extracellular GABA with high temporal and

spatial resolutions. It supports its utility for long-term mesoscale imaging of cortical inhibition under natural physiological conditions.

### 2.3.5 Intracortical Long-Range GABAergic Correlations Revealed by Seed-Pixel Analysis Across Brain States

To assess the organization of spontaneous extracellular GABA dynamics in the cortex, I used seed-pixel correlation mapping of iGABASnFR2 fluorescence to investigate intracortical long-range connectivity across different brain states. By placing seed pixels in primary sensory regions, I generated correlation maps of spontaneous GABA dynamics across awake, NREM, and REM sleep states [Fig. 5(a)]. In the awake state, these maps revealed strong bilateral synchrony and widespread long-range connectivity among distant cortical regions. These spatial patterns of functional connectivity closely resemble those previously observed with excitatory signals using iGluSnFR and Ca2. imaging, suggesting that spontaneous GABA activity also reflects underlying anatomical connectivity and shared network drive. During NREM sleep, seed-pixel correlations were reduced, indicating a decoupling of large-scale inhibitory networks consistent with cortical slow-wave activity. In contrast, REM sleep preserved many of the bilateral and local connections seen in wakefulness, although with moderate reductions in correlation strength. I further quantified interhemispheric connectivity using pairwise correlation matrices of bilateral cortical regions [Fig. 5(b)]. These patterns, consistently captured using iGABASnFR2, highlight the sensor's sensitivity to state-dependent fluctuations in extracellular GABA and its utility for mapping mesoscale inhibitory networks in vivo.

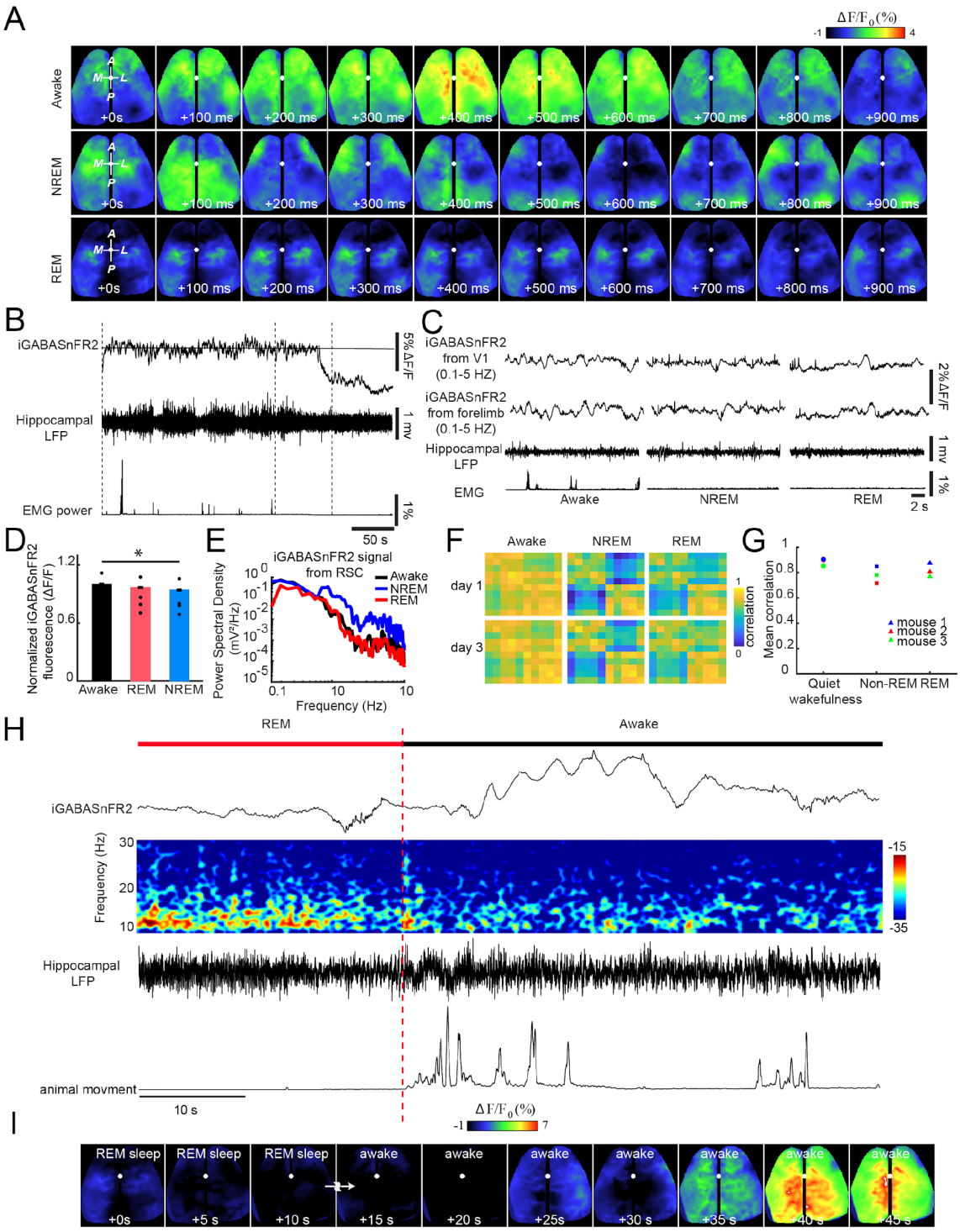


**Fig. 4 Combined electrophysiological recording and mesoscale iGABASnFR2 imaging of GABA activity during wakefulness and sleep.** Spatiotemporal dynamics of GABA activity over a 1-s period during wakefulness, NREM, and REM sleep. Scale bar, 2 mm. (b) Representative traces of GABA activity [retrosplenial cortex (RSC)], hippocampal LFP, and EMG power during wakefulness, NREM, and REM sleep in a head-fixed mouse. Baseline fluorescence (Fo) was

calculated as the mean signal over the recording session. (c) Expanded view of GABA activity, LFP, and EMG power corresponding to the time windows in panel (b). (d) Group mean normalized GABA signal across wakefulness, NREM, and REM sleep (n . 5 mice, Kruskal–Wallis test with Nemenyi post hoc correction; P . 0.003 overall, all pairwise comparisons significant at $P < 0.05$) (e) Spectral power of GABA signal in RSC across wakefulness, NREM, and REM sleep. (f) Cortical GABA activity correlation maps across quiet wakefulness, NREM, and REM sleep over two recording days. (g) Mean interhemispheric correlation of cortical GABA activity across wakefulness, NREM, and REM sleep (n . 3 mice). The mean correlation among units significantly increased from quiet wakefulness to NREM and REM sleep across all mice ($P < 0.05$, repeated measures ANOVA with Bonferroni-corrected paired t-tests). (h) Simultaneous recordings of cortical GABA signals, hippocampal LFP spectrogram, and EMG power during a REM-to-wakefulness transition. (i) Time-lapse montage showing cortical GABA dynamics during the REM-to-wake transition shown in (H). Scale bar: 2 mm.

### 2.3.6 Tiagabine Elevates Baseline GABA Levels but Dampens Sensory-Evoked Responses and Reorganizes Cortical Inhibitory Connectivity

To examine how pharmacological inhibition of GABA reuptake influences cortical GABA dynamics, I administered tiagabine—a selective GAT-1 inhibitor (Dalby, 2000) —under 1% isoflurane anesthesia and monitored extracellular GABA levels using iGABASnFR2. Mice were head-fixed throughout the experiment. I first recorded visually evoked GABA responses (∼6 min), followed by a ∼15- min baseline period of spontaneous activity. Although the mouse remained head-fixed, tiagabine was injected intraperitoneally. Spontaneous activity was then recorded for another ∼15 min before delivering a second round of visual stimulation to assess post-tiagabine responses. Before tiagabine injection, visual stimulation evoked robust and spatially localized increases in GABA signals within the contralateral primary visual cortex [Fig. 6(a)i]. Following tiagabine administration, the same sensory stimulus failed to evoke any detectable response [Fig. 6(a)ii]. This complete loss of evoked GABA activity is also evident in the time-series traces [Fig. 6(a)iii]. These recordings were acquired at 150 Hz using the blue fluorescence channel under continuous (non-strobing) illumination. To better understand this loss of evoked responsiveness, I analyzed spontaneous GABA activity using dual-wavelength strobing imaging (40 Hz blue and 40 Hz green). In the primary visual cortex, the raw blue fluorescence signal, averaged across six animals, showed a sustained elevation (Fink-Jensen et al., 1992; Wu et al., 2001) in baseline GABA levels following tiagabine

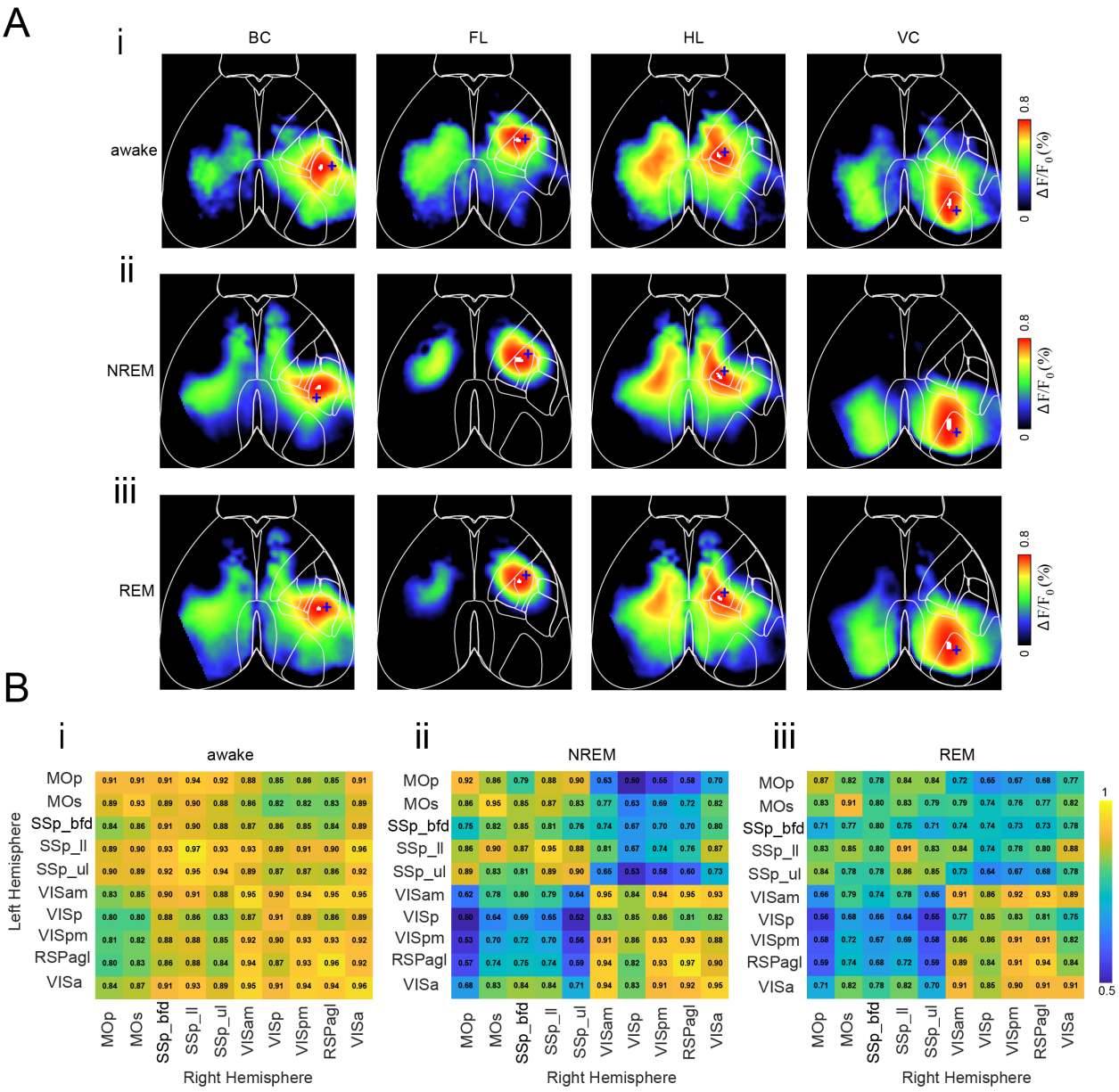


**Fig. 5 Brain state–dependent patterns of extracellular GABA dynamics measured by iGABASnFR2.** (a) Seed-pixel correlation maps (0.1 to 5Hz) of spontaneous iGABASnFR2 fluorescence across brain states. (i) Awake, (ii) NREM sleep, and (iii) REM sleep. Correlation maps are shown for seed regions in the BC, FL cortex, HL cortex, and VC. (b) Interhemispheric correlation matrices of spontaneous extracellular GABA signals across brain states. (i) Awake, (ii) NREM sleep, and (iii) REM sleep. Matrices display Pearson correlation coefficients among bilateral cortical regions based on iGABASnFR2 fluorescence. Regions include the following: Mop, primary motor area; MOs, secondary motor area; SSp_bfd, primary somatosensory area (barrel field); SSp_ll, lower limb; SSp_ul, upper limb; VISam, anteromedial visual area; VISp, primary visual area; VISpm, posteromedial visual area; RSPagl, agranular retrosplenial area; VISa, anterior visual area. Widespread interhemispheric connectivity is observed during wakefulness

and REM sleep, with reduced correlations during NREM sleep. Blue crosses indicate the location of the seed pixel used for correlation mapping. Number of animals = 5.

injection [Fig. 6(b)i], consistent with extracellular GABA accumulation due to GAT-1 blockade. Reflectance signal from the same region also increased post-injection [Fig. 6(b)ii], confirming the overall signal elevation. Quantitative analysis revealed that tiagabine significantly increased the duration, frequency, and peak amplitude of spontaneous GABA transients across animals [Fig. 6(b)iii], reflecting heightened inhibitory tone. To assess how elevated GABA levels affect network organization, I performed seed-pixel correlation analysis (0.1 to 5 Hz) of spontaneous iGABASnFR2 activity. Following tiagabine injection, seed regions in sensory cortices showed increased local synchrony and expanded spatial correlation patterns [Fig. 6(c)]. Interhemispheric correlation matrices also revealed stronger bilateral connectivity, particularly among homologous sensory areas [Fig. 6(d)]. These results further validate the ability of iGABASnFR2 to detect changes in extracellular GABA levels under both baseline and stimulated conditions, highlighting its sensitivity to dynamic alterations in cortical inhibition and its potential utility in pharmacological studies targeting GABAergic signaling.

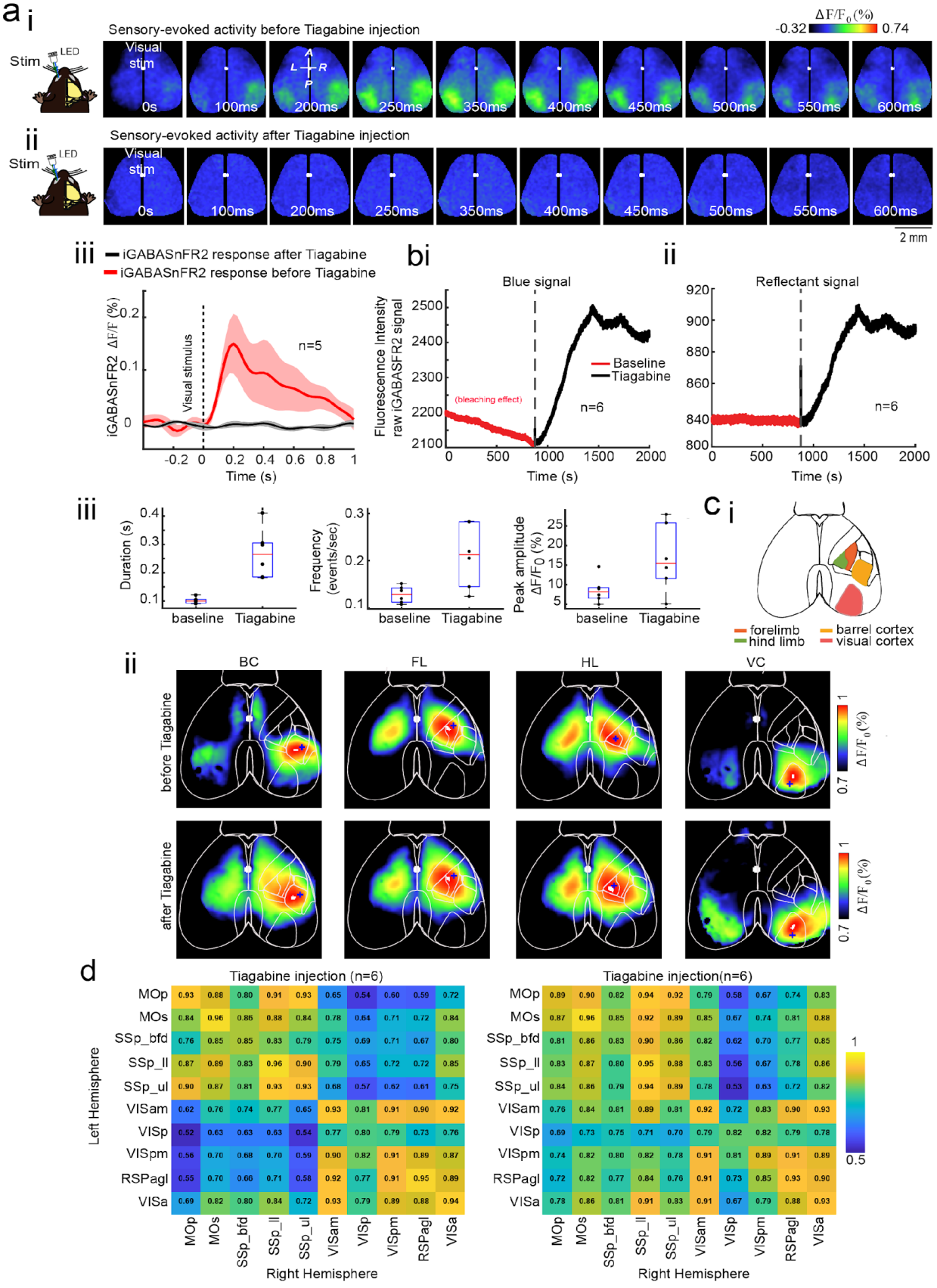
a i
Sensory-evoked activity before Tiagabine injection
ΔF/F0(%)
-0.32
0.74
Stim
LED
Visual stim
0s
100ms
200ms
250ms
350ms
400ms
450ms
500ms
550ms
600ms
ii
Sensory-evoked activity after Tiagabine injection
2 mm
iii
iGABASnFR2 response after Tiagabine
iGABASnFR2 response before Tiagabine
iGABASnFR2 ΔF/F (%)
Visual stimulus
n=5
Time (s)
bi
Blue signal
Fluorescence Intensity raw iGABASFR2 signal
(bleaching effect)
Baseline
Tiagabine
n=6
Time (s)
ii
Reflectant signal
n=6
Time (s)
iii
Duration (s)
Frequency (events/sec)
Peak amplitude ΔF/F0 (%)
baseline
Tiagabine
c i
forelimb
hind limb
barrel cortex
visual cortex
ii
BC
FL
HL
VC
before Tiagabine
after Tiagabine
ΔF/F0(%)
d
Tiagabine injection (n=6)
Tiagabine injection(n=6)
Left Hemisphere
Right Hemisphere
MOp
MOs
SSp_bfd
SSp_ll
SSp_ul
VISam
VISp
VISpm
RSPagl
VISa

**Fig. 6 Effect of tiagabine administration on extracellular GABA activity in mice expressing iGABASnFR2.** (a) Sensory-evoked GABA responses recorded with the blue channel (iGABASnFR2) at 150 Hz under continuous illumination (no strobing). (i) Representative montages of visually evoked GABAergic activity before tiagabine administration. (ii) The same stimulation after tiagabine injection. (iii) Time series of contralateral visually evoked iGABASnFR2 signals from the VISp. Traces represent mean ± SEM from five animals, extracted from 3 X 3 pixel ROIs (~0.04 mm2). (b) Tiagabine-induced changes in spontaneous GABA activity in VISp, recorded using dual-channel strobing acquisition (80 Hz total: 40 Hz blue and 40 Hz green). (i) Blue fluorescence signal (iGABASnFR2) from VISp, averaged across 6 animals. Traces show signal before (red) and after (black) tiagabine injection. The red trace shows a photobleaching trend; the black trace shows increased fluorescence post-injection. (ii) Reflectance signal from the same VISp region, averaged across six animals. (iii) Quantification of spontaneous iGABASnFR2 transients in VISp before and after tiagabine injection. Box plots show duration (left), frequency (middle), and peak amplitude (right) of fluorescence transients. Data represent mean ± SEM across six animals (n . 6). Tiagabine significantly increased the duration, frequency, and amplitude of spontaneous GABAergic transients compared with baseline. Statistical comparisons were made using paired t -tests; all changes were significant ($p < 0.05$). (c) Functional connectivity of spontaneous iGABASnFR2 activity, recorded with dual-channel strobing (40 Hz blue and 40 Hz green). (i) Schematic of cortical ROIs used for seed-pixel correlation analysis: barrel cortex (orange), forelimb (red), hind limb (green), and visual cortex (brown) (ii) Seed-pixel correlation maps (0.1 to 5 Hz) before and after tiagabine injection. Blue asterisks indicate seed pixel locations in the selected ROIs. (d) Interhemispheric correlation matrices of spontaneous iGABASnFR2 activity before and after tiagabine injection (n . 6 mice), showing enhanced bilateral cortical connectivity post-injection. Regions: Mop, primary motor area; MOs, secondary motor area; SSp_bfd, primary somatosensory area (barrel field); SSp_ll, lower limb; SSp_ul, upper limb; VISam, anteromedial visual area; VISp, primary visual area; VISpm, posteromedial visual area; RSPagl, agranular retrosplenial area; VISa, anterior visual area. The interior is at the top of all maps. Blue crosses indicate the location of the seed pixel used for correlation mapping.

## 2.4 Discussion

I used mesoscale imaging with the genetically encoded GABA sensor iGABASnFR2 to map the spatiotemporal dynamics of extracellular GABA across the intact mouse cortex in vivo. By characterizing extracellular GABA dynamics in both sensory-evoked and spontaneous across brain states—including anesthesia, quiet wakefulness, NREM, and REM sleep—I provide, for the first time, a comprehensive mesoscale imaging of GABA dynamics in the cortex. My results establish iGABASnFR2 as a valuable tool for investigating GABAergic tone and state-dependent fluctuations in extracellular GABA, complementing previous studies that used iGluSnFR and voltage-sensitive dyes to map excitatory signaling and depolarization across largescale cortical networks. The robust and state-dependent changes in extracellular GABA was observed—during

sensory stimulation, spontaneous activity, and pharmacological manipulation—demonstrate that inhibitory tone is dynamically regulated across brain states and cortical regions.

### 2.4.1 Interpreting iGABASnFR2 Signals

iGABASnFR2 fluorescence changes are likely shaped by a combination of GABA release from interneurons, diffusion through the extracellular space, and clearance by GABA transporters, particularly GAT-1 (Scimemi, 2014).The timing of sensory-evoked responses—characterized by a delayed onset (∼75 ms) and prolonged signal lasting several 100 ms—is consistent with the dynamics of SST-positive interneuron-mediated inhibition, which is known to follow the rapid activation of PV+ interneurons (Gabernet et al., 2005; Muñoz et al., 2017).The prolonged decay phase of iGABASnFR2 signals [Fig. 2(c)] suggests that extracellular GABA may persist longer, potentially contributing to modulatory or volume transmission effects (Farrant & Nusser, 2005).

### 2.4.2 Cortical GABA Responses to Sensory Input Are Conserved Across Brain States

Sensory-evoked results revealed robust, modality-specific patterns of extracellular GABA activation across the cortex, reflecting both localized responses and broader, network-level dynamics [Fig. 2(a)]. Each stimulus modality selectively activated its corresponding primary sensory area [Fig. 2(b)], with activity spreading from the focal point of stimulation to more distal, functionally connected cortical regions. This widespread response pattern suggests that inhibitory activity can propagate across large-scale networks, challenging the traditional view of inhibition as strictly local. In our study, contralateral responses were consistently stronger and faster than ipsilateral responses, likely reflecting direct thalamocortical projections to the primary sensory cortex. In contrast, the delayed and weaker ipsilateral responses are consistent with slower callosal transmission and interhemispheric integration [Figs. 2(b)–2(c)], as reported in previous studies of cortical sensory processing (Ferezou et al., 2007). In addition, despite the differences in global cortical state and arousal, sensory-evoked GABAergic responses were consistently observed across brain states, suggesting a preserved functional role of inhibition, even as response strength and timing are modulated [Figs. 3(b)–3(d)]. This robustness underscores the reliability of iGABASnFR2 for monitoring inhibitory dynamics and reflects the essential role of inhibition in

stabilizing excitation and regulating cortical gain, as also supported by prior calcium imaging studies in awake animals (Pakan et al., 2016).

### 2.4.3 Spontaneous GABA Dynamics Reveal State-Dependent Connectivity

In our study, interhemispheric GABA synchrony was lowest during NREM sleep [Figs. 4(d)-4(g)], suggesting that inhibition in this state becomes locally structured and functionally decoupled across hemispheres. REM sleep [Figs. 4(d)-4(g)] showed partial recovery of interhemispheric GABA synchrony, suggesting a reorganization of inhibitory networks distinct from both wakefulness and NREM. This contrasts with vascular-based findings; for instance, a study (Turner et al., 2020) reported strong bilateral hemodynamic coherence during both NREM and REM, reflecting broader, non-specific signals. However, they also noted that neurovascular signals integrate contributions from neurons, astrocytes, and metabolism, potentially decoupling them from electrophysiological activity. Our direct measurement of extracellular GABA provides a distinct view, revealing that strong vascular synchrony during NREM does not imply coordinated inhibitory signaling. Indeed, the low GABA synchrony I observe during NREM contrasts with the high bilateral (HbT) coherence reported by Turner et al., (Turner et al., 2020) highlighting a dissociation between vascular and inhibitory network dynamics. Similar patterns have been observed in BOLD fMRI studies, which report reduced largescale connectivity during NREMand partial restoration during REM (Horovitz et al., 2009; Larson-Prior et al., 2009; Tagliazucchi & Laufs, 2014).These converging lines of evidence highlight arousal state as a key factor in shaping both vascular and neural network dynamics and emphasize the central, yet state-specific, role of inhibition in large-scale brain coordination during sleep.

### 2.4.4 Functional Inhibitory Architecture Aligns with Cortical Structural Organization

Seed-pixel correlation results revealed structured long-range inhibitory connectivity [Fig. 5(a)]. In the awake state, I observed strong bilateral synchrony between homologous sensory areas and strong local correlations within modalities [Figs. 5(a)i and 5(b)i]. These maps are similar to those derived from excitatory indicators, including iGluSnFR and VSD (Xie et al., 2016; Mohajerani et al., 2013) supporting the view that inhibitory and excitatory networks are functionally integrated, but exhibit distinct temporal dynamics. In NREM sleep, long-range inhibitory connectivity

weakened, suggesting a shift toward localized processing [Figs. 5(a)ii and 5(b)ii] while REM sleep partially restored [Figs. 5(a)iii and 5(b)iii]. State-dependent changes highlight the flexibility of cortical inhibitory networks, which adapt dynamically to behavioural states, promoting broad coordination during wakefulness and preserving localized stability during sleep (Niethard et al., 2017)

### 2.4.5 Tiagabine Elevates Extracellular GABA and Disrupts Sensory-Evoked Responses via Altered Cortical Synchrony

Our data show that tiagabine disrupts sensory-evoked GABAergic responses by elevating extracellular GABA and altering cortical network dynamics. Before injection, visual stimulation produced robust, spatially confined increases in GABA sensor signals in the visual cortex [Fig. 6(a)]. After tiagabine administration, however, the same stimulus no longer evoked detectable GABA responses—despite a sustained increase in baseline fluorescence [Fig. 6(b)i], confirming that the sensor remained active. Although not used for quantification, an increase in green reflectance signal [Fig. 6(b)ii] suggested broader changes in cortical vascular or metabolic state. The absence of evoked activity in the presence of elevated GABA points to a non-linear relationship between inhibitory tone and sensory responsiveness. This may involve excessive tonic inhibition, desynchronized interneuron networks, or saturation of GABAergic circuits. In our study, tiagabine-induced increases in extracellular GABA were clearly detected by iGABASnFR2, with fluorescence peaking around 10 min post-injection—consistent with prior micro dialysis reports (Johansson et al., 1992). This elevation likely enhanced tonic inhibition via extrasynaptic GABA_A receptors, (Semyanov et al., 2004) reducing neuronal excitability and suppressing phasic, stimulus-driven responses. This mechanism helps explain the loss of stimulus-locked GABA transients. Similar effects have been observed in rodent EEG studies, where tiagabine increases low-frequency synchronization and, at higher doses, induces hypersynchronous activity resembling absence seizures—likely a result of widespread tonic inhibition (Lancel et al., 2009)

Our results align with these findings and demonstrate that iGABASnFR2 effectively detects sustained changes in extracellular GABA. However, the loss of evoked transients following tiagabine suggests the sensor may reach a functional ceiling under conditions of high ambient GABA, limiting its dynamic range. Though tiagabine does not directly cause transporter reversal,

elevated intracellular GABA and transporter saturation could still favor non-vesicular GABA release,67 further amplifying tonic signaling. Together, these findings highlight both the strengths and limitations of iGABASnFR2: it is sensitive to pharmacologically induced increases in extracellular GABA but may underestimate fast, transient responses when tonic levels are elevated. This underscores the importance of considering inhibitory tone and network state when interpreting GABA imaging data.

### 2.5 Conclusion

Our findings establish iGABASnFR2 as a robust sensor for wide-field imaging of extracellular GABA in the cortex, revealing both strong stimulus-locked responses and state-dependent dynamics. Our experiments show that inhibition is not merely local or reactive but is organized into large-scale motifs that shift with arousal state and can be pharmacologically tuned. For a long time, efforts to understand how excitation and inhibition interact across the cortex have been limited by the lack of tools that can monitor both processes in real time—especially in awake, behaving animals. That is now changing. Genetically encoded sensors such as iGABASnFR2, along with glutamate and calcium indicators, offer a new opportunity to resolve the dynamic interplay between excitatory and inhibitory signaling across cortical networks with high spatiotemporal precision.

Importantly, the development of red-shifted glutamate sensors, such as R-iGluSnFR, (Wu et al., 2018) now makes it possible to image GABA and glutamate simultaneously, opening the door to more complete views of circuit function in vivo. This capability will be essential for understanding how the Excitatory–inhibitory dynamics is regulated during normal brain function and how it becomes disrupted in neurological and psychiatric disorders. Many neurological and psychiatric disorders—such as epilepsy, autism, and schizophrenia—involve disruptions in Excitation–inhibition interaction. Simultaneous imaging of glutamate and GABA now enables researchers to observe how excitation and inhibition interact across space and time; how this interaction is modulated by behavioural state, neuromodulators, or genetic risk factors; and how it breaks down in coordinated excitation–inhibition dynamics and keep neural activity within a functional operating range in disease.

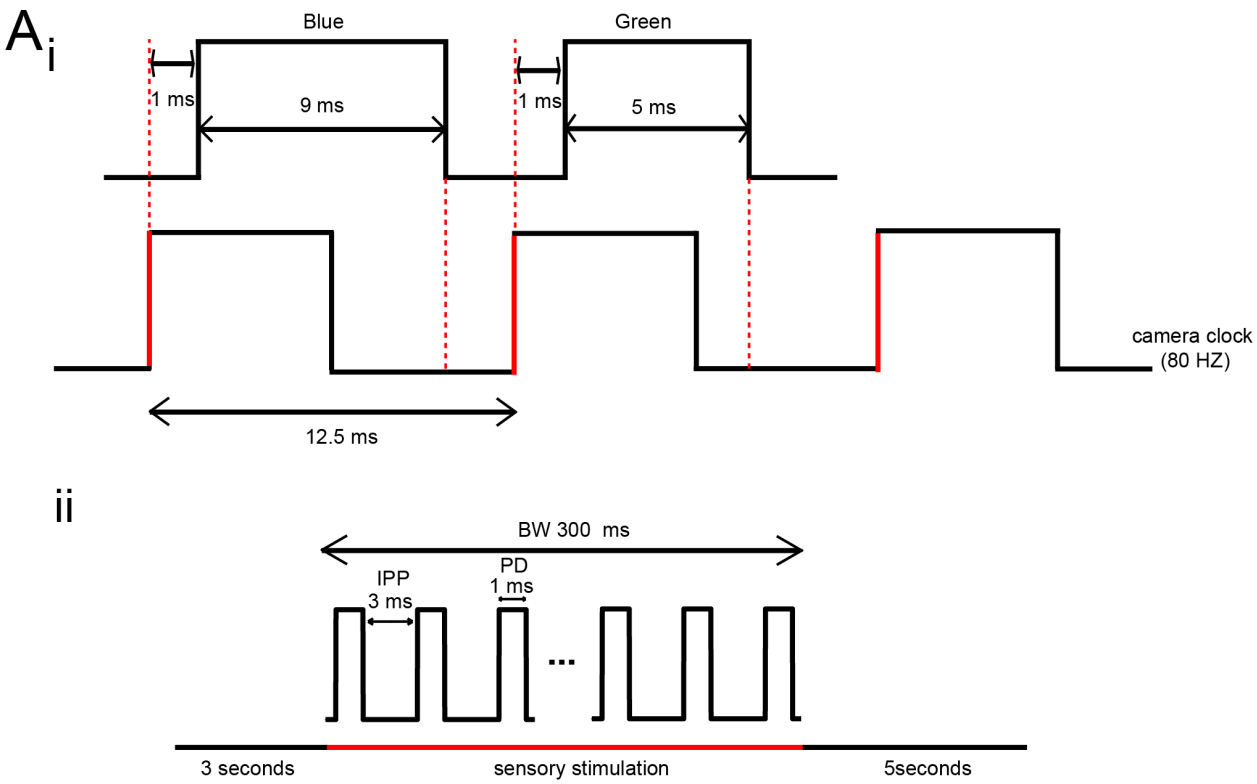


**Supplementary Figure 1. A. Imaging acquisition timing and sensory stimulation protocol.** (i) Diagram illustrating the timing of LED illumination and camera acquisition during dual-channel wide-field imaging at 80 Hz. Top, the timing of blue and green LED activation. Each TTL rising edge (red vertical lines) triggers an imaging frame. After a 1 ms delay, either the blue LED (9 ms ON) or green LED (5 ms ON) is activated, alternating every frame. This design ensures only one LED is active during each ~11 ms camera exposure, preventing spectral contamination. Bottom, the camera clock traces at 80 Hz. Each square pulse represents one frame, with a duration of 12.5 ms, matching the TTL trigger frequency. (ii) Timing diagram of the sensory stimulation protocol. Each trial includes an 8-second acquisition period, with 80 Hz imaging throughout. A piezoelectric actuator delivers mechanical stimulation between 3 and 3.3 seconds in the form of a burst (BW = 300 ms) of pulses (PD = 1 ms) spaced by a 3 ms inter-pulse period (IPP). A total of 40 trials were performed per condition.

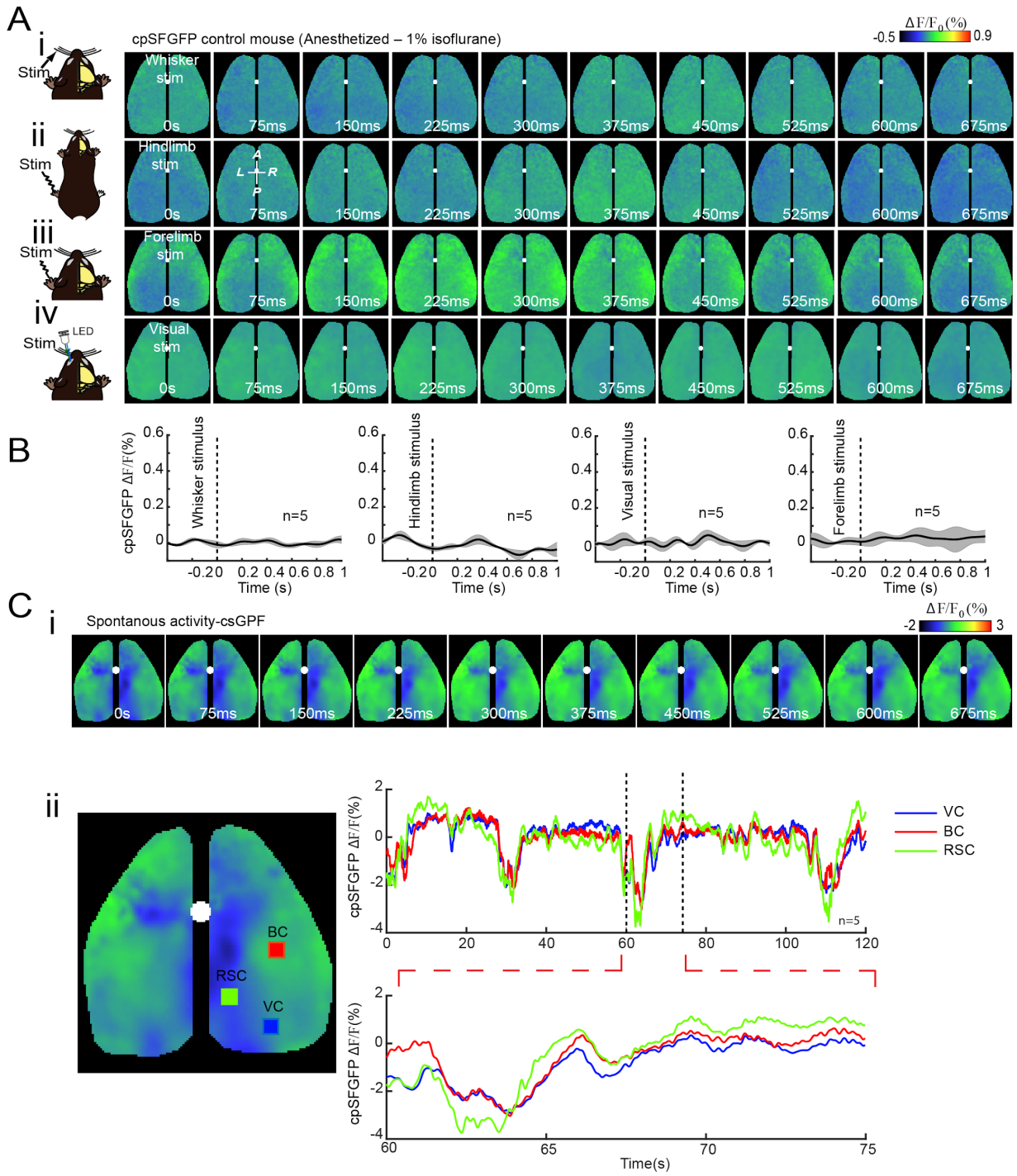


**Supplementary Figure 2. Sensory-evoked and spontaneous cortical responses under anesthesia using cpSFGFP as a control for iGABASnFR2.** (A) Montages showing cortical activation patterns in a mouse anesthetized with 1% isoflurane. A white circle marks Bregma. Sensory-evoked responses are shown for: (i) contralateral whisker (C2) stimulation, (ii) contralateral hindlimb stimulation, (iii) contralateral forelimb stimulation, and (iv) visual stimulation of the contralateral eye using an LED. Sensory responses emerge within 50–375 ms following stimulation, with activation localized to the primary sensory cortex (white arrows). Each

response is averaged over 40 trials. The second frame in the second row indicates anterior (A), posterior (P), medial (M), and lateral (L) orientations. (B) Time course plots of ΔF/F (%) for cpSFGFP signals in response to whisker (i), hindlimb (ii), forelimb (iii), and visual (iv) stimulation. Traces represent mean ± SEM from 3 × 3-pixel ROIs (~0.04 mm²); *n* indicates the number of animals. (C) Spontaneous cortical activity measured with cpSFGFP under isoflurane anesthesia. (i) Representative montages showing spontaneous cortical dynamics over time. (ii) Map showing selected ROIs in the right barrel cortex (red), visual cortex (blue), and retrosplenial cortex (orange). Time series plot (top right) displays spontaneous fluorescence fluctuations across 120 seconds. A magnified 15-second window is shown below for detail. Imaging was performed using dual-channel (blue and green) acquisition at 80 Hz.

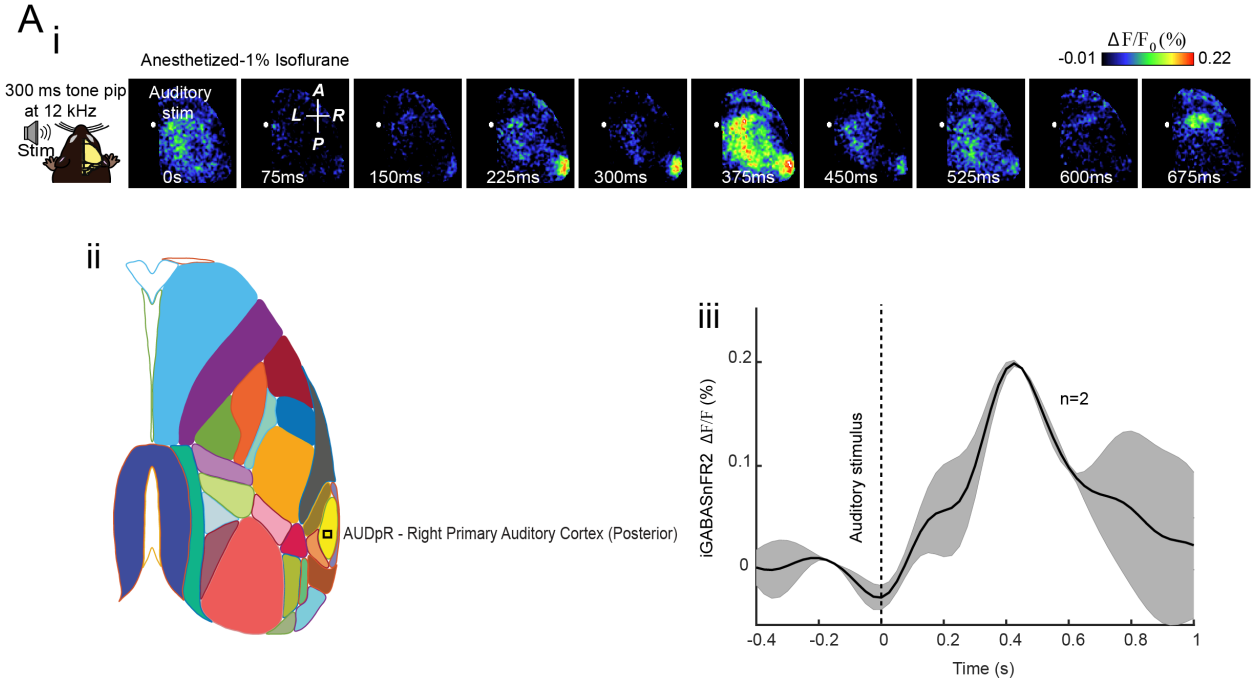


**Supplementary Figure 3. Auditory-evoked cortical GABA responses under anesthesia measured with iGABASnFR2.** (A) GABAergic activity in response to auditory stimulation in mice anesthetized with 1.1% isoflurane. (i) Representative montages show changes in iGABASnFR2 fluorescence following auditory stimulation (300 ms). Responses represent an average of 40 trials. The second image in the second row indicates anterior (A), posterior (P), medial (M), and lateral (L) directions. (ii) Time course of ΔF/F (%) from the contralateral auditory cortex, averaged across two animals. Data represent mean ± SEM from 3 × 3-pixel regions of interest (~0.04 mm²). The dashed vertical line marks the time of auditory stimulus onset (0 s).

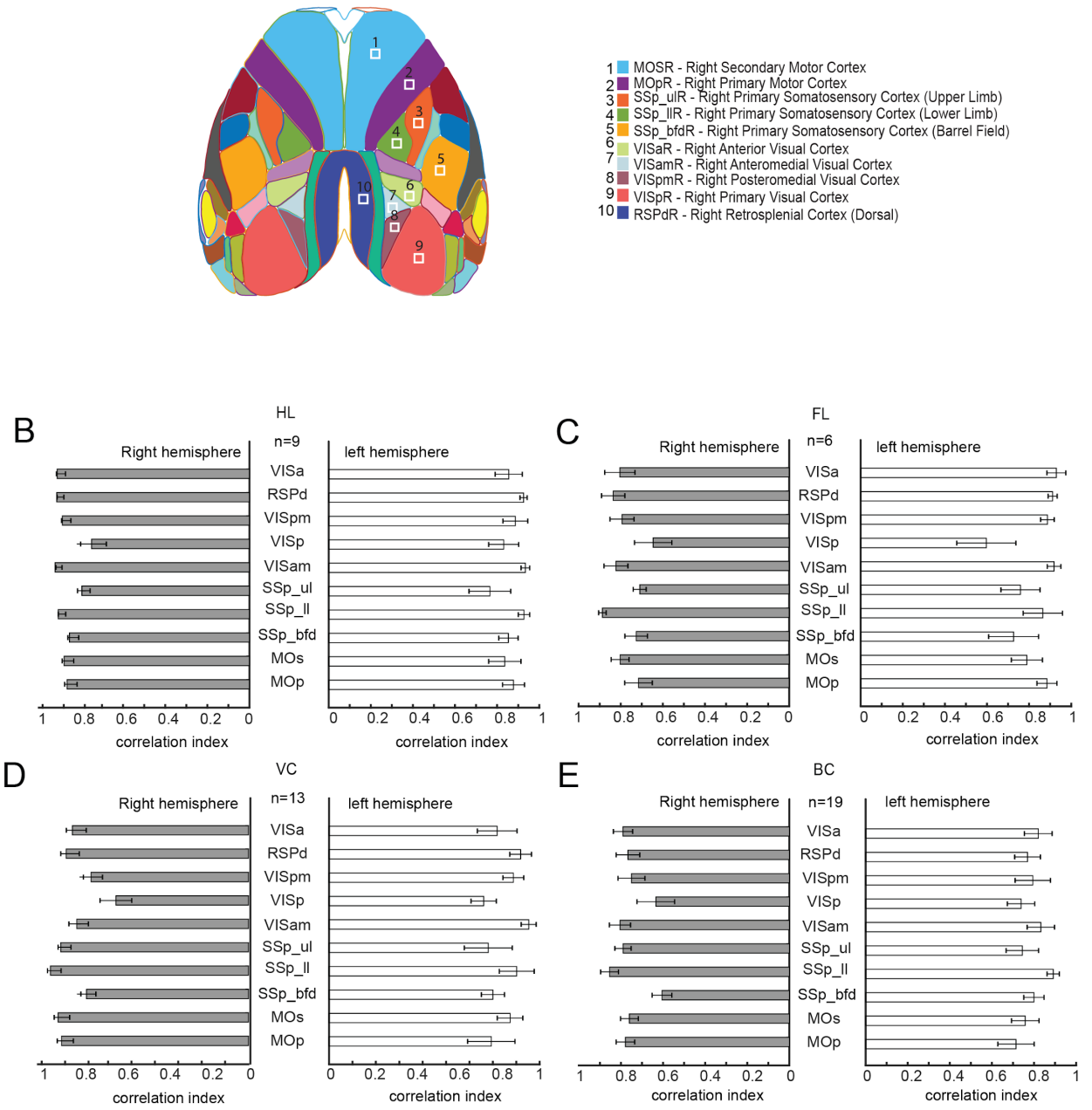


**Supplementary Figure 4. Intrahemispheric connectivity: Region-based comparison of sensory-evoked response**(A) Schematic of the right hemisphere showing the 10 cortical regions of interest (ROIs) used for intrahemispheric correlation analysis: 1) MOp – Primary motor cortex, 2) MOs – Secondary motor cortex, 3) SSp_bfd – Primary somatosensory area, barrel field, 4) SSp_ll – Primary somatosensory area, lower limb, 5) SSp_ul – Primary somatosensory area, upper limb, 6) VISam – Anteromedial visual area, 7) VISp – Primary visual area (V1), 8) VISpm – Posteromedial visual area, 9) RSPagl – Retrosplenial area, lateral agranular part, 10) VISa – Anterior visual area. To assess intrahemispheric connectivity, we calculated Pearson's correlation coefficients between the iGABASnFR2 signal from each primary sensory ROI and the 10 target

ROIs, based on 3 × 3-pixel regions of interest (~0.04 mm²). These analyses were performed separately for the right and left hemispheres during sensory-evoked conditions. (B–E) Bar plots display the pairwise correlation indices for the hindlimb (HL), forelimb (FL), visual cortex (VC), and barrel cortex (BC), respectively. **Statistical analysis:** Paired two-tailed *t*-tests were used to compare the correlation indices between the right and left hemispheres for each ROI. Bonferroni correction was applied to adjust for multiple comparisons across 10 ROIs. In addition, a two-way repeated-measures analysis of variance (ANOVA) was performed using a linear mixed-effects model with the fixed effects of (the right vs left hemispheres), *ROI*, and the *Condition* × *ROI* interaction. The degrees of freedom for marginal tests were computed using the residual method. **Hindlimb (HL, B):** No significant differences between the right and left hemispheres were observed (all Bonferroni-corrected $p > 0.05$). The ANOVA revealed a significant main effect of ROI ($F(9,158) = 2.19$, $p = 0.025$), but no main effect of between hemispheres ($F(1,158) = 0.045$, $p = 0.83$) or interaction ($F(9,158) = 0.50$, $p = 0.87$). **Forelimb (FL, C):** A trend toward reduced correlation in MOp in right hemispheres was observed ($t = –4.21$, uncorrected $p = 0.0135$, Bonferroni $p = 0.1355$), although not significant after correction. The ANOVA showed a significant main effect between hemispheres ($F(1,80) = 4.88$, $p = 0.030$), a trend for ROI ($F(9,80) = 1.79$, $p = 0.083$), and no significant interaction ($F(9,80) = 0.87$, $p = 0.55$). **Visual cortex (VC, D):** VISpm showed a trend toward decreased correlation in the right hemispheres ($t = –2.31$, $p = 0.0380$, Bonferroni $p = 0.3804$), with no other significant comparisons. The ANOVA revealed a significant main effect of ROI ($F(9,256) = 2.66$, $p = 0.0057$), but no significant main effect of between hemispheres ($F(1,256) = 2.17$, $p = 0.14$) or interaction ($F(9,256) = 1.48$, $p = 0.16$). **Barrel cortex (BC, E):** No statistically significant differences were found between the left and right hemispheres after correction (all Bonferroni $p > 0.05$), though SSp_bfd showed a trend ($t = –2.13$, $p = 0.0663$, Bonferroni $p = 0.6634$). The ANOVA indicated a significant main effect of ROI ($F(9,224) = 2.08$, $p = 0.032$), with no effect between hemispheres ($F(1,224) = 0.73$, $p = 0.39$) or interaction ($F(9,224) = 0.85$, $p = 0.58$). These results suggest that overall intrahemispheric GABAergic correlation patterns are largely stable across spontaneous and evoked conditions, with subtle region-specific modulations.

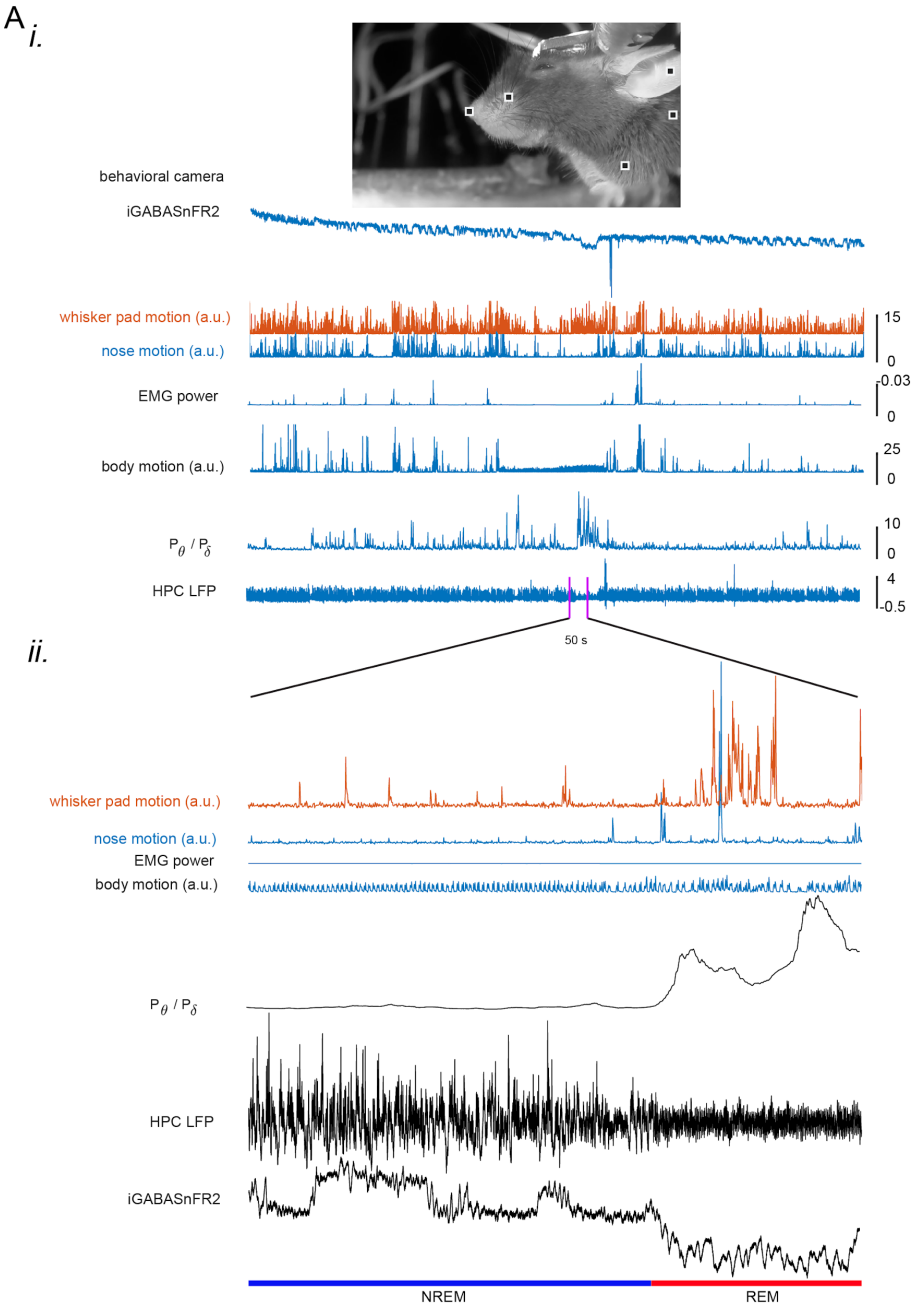


**Supplementary Figure 5. Motion signal, hippocampal LFP activity, and EMG power for sleep scoring in a head-fixed mouse.** Panel (i) presents a time-series analysis integrating motion and electrophysiological signals used for sleep scoring. The top schematic shows a spatial map of the mouse's head with rectangular regions of interest used to extract motion signals. The plots below display (from top to bottom): raw (non-preprocessed) iGABASnFR2 fluorescence, whisker pad and nose motion signals (z-scored) recorded at 25 Hz using a behavioural camera, EMG power indicating muscle activity, body motion (z-scored) representing gross movements, the theta-to-delta power ratio (Pθ/Pδ) derived from hippocampal local field potentials (LFPs) to differentiate NREM and REM sleep, and the raw hippocampal LFP signal reflecting underlying neural dynamics. Panel (ii) provides a magnified 50-second segment of the data shown in panel (i),

offering a detailed view of whisker pad and nose motion, EMG power, body motion, theta-to-delta ratio, raw hippocampal LFP signal and raw (non-preprocessed) iGABASnFR2 signal. The highlighted segment captures transitions between NREM and REM sleep, demonstrating how motion and neural signals align with behavioural state changes.

## Chapter 3

## Cortical GABAergic inhibition dynamics around hippocampal sharp-wave ripples


### Abstract

Cortical inhibition, mediated by GABA, is essential in balancing excitation and modulating neural processing, but it is unclear to what extent inhibitory dynamics are responsive to internally generated hippocampal activity, such as sharp-wave ripples (SWRs). Employing widefield imaging of extracellular GABA with iGABASnFR2 and hippocampal recordings, I characterized cortical inhibition during sleep–awake states first. Around SWRs, inhibition was state- and region-specific: during NREM, medial cortices (e.g., retrosplenial) increased GABA before SWRs, whereas sensory areas in the lateral cortices decreased it; during wake, GABA increased in lateral cortices after SWRs. These findings reveal that cortical inhibition is not static and ubiquitous but instead is dynamically characterized by brain state, orchestrating the flow of hippocampal outputs to the rest of the cortex. Inhibitory modulation, as our data reveal, forms a mechanism allowing selective gating of memory-related activity during wakefulness and sleep.

## 3.1 Introduction

Cortical function emerges from the coordinated interaction between excitation and inhibition that together determines the dynamics of neural circuits and behavioural (Isaacson and Scanziani, 2011). Excitatory neurons generate most cortical output and communicate long distance between brain regions. This excitatory flow must be tightly regulated to ensure stable network activity, accurate information processing, and adaptive behavioural output (Haider & McCormick , 2009). GABAergic interneurons, which comprise approximately 20–30% of cortical neurons, regulating circuit excitability, shaping neuronal response, and organizing rhythmic network activity. Cortical GABAergic interneurons are broadly classified into three major subtypes based on molecular expression: parvalbumin-positive (PV+), somatostatin-positive (SST+), and vasoactive intestinal peptide–positive (VIP+) interneurons. PV+ interneurons primarily target the perisomatic region of pyramidal neurons and exhibit fast-spiking firing properties, enabling them to provide powerful feedforward and feedback inhibition and to synchronize network activity. PV+ interneurons rapidly suppress pyramidal cell firing and generating gamma-frequency oscillations. SST+ interneurons, in contrast, inhibit distal dendrites of pyramidal neurons and provide feedback inhibition that regulates dendritic integration of top-down and long-range inputs. VIP+ interneurons inhibit other interneurons, particularly SST+ cells, thereby recruiting disinhibitory circuits that sustain pyramidal neuron output during behavioural states such as attention and changes in arousal (Isaacson & Scanziani, 2011; Markram et al., 2004; Rudy et al., 2011). GABAergic interneurons shape synaptic plasticity, tune excitatory drive, and synchronize communication across distributed cortical networks (Tremblay et al., 2016). The coordination between excitation and inhibition dynamically varies with behavioural state, including sleep, wakefulness, attention, and locomotion (McGinley et al., 2015). Disruption of GABAergic interneurons has been implicated in a broad spectrum of neuropsychiatric disorders, including epilepsy, autism spectrum disorder, and schizophrenia (Marín, 2012).

Recent studies have started to answer this question by describing excitatory cortical activity in response to hippocampal SWRs. A study using genetically encoded glutamate sensors indicated that cortical excitatory activity was strongly modulated by SWRs in a state-dependent manner. Karimi Abadchi et al. (Karimi Abadchi et al., 2020; Karimi Abadchi et al., 2023) demonstrated

that, during NREM sleep, the SWRs precede a period of suppression in the whole cortex that is followed by sequential activation originating in medial and in visual cortices, areas involved in the default mode system. During quiet wakefulness, however, SWRs are followed by robust suppression in agranular retrosplenial cortex, with late rebound in cortical glutamatergic activity. These studies demonstrate that SWRs have organized and state-specific excitatory patterns of excitation as their outcome. Cortical computation, however, is almost never regulated by excitation in isolation. Since excitatory drive is generally followed or accompanied by inhibition (Isaacson & Scanziani, 2011; Tremblay et al., 2016), the state-dependent patterns of excitation during SWRs thus inevitably bring to the forefront the question of the corresponding inhibitory patterns. Thus, to this point, whereas excitatory responses have been accurately described, the inhibitory aspect of the cortical responses to SWRs has remained uninvestigated. It is important to know how it is that GABAergic inhibition plays its part in this process, since the generation of the timing, spread, and functional significance of the cortical activation is controlled by the regulatory action of the inhibition mechanisms.

Here, I attempt to fill this gap; in the process, I employ wide-field imaging of extracellular GABA using iGABASnFR2 (Marvin et al., 2019), in combination with hippocampal electrophysiology, with the sensor expressed predominantly in cortical excitatory neurons, to track GABAergic dynamics in the dorsal cortex during different states of the brain such as NREM, REM, and wake. This approach tracks changes in extracellular GABA, which serve as an index of the GABAergic inhibitory milieu surrounding these neurons rather than a direct measure of postsynaptic inhibitory currents. Extracellular GABA primarily originates from synaptic release (Glykys & Mody, 2007) but it can also include contributions from non-synaptic sources such as astrocytic release (Kozlov et al., 2006). Moreover, the functional impact of GABA depends on state-dependent chloride gradients (Alfonsa et al., 2023). I therefore interpret the iGABASnFR2 signal as reflecting GABAergic signaling dynamics rather than absolute synaptic inhibition. I first establish the baseline by describing the spontaneous cortical GABA transients during these states, against which to gauge state-dependent GABAergic inhibition. I then inquired whether SWRs shape cortical GABAergic inhibition in time- as opposed to space-ordered patterns, as one would expect should hippocampal memory-related activity be selectively modulated by distributed inhibitory processes. Emphasizing the inhibitory aspect of the cortical response to SWRs, our study attempts to reveal a level of cortico-hippocampal organization that exists but moves beyond the level of the excitatory to the level of the inhibitory circuits that defines the flow of information across the brain.

## 3. 2 Materials and methods

### 3.2.1 Animals and experimental conditions

I employed eight adult (>2 months) EMX-Cre female and male mice of the C57BL/6J strain for imaging studies. For studying natural sleep, EMX-Cre mice were injected intracranially with AAV vectors in a Cre-dependent manner to drive the expression of the genetically encoded GABA sensor iGABASnFR2 in neocortical and hippocampal excitatory neurons. This enabled optical reporting of extracellular GABA in excitatory cortical circuits. Strong expression of iGABASnFR2 in targeted brain areas was validated through brain sectioning analysis as outlined in our previous publication (Rezaei et al., 2025). Mice were group-housed (two to five mice) under a 12-hour light-dark cycle and had ad libitum access to water and a standard laboratory mouse diet. For sleep recording studies, mice were singly housed after head-plate and electrode implantation surgery. All animal studies were approved by the University of Lethbridge Animal Care Committee and adhered to the Canadian Council for Animal Care guidelines.

### 3.2.2 Viral constructs and retro-orbital injection procedure

To enable selective detection of extracellular GABA dynamics in excitatory cortical circuits, I used EMX-Cre transgenic mice, in which Cre recombinase is primarily expressed in excitatory pyramidal neurons of the neocortex and hippocampus. This allowed for Cre-dependent expression of genetically encoded sensors specifically in those neurons. Two AAV vectors were used: AAV2/PHP.N-Syn-flex-iGABASnFR2, encoding the Cre-dependent GABA sensor, and AAV2/PHP.N-Syn-flex-cpSFGFP, a non-sensing cytosolic GFP control. Both constructs were obtained from the Canadian Neurophotonics Platform Viral Vector Core (RRID: SCR_016477) and purified to a final concentration of $1.5 \times 10^{13}$ genome copies per milliliter (GC $mL^{-1}$). Retro-orbital injections (Yardeni et al., 2011) outline systemic delivery using the PHP.N capsid (Chan et al., 2017). The animals were anesthetized using isoflurane (maintained at 1.5–2%), and Metacam (5 mg/kg) was given by subcutaneous. One drop of 0.5% proparacaine hydrochloride ophthalmic anesthetic was instilled prior to injection. The 30-gauge needle was inserted at an angle of 30° into the medial canthus, and $1.4 \times 10^{11}$ GC of the viral vector was delivered into the retro-orbital sinus.

iGABASnFR2 has a secretion signal (IgG kappa) and a transmembrane domain (from PDGFR). Combined those two sits target it to the plasma membrane, facing out. Without those, it will be expressed in the cytosol, and in theory could be used to detect cytosolic GABA. This method allowed widespread brain expression of iGABASnFR2 in excitatory neurons for the optical detection of extracellular GABA in mesoscale imaging studies. In addition to neuronal synaptic release, astrocytes are known to contribute to extracellular GABA via non-vesicular release mechanisms that generate tonic inhibition. Therefore, the iGABASnFR2 signal likely reflects the combined contribution of neuronal and glial sources of extracellular GABA.

### 3.2.3 Surgical procedure and electrophysiological recording setup

The animals were given buprenorphine (0.05–0.1 mg/kg, subcutaneously) 30 minutes prior to surgery, and then isoflurane (1–2% oxygen) was administered via a nose cone. The scalp was shaved and sterilized, and the skull was covered with C&B Metabond (Parkell, Inc.), to which a custom-designed headplate was attached over the skull. A 12-mm glass coverslip (Carolina Biological Supply, Cat. No. 633005) was then cemented to establish a chronic cranial window to image at the mesoscale. The LFP recordings were obtained through teflon-coated 50 µm stainless steel wires (A-M Systems) implanted for electrophysiology. A bipolar electrode was positioned in the right hippocampus through craniotomy at approximately 2.6 mm laterally from the midline, tangent to the posterior edge of the occipital suture. The electrode was advanced at a 57° angle relative to vertical while monitoring neural signals both visually and audibly. Once optimal signal quality was achieved, the electrode was fixed in place using Krazy Glue and C&B Metabond. In addition, a bipolar EMG electrode was implanted in the nuchal muscles to record muscle tone. LFP signals from hippocampal electrode was amplified (×1,000), bandpass filtered (0.1–10,000 Hz) using a Grass A.C. pre-amplifier (Model P511, Artisan Technology Group), and digitized at 20 kHz using a Digidata 1440 acquisition system (Molecular Devices Inc.).

### 3.2.4 Habituation for head-restraint sleep and wakefulness experiments

They were then gradually introduced to the recording device after 14 days of recovery by positioning the animals on the recording platform. The first step consisted of letting the animals get to the platform and adapt to the environment. On subsequent days, having settled, they were

positioned on head restraint in step increases in the period of head fixation, initiated at five minutes during the first day and incremented in five-minute increases to a period of one hour total.

### 3.2.5 GABA imaging during wakefulness

Following the habituation, every animal was recorded every three days, with three to four sessions being done on each mouse. The recording was always done at the same time of the day to reduce variability and stress. Finally, the animals were put back into their home cages in the housing pod, where they rested and recovered before the subsequent recording.

### 3.2.6 GABA imaging during natural sleep

Sleep recordings were performed after the completion of all wakefulness sessions. To optimize conditions for natural sleep under head restraint, the day before recording, the animals were moved from their home cage in the colony room to a separate room at noon. Sleep was restricted to ~6 hours by gently stimulating the mice with a cotton-tip stick whenever they showed signs of drowsiness. The animals were then transferred to a larger cage containing new objects, such as a running wheel, Cheerios, and a water container, and left in surgical recovery where the temperature was controlled. The next day, the animals were transferred to the imaging room, and sleep recordings began at ~7:00 AM. Once recording finished, the animals were returned to their home cages in the podding room and allowed to sleep freely for at least three days before repeating the procedure for another recording.

### 3.2.7 GABA imaging

Imaging was undertaken with a custom macroscope comprising a front-to-front video lens setup, 8.6 × 8.6 mm field of view. The focal plane was set ~0.5–1 mm below the cortical surface. Fluorescence signals were recorded with a 12-bit CCD camera (1M60 Pantera, Dalsa, Waterloo, ON) attached to an EPIX E8 frame grabber and operated by XCAP 3.8 software (EPIX, Inc., Buffalo Grove, IL), imaging at a frame rate of 80 Hz. Imaging parameters have been used in previous studies, including voltage-sensitive dye imaging (Mohajerani et al., 2013; Vanni &

Murphy, 2014; Silasi et al., 2016). Sequential illumination was provided using alternating blue (473 nm) and green (530 nm) LEDs (Thorlabs) (Xiao et al., 2021). Blue light (473 nm, filtered through a 467–499 nm bandpass) was employed to excite the iGABASnFR2 indicator, and green light (530 nm, filtered through a 527/42 nm bandpass) for intrinsic signal imaging of blood volume. A bandpass emission filter was placed in front of the CCD camera to facilitate selective detection of either fluorescence or reflectance signals. Blue and green light-emitting diodes (LEDs) were used as illumination sources. They were alternatively synchronized and frame-by-frame, utilizing transistor–transitor logic (TTL) triggering, to offer temporal control precisely so as to interleave acquisitions of reflectance and fluorescence images at 40 Hz per channel. Reflectance images, which may be used for corrections of blood artifacts (Kramer & Levitan, 1979; Ma et al., 2016; Scott et al., 2018), were analyzed as well within our current pipeline.

### 3.2.8 Preprocessing

Image data were transferred into MATLAB; blue and green frames were differentiated based on reference frames to set up illumination origins. Only the region of interest (ROI) was selected utilizing a binary mask. Slow baseline drifts were eliminated utilizing a local detrending algorithm, based on a filter of the Chebyshev type. The ratio of $\Delta F/F_0$ was normalized to the fluorescence signals (F) based on the following formula: $\Delta F/F_0 = (F - F_0) / F_0 \times 100$, where the detrended, curve provided an estimate of $F_0$. To filter out high frequency noise, a low-pass finite impulse response (FIR) filter, utilizing a 6 Hz cut-off, was used on the time series of $\Delta F/F_0$. Hemodynamic artifacts in the blue channel were corrected by linear regression, using the green reflectance signal as a regressor. To denoise the data further, singular value decomposition (SVD) was applied to the corrected blue channel, and the first 300 components were used for reconstruction.

### 3.2.9 Sleep scoring

Motion data were obtained from behaviour camera (frame rate = 25HZ) by the FaceMap (Syeda et al., 2024), which computes frame-to-frame pixel intensity differences in manually defined regions of interest (ROIs). Five ROIs—nose, whisker pad, ear, shoulder, and trunk—were selected to monitor both subtle facial expressions and body movement. Motion signals were time-locked to electrophysiological recordings. Wakefulness in this study was identified by clear motor activity

in video recordings and high EMG amplitude. NREM sleep was determined by decreased EMG tone, low hippocampal theta-to-delta power ratio, and the occurrence of large irregular activity in the hippocampal LFP. REM sleep was characterized by EMG suppression, sustained hippocampal theta oscillations, and high theta-to-delta ratios.

### 3.2.10 SWR detection

SWRs were determined based on a modified Karimi Abadchi et al. (Karimi Abadchi et al., 2020) protocol. The raw LFP signals of the hippocampus were initially down-sampled at 2 kHz and band-filtered between 110 to 250 Hz (ripple band) on a real-valued MATLAB (MathWorks) Morlet wavelet. The ripple-band signal was then rectified and smoothed. screened SWRs were detected when ripple power crossed above a threshold set as the mean plus a multiple of the standard deviation of the baseline. The multiplier was set for each animal to compensate for inter-individual differences in signal quality. Onset and offset times were set using a second threshold of 75% of the detection threshold. To further refine event detection, only those SWRs with an appropriate duration were kept. For each event window, event center was defined as the time of the greatest negative deflection (trough) of the ripple-band sound. Events within 50 ms of an event were grouped into one SWR.

### 3.2.11 Normalization of peri-SWR neocortical activity using Z-scoring

To normalize peri-SWR neocortical GABA activity, random timestamps were created by shuffling of the inter-SWR intervals within individual recording sessions. Imaging stacks 0.5 seconds before and 0.5 seconds after the timestamp were sampled and time-aligned for each random event. Averaging peri-event stacks across all random timestamps were then calculated to compute a baseline mean stack, as well as a parallel SD stack for standard deviation. These mean and SD stacks served as references to z-score normalization. The peri-SWR imaging stacks were then all normalized by subtraction of the baseline mean stack and division by the SD stack on a pixel-by-pixel basis to provide a z-scored representation of neocortical activity.

### 3.2.12 Statistical Analysis

All statistical analyses were conducted using built-in functions in MATLAB.

### 3.2.13 Data availability

All data and custom software/algorithms necessary to interpret and replicate the findings and methods of this article are available upon request.

## 3.3 Results

### 3.3.1 Experimental protocol for investigating neocortical GABA dynamics

I retro-orbitally injected AAV2/PHP.N-Syn-Flex-iGABASnFR2 or control construct (cpSFGFP) into animals (see Figure 1A). The configuration of our recording involved mesoscale GABA imaging, in-vivo electrophysiological recordings, and monitoring of behaviour (see Figure 1B). Protocols of imaging were conducted at 80 Hz cycling blue (470 nm) and green (530 nm) LEDs alternating with a CCD camera. LFPs were recorded from the right dorsal CA1 to study hippocampal sharp-wave ripples (SWRs), with neck EMG and a camera for monitoring behaviour.A schematic of the headplate placement and the 17 cortical regions imaged in the right hemisphere is shown in **Figure 1Ci–ii**. Example cortical images are shown in Figure **1Ciii–iv**, with the dorsal retrosplenial cortex (dRSC) marked as a representative region of interest (ROI). To correct for hemodynamic artifacts, GABA fluorescence signals were normalized to simultaneously recorded reflectance traces (**Figure 1Cv–vi**). Frames of images were registered to the center of SWR activity (see Figure 1Di), averaged and concatenated into single peri-ripple montages (see Figure 1Di–ii). To reveal cortical GABAergic inhibition dynamics, I provide two companion videos. **Video 1** provides spontaneous neocortical GABA dynamics during wakefulness, as $\Delta F/F_0$ signals via iGABASnFR2, together with hippocampal local field potential (LFP) and electromyography (EMG) traces verifying wakefulness. **Video 2** illustrates the multimodal sleep-scoring method, in combination of hippocampal ripple-band power, EMG power, raw EMG traces,

pupil diameter, as verified in synchronized infrared video, to distinguish wakefulness, non-rapid eye movement (NREM) sleep, and rapid eye movement (REM) sleep.

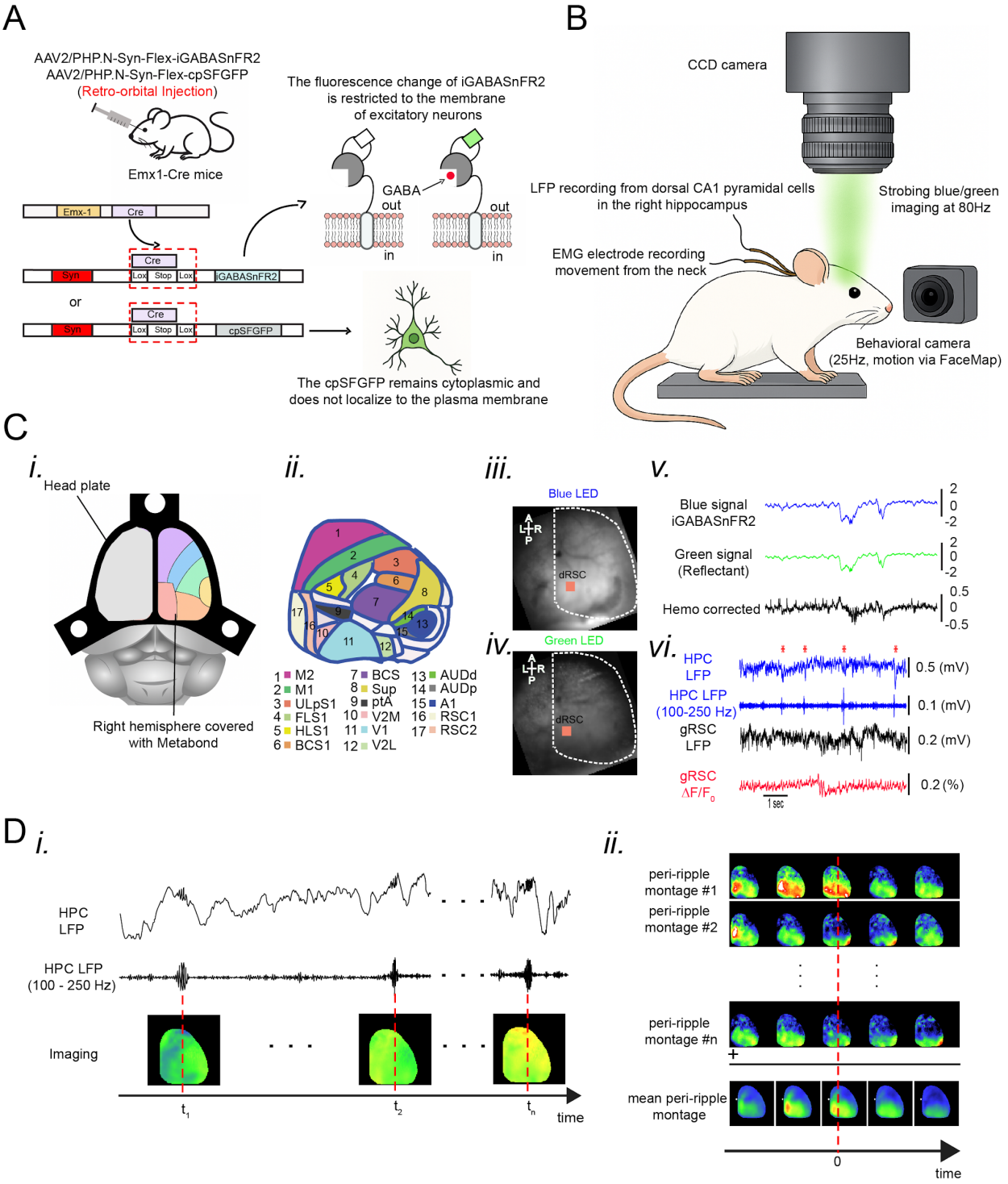


**Figure 1. Experimental protocol for imaging neocortical GABA dynamics during sleep and hippocampal ripples.** (A) Schematic of viral delivery and genetic targeting. Emx1-Cre mice

received retro-orbital injections of either AAV2/PHP.eB-Syn-Flex-iGABASnFR2 or AAV2/PHP.eB-Syn-Flex-cpSFGFP as a control. In Emx1-Cre mice, Cre recombinase drives expression of the GABA sensor iGABASnFR2 or control construct specifically in cortical excitatory neurons. iGABASnFR2 is membrane-bound and reports extracellular GABA binding via fluorescence increases, whereas cpSFGFP is cytosolic and does not respond to GABA. (B) Diagram of the in vivo imaging and recording setup. A CCD camera captures widefield fluorescence from the dorsal cortex through a cranial window. Imaging is synchronized to alternating blue (470 nm) and green (530 nm) LED strobes at 80 Hz for excitation of iGABASnFR2 and collection of reflectance signals, respectively. Simultaneous recordings include hippocampal LFPs from dorsal CA1 to detect SWRs, neck EMG for movement and arousal state, and a behavioural camera (25 Hz) for motion tracking via FaceMap. (C) Imaging coverage and signal correction. (i)Schematic showing the imaging configuration: the right hemisphere was exposed for imaging, which was sealed it with Metabond, while the left hemisphere remained intact. (ii) Schematic showing the 17 identified cortical regions used in ROI-based analyses. (iii–iv) Example cortical images under blue and green LED illumination. The red box marks the dorsal retrosplenial cortex (dRSC), one of the key analysis regions. (v) Traces from the same site showing raw iGABASnFR2 fluorescence (blue), reflectance (green), and the hemodynamically corrected signal (black). (vi) Example traces showing simultaneous hippocampal LFPs (broadband and ripple-filtered), local dRSC LFP, and corrected GABA fluorescence from dRSC. Detected SWRs are aligned with both GABA and LFP signals. (D) Alignment and averaging of peri-ripple GABA activity. (i) Example SWRs from the ripple-band filtered LFP (100–250 Hz) are aligned with concurrent widefield GABA imaging frames. (ii) For each detected SWR, peri-event GABA imaging frames are extracted, aligned to the ripple center (t = 0), and assembled into individual montages. Mean peri-ripple maps are generated across events to characterize spatiotemporal GABA dynamics around SWRs.

### 3.3.2 Cortical GABA Dynamics Across Sleep-Wake State Transitions

To examine the spatiotemporal dynamics of neocortical GABA activity in state transitions, I unilaterally imaged fluorescence signals from the GABA-sensing reporter iGABASnFR2 by widefield imaging. Representative spatial montages and time series traces were analyzed to evaluate GABA dynamics between cortical regions during transitions from NREM to wakefulness and wakefulness to NREM sleep.

#### 3.3.2.1 NREM to awake Transition

**Figure 2Ai** represents spatial montages of neocortical GABA activity at transition to wake (**Video 3**) with overall increases in fluorescence signal (z-scored ΔF/F) on transition, indicative of increased levels of extracellular GABA. The phenomenon is quantified further in (**Figure 2Aii**),

which reveals regions such as V1, RSC2, and FLS1 exhibit a ramp-like build-up of GABA activity begun several seconds before transition and peaking a short time after wake onset.

#### 3.3.2.2 Wake to NREM Transition

At wake-to-NREM transition (**Figure 2Bi**), spatial montages reveal a prominent reduction of GABA fluorescence across the neocortex (**Video 4**). Time series traces in (**Figure 2Bii**) from the same three areas exhibit a progressive decline in activity, starting approximately 5 seconds prior to transition and persisting into early NREM.

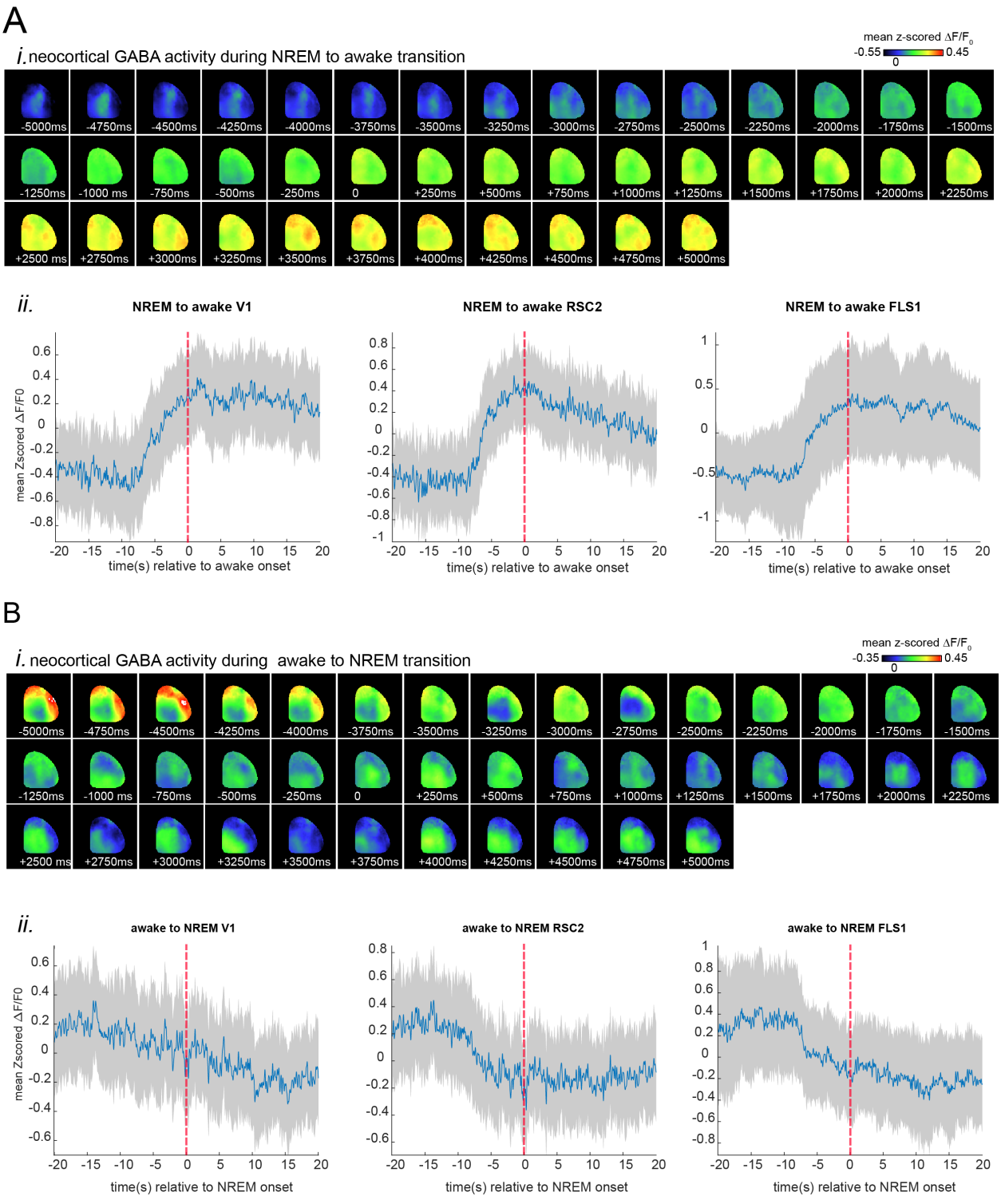


**Figure 2. Neocortical GABA activity during NREM to awake and awake to NREM transitions.** (A) Transition from NREM to Awake. (i) Representative montage of mean neocortical GABA activity during wake-NREM transition recorded with the GABA-sensing fluorescent reporter iGABASnFR2. Images present 5-second time bins, and zero s-time marks

wake onset. Data were scaled and z-scored to the shown color bars (n=5). (ii) Representative sample traces of iGABASnFR2 signals from regions indicated in (i). The plots present the mean optical signals recorded in 3 × 3-pixel boxes (~0.04 mm²) throughout cortical regions. Width of shading surrounding each plot indicates standard error of the mean (SEM). The time 0 s indicates wake onset. (B) Transition from Awake to NREM. (i) Representative montage of mean neocortical GABA activity during wake-NREM transition. Images present 5-second time bins, and zero s-time marks NREM onset. Data were scaled and z-scored to the shown color bars (n=5). (ii) Representative sample traces of iGABASnFR2 signals from regions indicated in (i). The plots present the mean optical signals recorded in 3 × 3-pixel boxes (~0.04 mm²) throughout cortical regions. Shaded areas surrounding each trace indicate reproducibility, which is confirmed. The time 0 s indicates NREM sleep onset.

#### 3.3.2.3 NREM to REM Transition

**Figure 3Ai** depicts the spatial dynamics of GABA activity in NREM to REM transitions (**Video 5**). GABA activity seemed more spatially diverse than in other transitions, with some areas showing transient increases and others remaining stable. Time series in **Figure 3Aii** indicate a modest, transient increase in GABA levels in all three regions, followed by gradual suppression throughout the REM episode.

#### 3.3.2.4 REM to Wake Transition

As illustrated in **Figure 3Bi**, the REM-to-wake transition (**Video 6**) is characterized by a trough in GABA signal at the time of transition, followed by an abrupt rebound. The time courses of **Figure 3Bii** indicate this transient inhibition most prominently in V1 and FLS1, and thus also indicate a transient phase of disinhibition during transitioning out of REM.

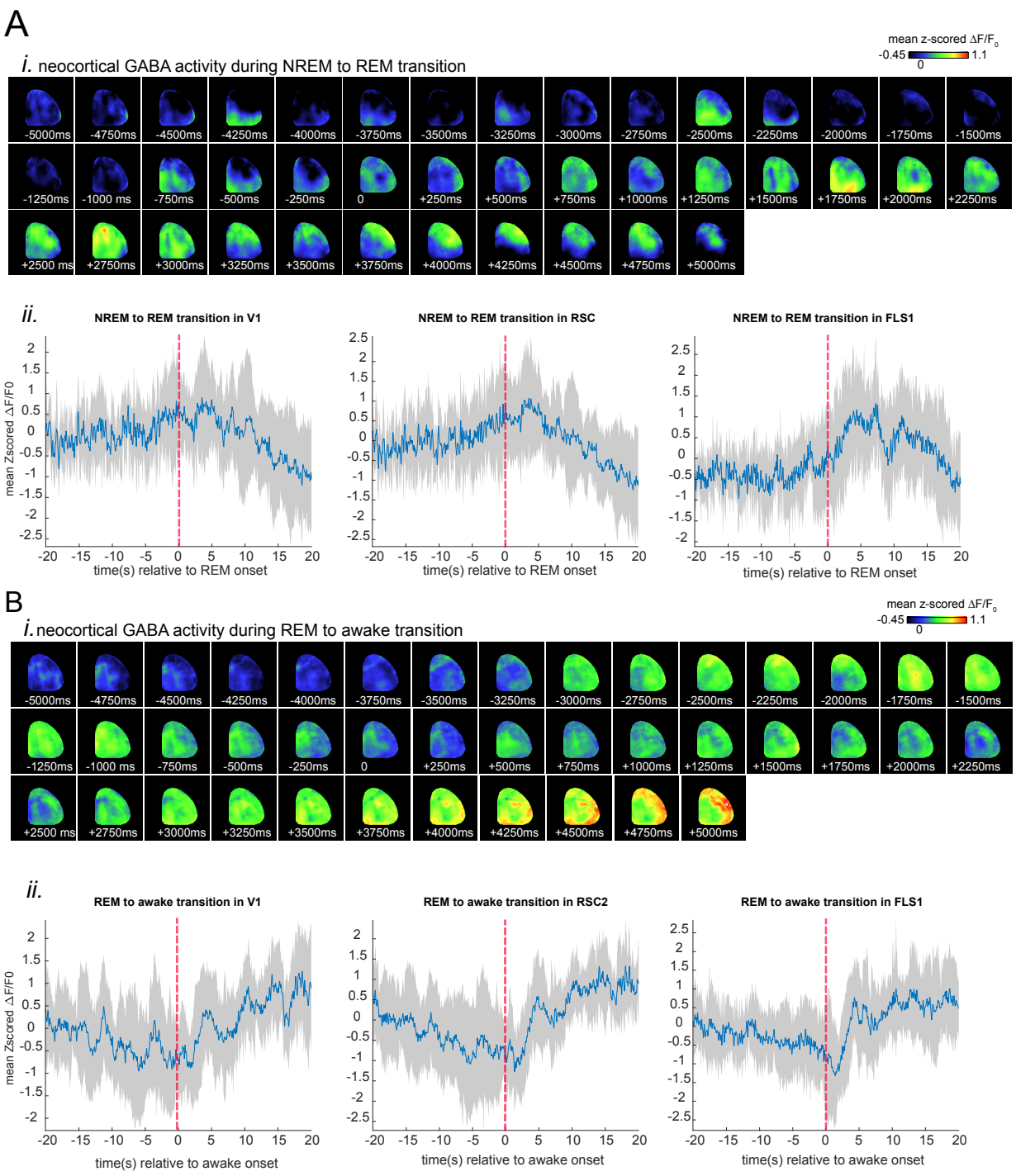
A
i. neocortical GABA activity during NREM to REM transition
mean z-scored ΔF/F0
-0.45
0
1.1
-5000ms
-4750ms
-4500ms
-4250ms
-4000ms
-3750ms
-3500ms
-3250ms
-3000ms
-2750ms
-2500ms
-2250ms
-2000ms
-1750ms
-1500ms
-1250ms
-1000 ms
-750ms
-500ms
-250ms
0
+250ms
+500ms
+750ms
+1000ms
+1250ms
+1500ms
+1750ms
+2000ms
+2250ms
+2500 ms
+2750ms
+3000ms
+3250ms
+3500ms
+3750ms
+4000ms
+4250ms
+4500ms
+4750ms
+5000ms
ii.
NREM to REM transition in V1
NREM to REM transition in RSC
NREM to REM transition in FLS1
mean Zscored ΔF/F0
time(s) relative to REM onset
B
i. neocortical GABA activity during REM to awake transition
mean z-scored ΔF/F0
-0.45
0
1.1
ii.
REM to awake transition in V1
REM to awake transition in RSC2
REM to awake transition in FLS1
mean Zscored ΔF/F0
time(s) relative to awake onset

**Figure 3. Neocortical GABA Activity During NREM to REM and REM to Awake Transitions.** (A) Transition to REM. (i) Montage of mean neocortical GABA activity recorded using the GABA-sensing fluorescent reporter iGABASnFR2 during natural sleep. Images represent 5-second epochs, and zero s-time represents REM onset. Data were z-scored and normalized to the color bars shown (n=5). (ii) Representative traces of iGABASnFR2 signals from regions marked in (i) in an exemplary animal. The plots show the mean optical signals recorded in 3 × 3-pixel boxes (~0.04 $mm^2$) within the visual (V1), retrosplenial (RSC), and forelimb somatosensory (FLS1; magenta) cortices. The thickness of the shading around each plot gives the SEM. The time 0 s represents REM onset. (B) Transition to wake at wake-onset. (i) Montage of mean neocortical GABA activity recorded using the GABA-sensing fluorescent reporter iGABASnFR2 during wake-onset transition from REM. Images represent 5-second epochs, and zero s-time represents wake-onset. Data were z-scored and normalized to the color bars shown (n=5). (ii) Representative traces of iGABASnFR2 signals from regions marked in (i) in an exemplary animal. The plots show the mean optical signals recorded in 3 × 3-pixel boxes (~0.04 $mm^2$) within the visual (V1), retrosplenial (RSC2), and forelimb somatosensory (FLS1; magenta) cortices. The thickness of the shading around each plot gives the SEM. The time 0 s represents wake-onset.

### 3.3.3 State-dependent spatiotemporal patterns of cortical inhibition around sharp-wave ripples

Studies have shown that sharp-wave ripples (SWRs) mediate communication between the hippocampus and cortex in offline brain states, such as sleep and quiet wakefulness (Buzsáki, 2015; Wilson & McNaughton, 1994; Peyrache et al., 2009). It has been shown that the disruption of SWRs impairs memory consolidation, thus demonstrating their functional importance (Ego-Stengel & Wilson, 2009; Girardeau et al., 2009). These events represent an excellent portal for investigating localized, temporally specific manipulation of cortical GABAergic inhibition. Following this background, I next addressed the question of how neocortical GABAergic inhibition responds to SWRs events. Using the iGABASnFR2 sensor, I combined unilateral imaging of neocortical extracellular GABA with local field potential (LFP) recordings from CA1 pyramidal cells to study the spatiotemporal features of extracellular GABA dynamics across the dorsal cortex in relation to hippocampal sharp-wave ripples (SWRs) in natural sleep and wakefulness.

Montages of **Figure 4A**, reveal neocortical GABA's temporal and spatial pattern across different states of the brain. Importantly, in time with NREM sleep (**Figure 4Ai**) neocortical GABA activation began relatively early (**Video 7**), at approximately 100 ms before the SWR center (t = 0). The activation peaked in retrosplenial cortex (RSC) and occurred before the SWR

center (**Figure 4Bi**). The temporal profile of the activation was medial-to-lateral in direction, and medial parts of the brain like the RSC exhibited earliest and greatest activation. Besides strong activation, a clear GABA deactivation pattern was seen in lateral areas before the SWR center. These observations lead us to speculate on the broader significance of GABAergic signaling in sleep and wakefulness. Conversely, during wakefulness (**Figure 4Aii**), no initial GABA activation was observed (**Video 8**). Rather, extracellular GABA activity within neocortical areas slowly built up following the SWR center (t = 0), peaking ~ 500 ms after SWR (Figure 4Biii–iv). Interestingly, wakefulness activation evolved in lateral-to-medial sequence, initiating in visual and somatosensory cortices regions and spreading to medial regions. Deactivation of wakefulness was much less strong and little suppression took place across regions before the SWR center, which gave extra support to the state-dependent difference in the GABA modulation.

To explore the spatial organization of peri-SWR GABA activity in more depth, I examined four major neocortical subnetworks: medial, visual, auditory, and somatomotor—as outlined in **Figure 4Ci**. Amplitude of activation were determined by taking mean of the complete signal in whole full width at half-maximum (from $t_1$ to $t_2$), as in **Figure 4Cii**. Repeated measures ANOVA confirmed sub-network-based effects for NREM sleep and wakefulness. In NREM sleep (**Figure 4Civ**), the sub-network-based effect attained significance ($F(3,12) = 21.608$, $p = 3.96 \times 10^{-5}$, Greenhouse-Geisser adjusted $p = 0.0017$). Follow-up post-hoc analyses verified medial subnetwork had highest activation, which was statistically significant comparing to auditory ($p = 0.0305$) and somatomotor ($p = 0.0366$) subnetworks. The visual subnetwork had intermediate activation, and its amplitudes were higher comparing to auditory ($p = 0.0146$) and somatomotor ($p = 0.0366$) subnetworks. In wakefulness (**Figure 4Cv)**, ANOVA results showed significant subnetwork effect ($F(3,18) = 30.051$, $p = 3.18 \times 10^{-5}$; Greenhouse-Geisser adjusted $p = 7.03 \times 10^{-5}$). Follow-up post-hoc analyses verified medial subnetwork had highest activation amplitudes, which were higher comparing to auditory ($p = 0.0075$) and somatomotor ($p = 0.0027$) subnetworks. The visual subnetwork had higher activation amplitudes comparing to auditory ($p = 0.0025$) and somatomotor ($p = 0.0053$) subnetworks.

Amplitudes of deactivation (**Figure 3D**) were explored and were found to exhibit state- and specific patterns during wakefulness and NREM. During NREM sleep (**Figure 4Di**), deactivation amplitudes were significantly larger, with repeated measures ANOVA indicating a strong

subnetwork effect ($F(3,12) = 21.608$, $p = 3.96 \times 10^{-5}$; Greenhouse-Geisser corrected $p = 0.0017$). Post hoc tests indicated significant differences between the auditory and visual ($p = 0.015$), auditory and medial ($p = 0.031$), and somatomotor and visual ($p = 0.010$) subnetworks. During wakefulness (**Figure 4Dii**), the deactivations were attenuated but had robust subnetwork effects ($F(3,12) = 13.869$, $p = 0.00033$, Greenhouse-Geisser adjusted $p = 0.0047$). The post-testing indicated that auditory subnetwork had less deactivation compared to visual ($p = 0.032$) and medial ($p = 0.041$) subnetworks. The visual subnetwork had greater deactivation than the somatomotor ($p = 0.061$) subnetwork.

To investigate state-dependent modulation more, I recorded amplitudes of GABA activation and deactivation in different neocortical regions during wakefulness and sleep (**Figure S2A**). Activation and deactivation were comparable across states, as confirmed by correlation analyses (**Figure S2B**). Moreover, the comparisons of activation and deactivation amplitude at the subnetwork-specific levels discovered no statistically significant differences between NREM and wakefulness, again highlighting unique modulation profiles for both states (**Figure S2C**). **Activation Amplitudes:** A mixed repeated-measures ANOVA revealed a significant main effect of state on activation amplitudes ($F(1,10) = 28.266$, $p = 0.00034$), with NREM sleep exhibiting higher overall amplitudes. Subnetwork effects were also significant across states ($F(3,30) = 51.895$, $p = 5.50 \times 10^{-12}$), indicating robust differences among regions. However, the interaction between state and subnetwork was not significant ($F(3,30) = 1.605$, $p = 0.209$), suggesting that the relative differences among subnetworks were preserved across states. **Deactivation Amplitudes:** Similarly, for deactivation amplitudes, a mixed repeated-measures ANOVA showed a significant main effect of state ($F(1,8) = 18.571$, $p = 0.0026$), with NREM showing stronger deactivation than wakefulness. Subnetwork effects were again significant ($F(3,24) = 35.134$, $p = 6.08 \times 10^{-9}$), while the interaction between state and subnetwork was not significant ($F(3,24) = 1.686$, $p = 0.197$), indicating that subnetwork-specific patterns remained consistent across brain states.

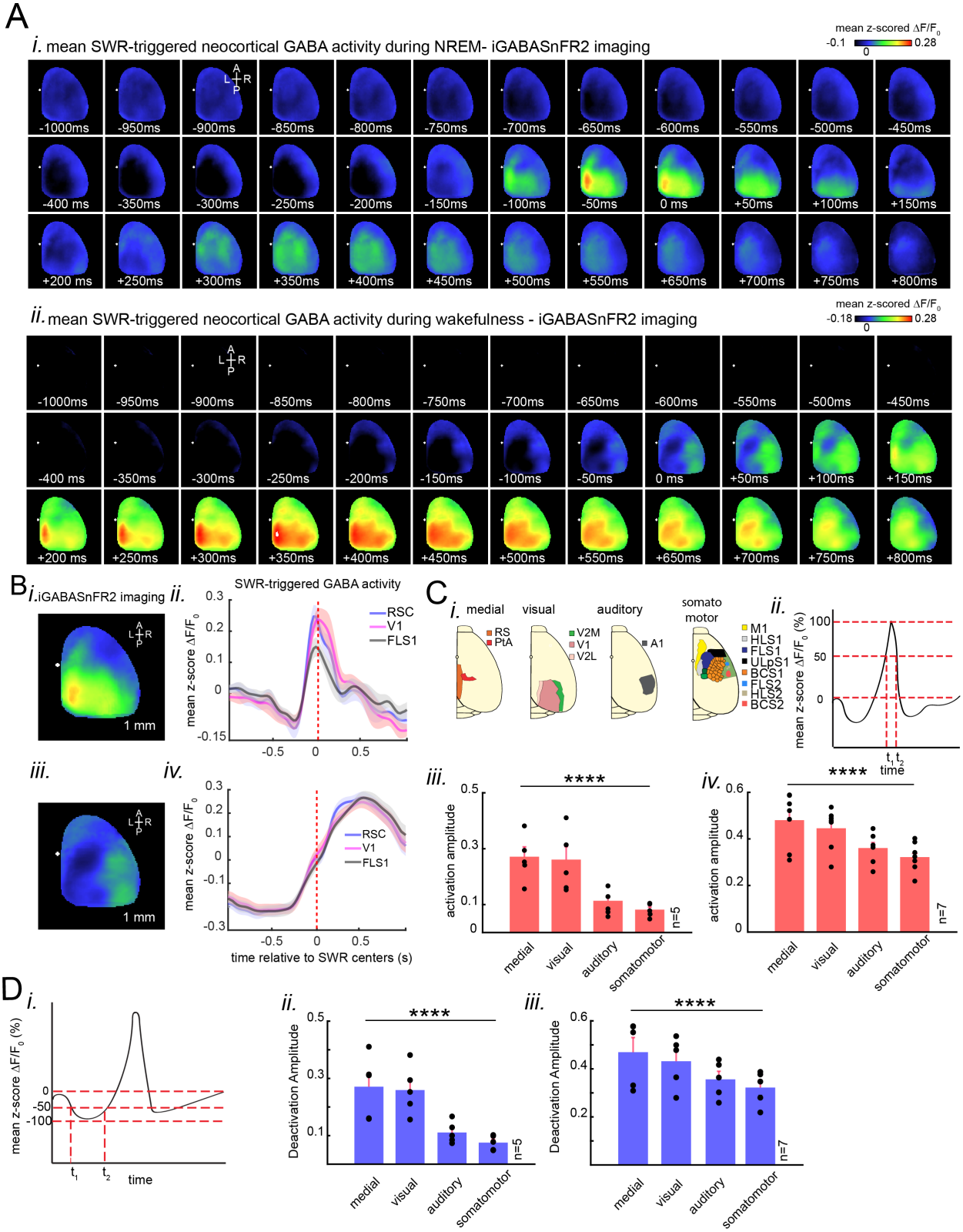
A
i. mean SWR-triggered neocortical GABA activity during NREM- iGABASnFR2 imaging
mean z-scored ΔF/F0
-0.1
0.28
0
-1000ms
-950ms
-900ms
-850ms
-800ms
-750ms
-700ms
-650ms
-600ms
-550ms
-500ms
-450ms
-400 ms
-350ms
-300ms
-250ms
-200ms
-150ms
-100ms
-50ms
0 ms
+50ms
+100ms
+150ms
+200 ms
+250ms
+300ms
+350ms
+400ms
+450ms
+500ms
+550ms
+650ms
+700ms
+750ms
+800ms
ii. mean SWR-triggered neocortical GABA activity during wakefulness - iGABASnFR2 imaging
-0.18
0.28
B
i. iGABASnFR2 imaging
1 mm
ii.
SWR-triggered GABA activity
mean z-score ΔF/F0
RSC
V1
FLS1
time relative to SWR centers (s)
iii.
iv.
C
i.
medial
visual
auditory
somato motor
RS
PtA
V2M
V1
V2L
A1
M1
HLS1
FLS1
ULpS1
BCS1
FLS2
HLS2
BCS2
ii.
mean z-score ΔF/F0 (%)
time
iii.
activation amplitude
****
n=5
medial
visual
auditory
somatomotor
iv.
n=7
D
i.
mean z-score ΔF/F0 (%)
time
ii.
Deactivation Amplitude
iii.

**Figure 4. Peri-SWR neocortical GABA activity: activation and deactivation patterns across sleep and wake states**. (A) Characteristic montage of mean peri-SWR neocortical GABA activity, as visualized with the GABA-sensing fluorescent reporter iGABASnFR2, during head-restrained natural sleep (i) and wakefulness (ii). Time 0 marks SWR centers. Images z-scored and scaled to respective color bars. (B) (i–iv) Sample traces of iGABASnFR2 signals. Panels (Bi, Bii) show natural sleep traces, and (Biii, Biv) show wake traces, taken from sample regions in panels (Ai) and (Aii). Traces show mean optical signals from 3 × 3-pixel boxes (~0.04 $mm^2$) within retrosplenial (blue), visual (black), and forelimb somatosensory (magenta) cortices. Shaded areas around regions of each plot are SEM. SWR centers mark time 0. (C) (i) Four large neocortical subnetworks (medial, visual, auditory, and somatomotor), structurally delimited. (ii) Quantification of activation amplitude schema, defined as mean within-whole-width-at-half-maximum (t1 to t2) of the mean. (iv–v) Grand average (n = 7 animals) of activation amplitudes across subnetworks during sleep and wakefulness, ordered in decreasing order. Each data point represents average activation amplitude for all regions within a subnetwork for one animal. Statistical Analysis: Awake data had a significant subnetwork influence ($F(3,18) = 30.051$, $p = 3.18 \times 10^{-7}$, Greenhouse-Geisser adjusted $p = 7.03 \times 10^{-5}$), and post-hoc differences were found between auditory and medial ($p = 0.0075$), auditory and visual ($p = 0.0025$), medial and somatomotor ($p = 0.0027$), and somatomotor and visual ($p = 0.0053$). Sleep data also revealed a significant subnetwork effect ($F(3,12) = 21.608$, $p = 3.96 \times 10^{-5}$, Greenhouse-Geisser corrected $p = 0.0017$), with posthoc differences between auditory and medial ($p = 0.0305$), auditory and visual ($p = 0.0146$), and medial and somatomotor ($p = 0.0366$). (D) (i–iii) neocortical deactivations preceding SWRs. (Di, Dii) show results for sleep and wakefulness, respectively. Deactivation amplitudes were rectified for group comparison, with higher values indicating more substantial deactivation. Bar plots depict mean ± SEM. Statistical Analysis: Awake data recorded a significant subnetwork effect ($F(3,12) = 13.869$, $p = 0.00033$, Greenhouse-Geisser corrected $p = 0.0047$), and posthoc differences between auditory and visual ($p = 0.032$), medial and somatomotor ($p = 0.041$), and visual and somatomotor ($p = 0.061$) regions. Sleep data recorded a significant subnetwork effect ($F(3,12) = 21.608$, $p = 3.96 \times 10^{-5}$, Greenhouse-Geisser corrected $p = 0.0017$), and posthoc differences between auditory and visual ($p = 0.015$), auditory and medial ($p = 0.031$), and somatomotor and visual ($p = 0.010$) regions. There are five supplementary panels in the figure.

### 3.3.4 Temporal mapping of cortical GABA peaks reveals brain-state-dependent propagation during SWRs

I then investigated the temporal profile of peak GABA activation across cortical areas. The time of peak neocortical GABA activation ($t_p$) was approximated, as the time of peak GABA signaling from the center of the SWR (**Figure 5Ai**), to measure the spatiotemporal extent of inhibition in SWRs in NREM sleep and wakefulness. $t_p$ values in NREM sleep were highly regionally heterogeneous (**Figure 5Aii**), as confirmed by repeated-measures ANOVA ($F(10,40) = 5.0973$, $p = 8.91 \times 10^{5}$). Analysis of linear trends showed a weak but significant medial-to-lateral gradient

in the time profile of activation (slope = 0.0113 s/region, p = 0.047). Spatial maps (**Figure 5Av**) showed the trend, with medial regions like RSC1 and RSC2 with earlier activation than the later activation of lateral cortices. In wakefulness, $t_p$ values had increased and more organized regional heterogeneity (**Figure 5Aiii**), and signification effect confirmed by repeated-measures ANOVA ($F(10,60) = 20.156$, $p = 1.12 \times 10^{15}$). The linear trend discovered was stronger (slope = 0.0272 s/region, p = 0.024), and representative of a greater medial-to-lateral gradient.

Spatial maps (**Figure 5Avi**) confirmed this reversal of patterns: medial regions had later peak GABA activation compared to lateral regions. Line-by-line comparison of trend slopes between brain states (**Figure 5Aiv**) identified that the medial-to-lateral gradient was much greater during wake than during NREM. In aggregate, these results define a state-dependent reorganization of peak neocortical GABA timing: gradual and subtle during NREM sleep, but more sudden and orderly during wakefulness. I compared rise times of extracellular GABA signals between regions and states (**Figure S3A**). Rise times were similar in all cases, so variation in $t_p$ found is better ascribed to differences in timing, as opposed to in speed of activation. In addition, in wakefulness,.$t_p$ values were positively correlated ($r = 0.558$, $p = 0.011$; **Figure S3Bii**) with lateral cortical location, as would be expected for a lateral-to- medial propagation of GABA activation. In NREM sleep, however, there was a significant negative correlation ($r = –0.391$, $p = 0.040$; **Figure S3Biii**), indicative of medial regions' earlier activation. These results lend further support to a state-dependent reorganization of spatiotemporal characteristics of neocortical GABAergic signaling during hippocampal SWRs.

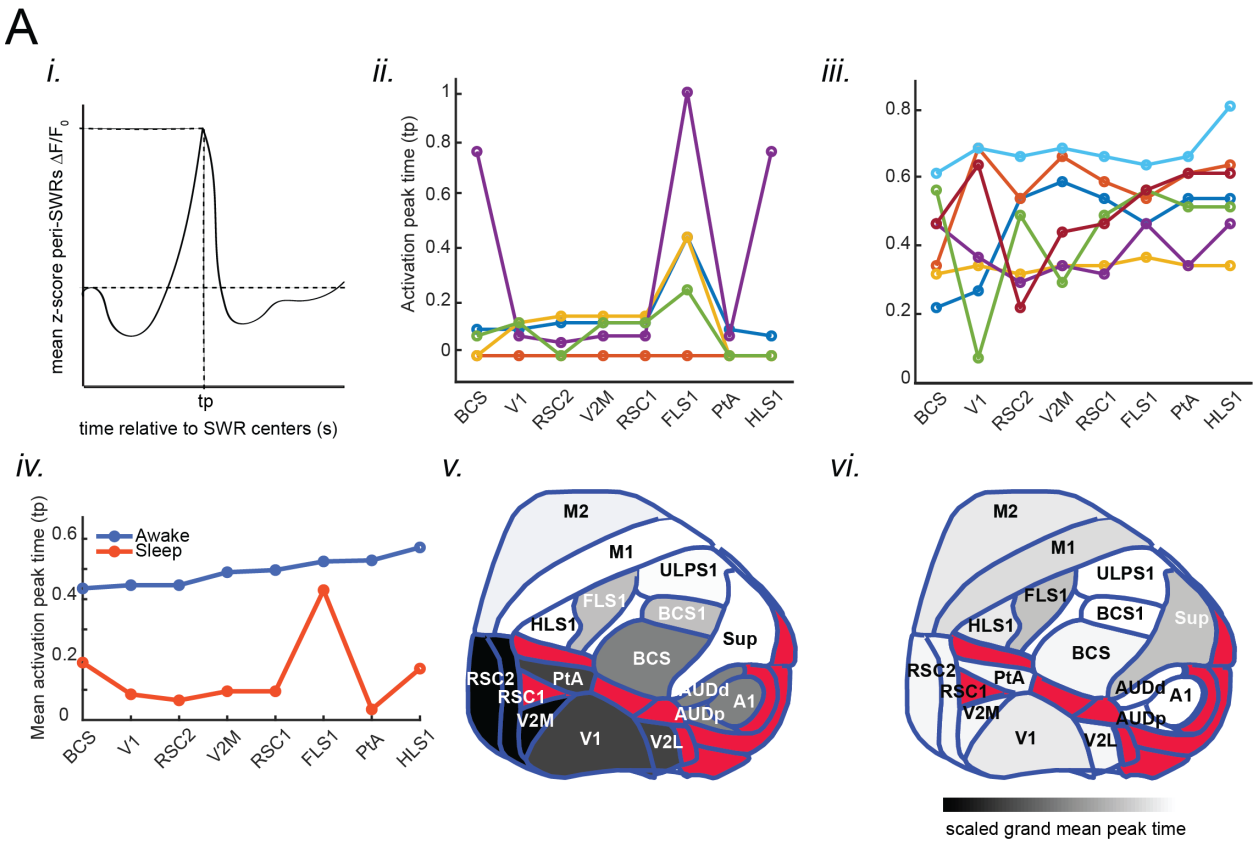


**Figure 5. Cortical regions exhibit state-dependent peak GABA activation dynamics around SWRs during natural sleep and wakefulness.** (A) (i) Peak GABA activation time (tp) for peri-SWR in each cortical region was determined as peak time of mean peri-SWR GABA activity trace (blue trace) and provides an index of peak GABA activation time relative to center of SWR. (ii) Sleep Condition: Repeated-measures ANOVA revealed significant regional variation in tp ($F(10,40) = 5.0973$, $p = 8.9111e{-}05$). A statistically significant positive linear trend (slope=0.011273 s/region,p=0.047249) discloses medial-to-lateral progression of tp during sleep, consistent with a subtle medial-to-lateral propagation of GABA activation. (iii) Awake Condition: Repeated-measures ANOVA revealed strong and statistically significant regional variation in tp ($F(10,60) = 20.156$, $p = 1.116e{-}15$). Post-hoc linear trend analysis confirmed a statistically significant positive slope (slope=0.02724 s/region, p=0.024326), which discloses a consistent and systemicdelayed,tp from medial toward lateral regions in wake stage. (iv) Post-hoc Linear Trend Analysis: Linear trend analysis confirmed state-dependent dynamics. In wake, a statistically significant positive slope (0.02724 s/region=0.024326) discloses a robust medial-to-lateral gradient. In sleep, a negligibly but statistically significant smaller slope (0.011273 s/region=0.047249) reveals less strenuous regional variations. The corresponding graph reveals the result, which shows steep and consistent regional variation in awake data compared with sleep. (v) Spatial maps during sleep (n=5) reveal higher earlier peak tp in medial regions like RSC1, RSC2, and PtA, and subsequent lateral propagation of activation. The result discloses an orchestrated medial-to-lateral propagation of GABAergic activation during natural sleep. (vi) Spatial maps for wakefulness (n=7) indicate delayed activation in medial regions and a more homogeneous distribution of tp values throughout cortical regions. The pattern indicates

characteristic cortical dynamics in wakefulness, with a strong medial-to-lateral gradient in GABA activation timing.

### 3.3.5 Spatial and temporal modes of peri-ripple iGABASnFR2 activity and region-specific dynamics

I then examined if ripple-related neocortical GABA dynamics show unique spatial motifs and temporal structures at the network level. To decompose spatiotemporal neocortical GABA activity into general spatial and temporal structures, I applied singular value decomposition (SVD) to GABA signals close to SWRs **(Figure 6A, B**). Component 1 mapped diffuse activation of GABA (Components 1i), and the corresponding temporal trace (Component 1ii) consisted of a punctuate onset of extracellular GABA at ripple onset (t = 0). Components 2–5, on the other hand, detected state-specific characteristics. In NREM sleep (**Figure 6A**), higher-order spatial components detected heightened recruitment of medial regions, including the retrosplenial cortex (RSC). The temporal components in NREM were slow and less well time-locked to onset of ripples compared to wakefulness. In wakefulness (**Figure 6B**), spatial maps (Components 2–5i) illustrated regionally localized activation of GABA in lateral regions, but corresponding temporal traces (Components 2–5ii) contained transient, fast features, suggesting fast, region-specific inhibition.

I also reconstructed neocortical GABA activity in the neocortex close to SWRs in five representative neocortical locations: RSC, BC, V1, auditory cortex (AUD), and forelimb somatosensory cortex (FLS1) (**Figure 6C, D**). Under wakefulness (**Figure 6C**), BC and V1 had sharp, high-amplitude GABA transients (**Figure 6Cii**), and statistical comparisons revealed heightened GABA responses in sensory areas compared to the RSC (**Figure 6Ciii**). During NREM sleep (**Figure 6D**), RSC has the strongest activation (**Figure 6Dii–iii**). Combined, these results show that while a global elevation of inhibitory tone accompanies hippocampal ripples in both brain states, fine-scale spatiotemporal patterns of neocortical GABA dynamics depend on brain state. Wakefulness involves rapid, GABA activation in lateral sensory cortices, while NREM sleep recruits more widespread, slower inhibitory responses with a focus on medial areas.

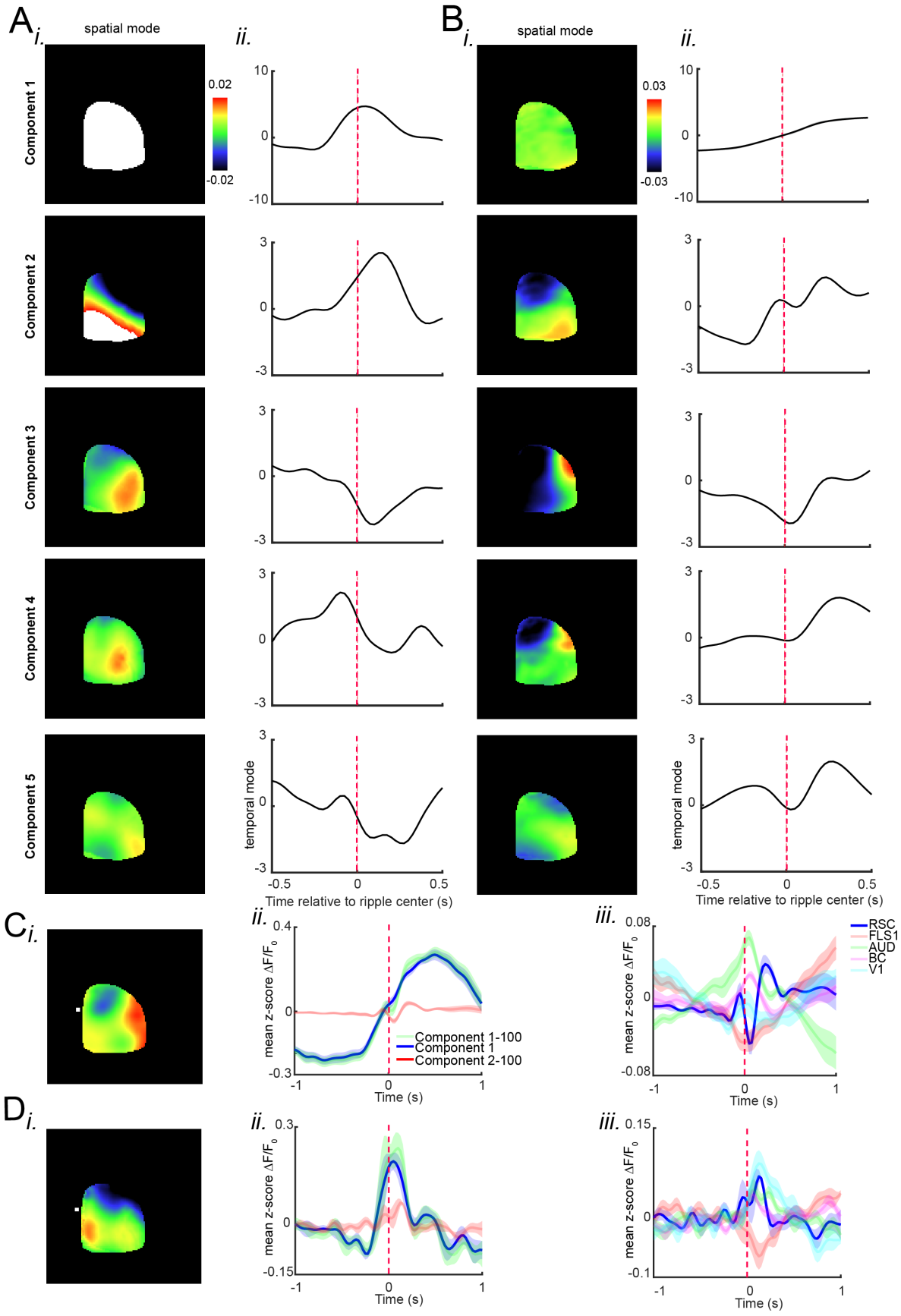
A
i.
spatial mode
ii.
Component 1
Component 2
Component 3
Component 4
Component 5
0.02
-0.02
temporal mode
Time relative to ripple center (s)
B
i.
spatial mode
ii.
0.03
-0.03
temporal mode
Time relative to ripple center (s)
C
i.
ii.
mean z-score ΔF/F0
Component 1-100
Component 1
Component 2-100
Time (s)
iii.
RSC
FLS1
AUD
BC
V1
mean z-score ΔF/F0
Time (s)
D
i.
ii.
mean z-score ΔF/F0
Time (s)
iii.
mean z-score ΔF/F0
Time (s)

**Figure 6 Spatial and Temporal Modes of Peri-Ripple iGABASnFR2 Activity and Region-Specific Dynamics.** (A, B) Spatial (i) and temporal (ii) modes of the five largest singular components obtained from singular value decomposition (SVD) of the peri-ripple iGABASnFR2 activity stack during NREM sleep (A) and wakefulness (B). Component 1 represents the dominant mode of peri-ripple GABA dynamics, capturing the largest fraction of variance and reflecting the most consistent spatial and temporal pattern of extracellular GABA fluctuations across ripple events. Components 2–5 capture additional structured variability in peri-ripple GABA activity and reveal clear brain-state–dependent differences in the spatiotemporal organization of cortical GABA dynamics. During NREM sleep (A)**,** higher-order components exhibit broader and more spatially distributed cortical patterns, with prominent contributions from associative regions such as retrosplenial cortex (RSC) and comparatively reduced spatial localization within primary sensory areas. Their corresponding temporal modes show slower and smoother dynamics around ripple onset. In contrast, during wakefulness (B)**,** spatial modes of Components 2–5 display more localized cortical patterns, with strong contributions from primary sensory regions including barrel cortex (BC) and visual cortex (V1). The corresponding temporal modes exhibit sharper, temporally precise deflections aligned to ripple initiation, indicating faster and more temporally constrained peri-ripple GABA dynamics during wakefulness. (C, D) Peri-ripple regional GABA activity reconstructed for significant regions of interest (ROIs)—retrosplenial cortex (RSC), barrel cortex (BC), visual cortex (V1), auditory cortex (AUD), and forelimb somatosensory cortex (FLS1)—reveals clear brain-state–dependent peri-ripple dynamics. During wakefulness (C)**,** BC and V1 exhibit well-defined, high-amplitude peaks in their peri-ripple temporal profiles (Cii). Statistical comparison across regions (Ciii) demonstrates significantly stronger peri-ripple GABA responses in sensory cortices compared with associative regions such as RSC.In contrast, during NREM sleep (D)**,** peri-ripple GABA activity is more broadly distributed across cortical regions, with RSC emerging as the dominant region exhibiting prolonged and comparatively larger-amplitude activity (Dii). Sensory regions such as BC and V1 show attenuated peri-ripple responses during sleep. Statistical comparison (Diii) further highlights the relative enhancement of RSC activity with respect to sensory cortices in the sleeping state.

Shaded regions in the temporal profiles (Cii, Dii) indicate the standard error of the mean (SEM).

## 3.4 Discussion

### 3.4.1 Summary of the Study

In this study, I investigated how neocortical GABA dynamics are temporally and spatially organized around internally generated hippocampal sharp-wave ripples (SWRs) across behavioural states. Using mesoscale imaging of extracellular GABA with the iGABASnFR2 sensor together with simultaneous recordings of CA1 pyramidal neuron activity, I first characterized GABA activity during spontaneous transitions between sleep and wakefulness. I then examined the spatiotemporal dynamics of neocortical GABA around hippocampal SWRs and

observed that cortical GABA activity is spatially structured, exhibits propagating dynamics, and is modulated by brain state. Specifically, I found distinct propagation patterns: medial-to-lateral during NREM sleep and lateral-to-medial during wakefulness. These findings indicate that cortical GABA signaling is influenced by hippocampal output and that this modulation varies across cortical subnetworks and vigilance states. To examine these dynamics, I employed the genetically encoded GABA sensor iGABASnFR2, which enables direct optical measurement of extracellular GABA in vivo. Widefield imaging through a large cranial window over the right hemisphere allowed us to monitor GABAergic activity across the dorsal cortex, while local field potentials were simultaneously recorded from the ipsilateral dorsal hippocampus to capture hippocampal output. This unilateral approach was guided by prior evidence of strong interhemispheric synchrony in both neocortical activity and hippocampal SWRs (Mohajerani et al., 2010; Buzsáki, 1989; Buzsáki, 2015), supporting its suitability for describing ripple–cortical interactions. Together, this configuration provided high temporal and spatial resolution to investigate state-dependent neocortical GABA dynamics during natural sleep and wakefulness.

### 3.4.2 Cortical GABA Dynamics During State transitions

First, I examined the changes in cortical GABA levels that take place during spontaneous behavioural state transitions, and I complemented this analysis with coherence and correlation-based network methods to reveal their implications at the circuit level. As the brain transitioned from NREM sleep to wakefulness, I observed a dramatic increase in GABA activity, which was replicated across different cortical areas (**Figure 2Ai–ii**) This increase in inhibitory tone, coupled with increased synchrony, can reflect an active gating or stabilization process during the arousal process, promoting the coordination of sensory and motor pathways as the brain prepares for the state of behavioural responsiveness (Lee & Dan, 2012; McGinley et al., 2015; Gentet et al., 2012). In contrast, transitions from wakefulness to NREM sleep were correlated with a decrease in extracellular GABA (**Figure 2Bi–ii**). These are likely to represent a switch from fast, phasic inhibitory mechanisms to slower, synchronous, oscillatory modes typical of NREM sleep (Niethard et al., 2018; Zielinski et al., 2019), in favor of the commencement of cortical downscaling and memory consolidation.

The dynamics of GABA in the neocortex across transitions involving REM sleep showed increasingly complex and varied dynamics. The transition from NREM to REM sleep was marked by modest, regionally specific increases in GABA levels, which were then followed by suppression (**Figure 3Ai–ii**). In contrast, the transition from REM sleep to wakefulness showed a large drop in GABA at the point of awakening (**Figure 3Bi–ii**), followed by rapid re-engagement, reflecting a brief release from inhibitory control (Niethard et al., 2016; Desrosiers & Basha, 2023; Tossell et al., 2023). Together, these findings highlight the dynamic and state-specific regulation of GABAergic tone across the neocortex, indicating that changes in inhibitory signaling are closely intertwined with macroscale network reconfiguration across sleep-wake transitions.

### 3.4.3 Ripple-triggered GABA responses are brain-state dependent

Past work using iGluSnFR has demonstrated that hippocampal sharp-wave ripples (SWRs) are coordinated by state-dependent neocortical excitation and can be preceded by cortical activation, challenging a strictly hippocampus-driven model of ripple generation (Karimi Abadchi et al., 2020). Here, I extend this framework by showing that extracellular GABA dynamics are likewise organized in a state-dependent and spatially structured manner around SWRs. During NREM sleep, medial cortical regions exhibited an early increase in extracellular GABA that began approximately 100 ms before the SWR center and reached its peak around 50 ms prior to the ripple. This early inhibitory recruitment mirrors the leading neocortical excitation reported by Karimi Abadchi et al. and follows the canonical excitation–inhibition sequence within cortical circuits. The peri-ripple GABA increase emerged first in medial cortex and subsequently propagated toward lateral regions. This organization parallels prior reports of retrosplenial engagement during slow-wave sleep (Opalka et al., 2020) and is consistent with established retrosplenial–hippocampal coordination in memory-related processing (Alexander et al., 2018; Wang & Ikemoto, 2016). In contrast, during wakefulness, extracellular GABA increased primarily after ripple onset, appearing first in lateral sensory cortices and then propagating toward medial regions, as shown in the SWR-triggered montages and time courses. Together, these findings demonstrate that SWRs are accompanied by state-dependent and spatially ordered changes in extracellular GABA, revealing distinct network-level coordination patterns across sleep and wakefulness. Consistent with this interpretation, quantitative activation analyses (Figure 4C–D) confirm that all cortical subnetworks

exhibit robust peri-SWR increases in extracellular GABA, with the earliest and strongest responses in medial cortex during NREM sleep and a reversed lateral-to-medial organization during wakefulness.

### 3.4.4 Temporal gradients reveal propagation of inhibitory signals

Time-to-peak ($t_p$) of neocortical GABA dynamics throughout different cortical areas showed medial-to-lateral propagation during NREM sleep, consistent with glutamate dynamics [19] and memory-related information flow direction between default-mode network structures. During wakefulness, direction of propagation was reversed, and propagation went from lateral to medial cortical compartments. These results are in concert with the suggestion that cortical inhibition characteristically follows excitation with a characteristic temporal delay (Isaacson & Scanziani, 2011; Atallah & Scanziani, 2009; Okun & Lampl, 2008) Neocortical inhibition in this case can function as a state-dependent gate of the hippocampal output, orchestrating temporally the inhibition control with the current sensory or cognitive demands. Directional asymmetry of propagation patterns uncovers the cortex to rescale not only the strength but also the spatiotemporal organization of inhibition in accordance with internal state.

### 3.4.5 SVD reveals global vs. local components of ripple-evoked inhibition

The SVD analysis of neocortical iGABASnFR2 signals during hippocampal SWRs revealed distinct spatial and temporal motifs of inhibitory dynamics. The dominant component reflected a widespread, near-global increase in GABA activity across cortex, consistent with a coordinated inhibitory response that may help stabilize cortical excitability during hippocampal output. Higher-order components captured localized and state-dependent features. During wakefulness, these modes revealed brief, regionally confined GABA transients in lateral sensory and motor areas, suggesting selective modulation of cortical circuits that could transiently gate sensory processing during ripple events. In contrast, during NREM sleep, GABA activity became broader and more sustained, particularly within medial regions such as the retrosplenial cortex (RSC), a hippocampal-interconnected hub implicated in systems consolidation. Together, these findings suggest that ripple-evoked inhibition comprises a global inhibitory scaffold modulated by state-

specific, spatially organized components, providing a flexible substrate for coordinating memory-related communication between hippocampus and cortex across behavioural states.

### 3.5 Conclusion

In the current study, mesoscale imaging of iGABASnFR2 was used to map the dynamics of extracellular GABA over the dorsal cortex during sleep-wake transitions and in response to hippocampal sharp-wave ripples. The results show that cortical GABAergic inhibition is spatially patterned and under strong control of behavioural states, suggesting that neocortical GABA dynamics play an active role in the routing and filtering of memory-related outputs from the hippocampus. While our imaging approach provides high temporal and spatial resolution over large cortical areas, it remains nonspecific about cell types and depth resolution. Therefore, it would not be possible to distinguish between the Behaviours of PV+, SST+, or VIP+ interneurons, or clarify the inhibitory roles at the subcortical level. To further define the circuit mechanisms underlying state-dependent and ripple-dependent inhibition, future studies employing iGABASnFR2 in conjunction with optogenetic manipulation, cell-type-specific marker labeling, or multiphoton microscopy will be necessary. In addition, with recent advances in genetically encoded sensors (Aggarwal et al., 2025), it is now possible to simultaneously measure excitation and inhibition in vivo. Combining iGABASnFR2 with glutamate sensors will enable direct assessment of excitation–inhibition balance in both healthy and disease models, offering new insights into how this balance is altered in disorders such as epilepsy or schizophrenia.

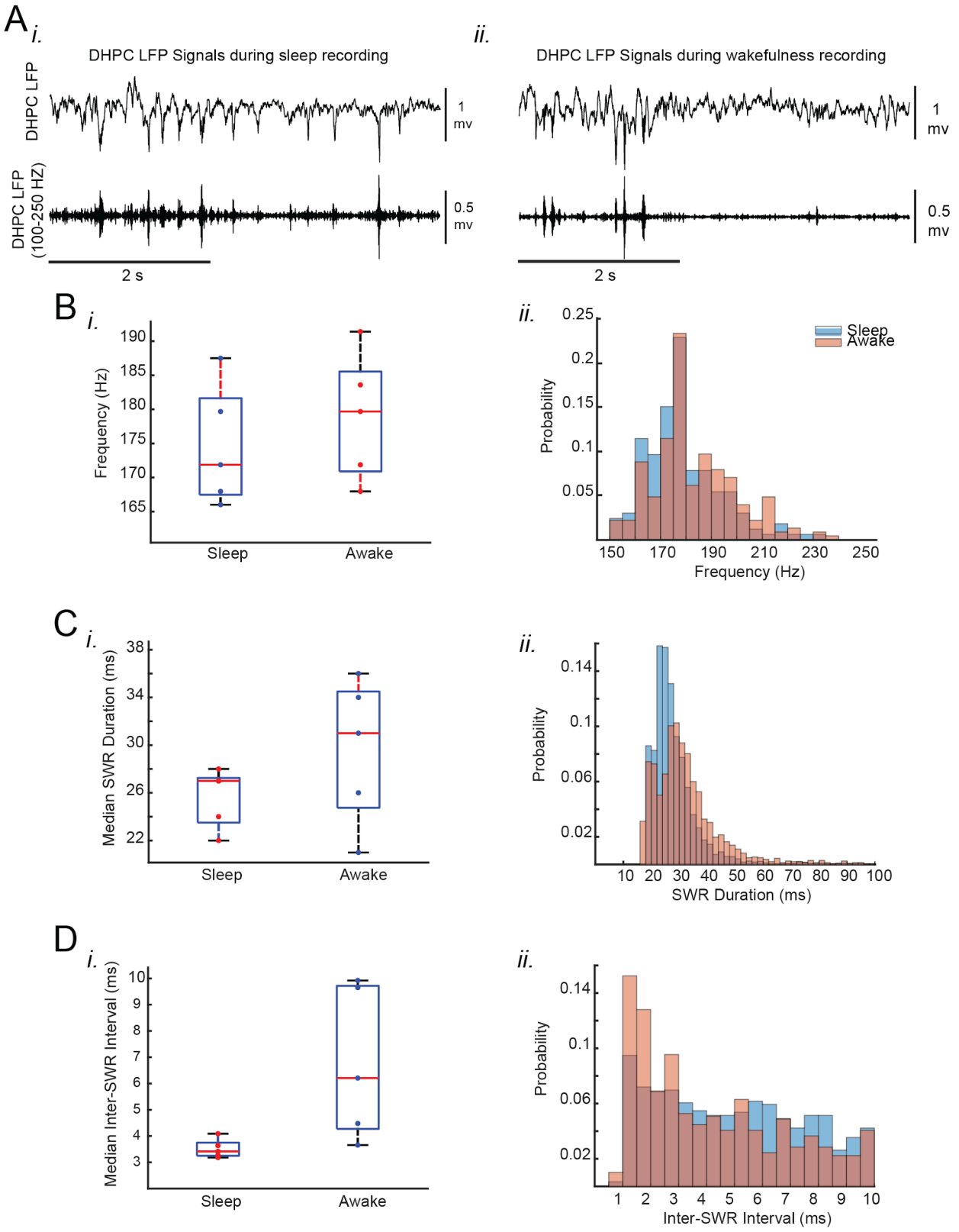


**Supplementary Figure 1. Characteristics of SWRs recorded in head-restrained naturally sleeping and wakeful mice.** (A) Representative DHPC (dorsal hippocampus) LFP signals were

recorded during sleep (i) and wakefulness (ii). The top traces show raw LFP signals, and the bottom traces display band-pass filtered LFP signals (100–250 Hz). The filtered signals highlight the occurrence of sharp wave ripples (SWRs). Scale bars indicate 2 seconds. (B) (i) Median peak spectral frequency of hippocampal SWRs recorded during head-restrained sleep and wakefulness. Each data point represents the median peak frequency for a given animal (n = 7 for sleep, n = 5 for wakefulness). SWRs detected during head-restrained sleep tend to have lower peak frequencies than wakefulness. Red plus signs represent outliers beyond the interval containing 99.3% of the data points. (ii) Histograms showing the distribution of peak spectral frequencies of hippocampal SWRs pooled across all animals and experimental conditions. Sleep recordings exhibit a more clustered and lower frequency distribution, whereas wakefulness displays a broader frequency range. (C) (i) Median SWR durations during head-restrained sleep and wakefulness. Each data point represents the median value for a given animal. SWRs detected during sleep are significantly shorter than those recorded during wakefulness. (ii) Histogram distributions of SWR durations pooled across all animals and experimental conditions. Sleep recordings show a higher probability of shorter durations, whereas wakefulness is associated with more variability and longer durations. (D) (i) Median inter-SWR intervals during head-restrained sleep and wakefulness. Each data point represents the median value for a given animal. SWRs detected during sleep tend to have shorter inter-SWR intervals compared to wakefulness. (ii) Histogram distributions of inter-SWR intervals pooled across all animals and experimental conditions. Sleep recordings are associated with shorter intervals and more tightly clustered distributions, whereas wakefulness exhibits a broader range of intervals, with longer durations being more frequent.

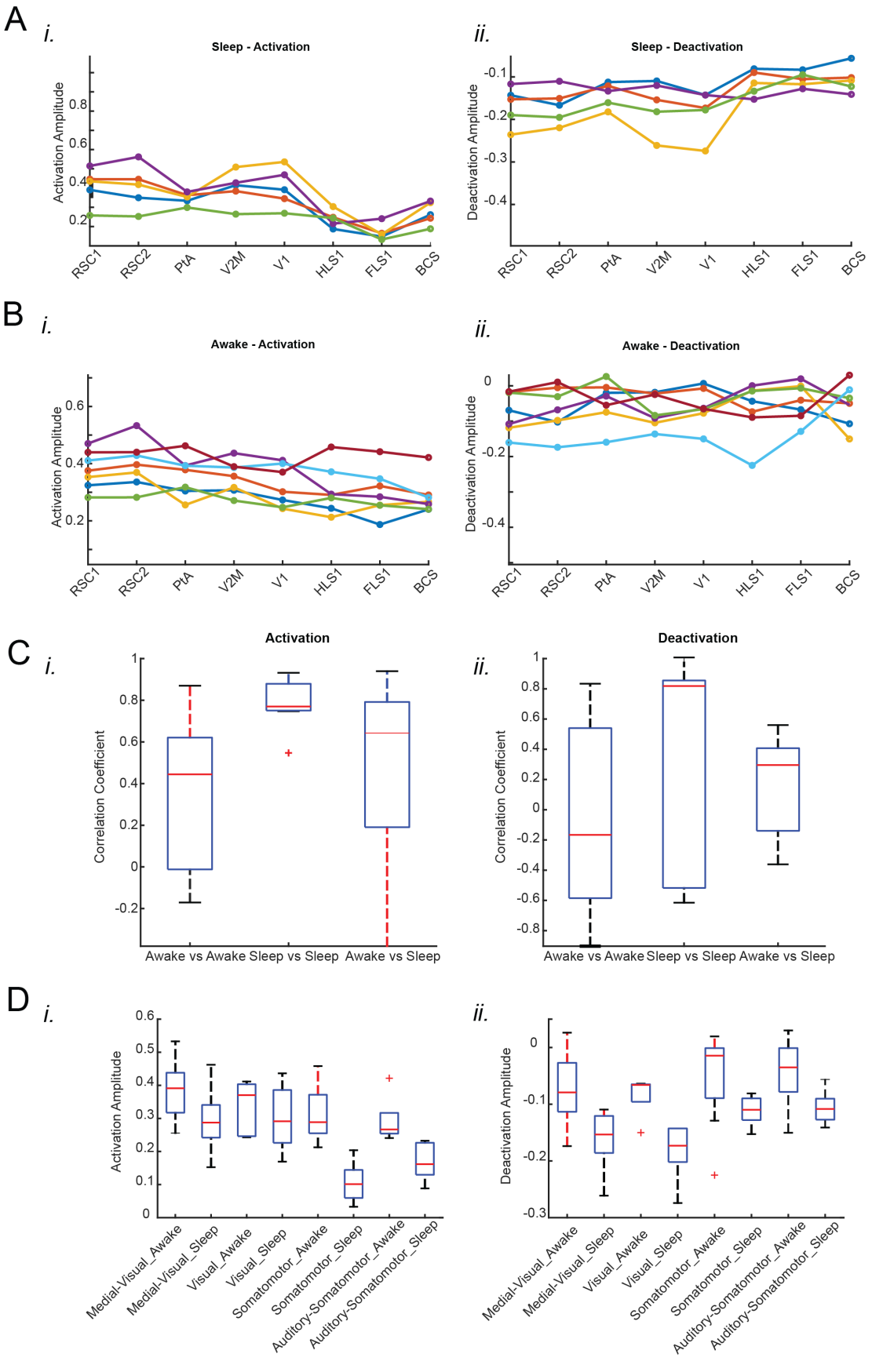
A
i.
Sleep - Activation
Activation Amplitude
RSC1
RSC2
PtA
V2M
V1
HLS1
FLS1
BCS
ii.
Sleep - Deactivation
Deactivation Amplitude
B
i.
Awake - Activation
ii.
Awake - Deactivation
C
i.
Activation
Correlation Coefficient
Awake vs Awake
Sleep vs Sleep
Awake vs Sleep
ii.
Deactivation
D
i.
Activation Amplitude
Medial-Visual_Awake
Medial-Visual_Sleep
Visual_Awake
Visual_Sleep
Somatomotor_Awake
Somatomotor_Sleep
Auditory-Somatomotor_Awake
Auditory-Somatomotor_Sleep
ii.
Deactivation Amplitude

**Supplementary Figure 2. State-dependent modulation of neocortical GABA dynamics during hippocampal sharp-wave ripples (SWRs).** (A, B) Peri-SWR GABA activation (i) and deactivation (ii) amplitudes across neocortical regions during NREM sleep (A) and wakefulness **(B)**. Regions are ordered along the x-axis according to descending activation amplitude during NREM sleep (A-i) and wakefulness (B-i), respectively. Each colored trace represents data from a single animal (n = 5 for NREM sleep; n = 7 for wakefulness).**(C)** Quantification of similarity in regional activation (i) and deactivation (ii) amplitude profiles across behavioural states. Box plots show distributions of Pearson correlation coefficients computed between all pairs of regional amplitude profiles for wakefulness vs wakefulness, sleep vs sleep, and wakefulness vs sleep. Red horizontal lines indicate medians; red crosses denote outliers. (D) Subnetwork-level comparison of peri-SWR activation (i) and deactivation (ii) amplitudes between wakefulness and NREM sleep. Box plots summarize regional amplitudes grouped into medial–visual, visual, somatomotor, and auditory–somatomotor subnetworks for each behavioural state.

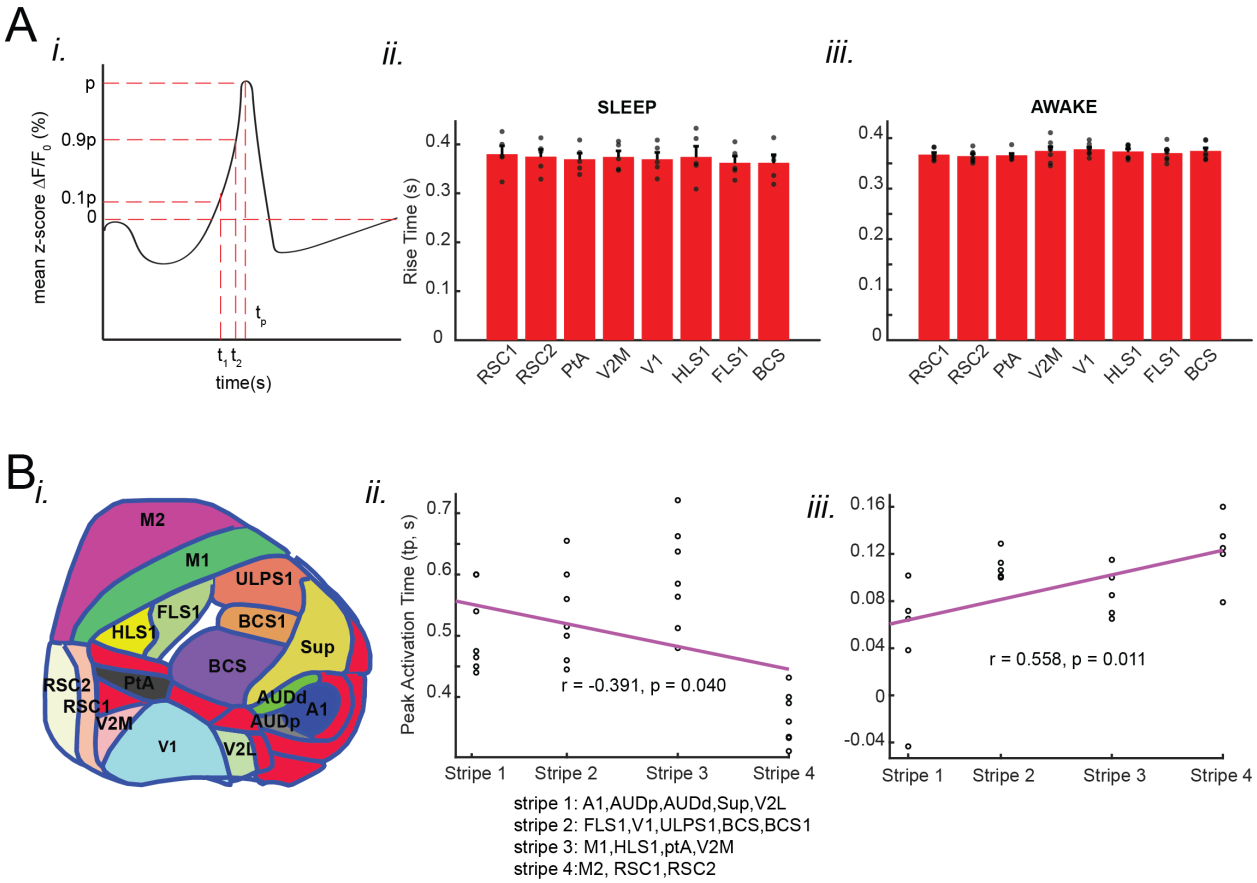


**Supplementary Figure 3. Sequential GABA Activation Across Neocortical Regions During Hippocampal SWRs: Lateral Dominance in Wakefulness and Medial Dominance in NREM Sleep (A)** GABA activation rise time in neocortical regions: (i) Measurement of GABA rise time: GABA rise time was calculated as the time taken for the signal to increase from 10% (0.1p) to 90% (0.9p) of its peak value (p). (ii) rise time during wakefulness: mean GABA rise times show no significant differences across neocortical regions. All regions activate at a similar rate. (iii) rise

time during sleep: GABA rise time is also consistent across neocortical regions, with no significant regional differences. Bar graphs represent mean ± SEM, with individual data points shown. (B) sequential activation of GABA in neocortical regions relative to SWRs: (i) schematic of neocortical regions: neocortex divided into four vertical stripes from medial to lateral regions. (ii) wakefulness: A significant positive correlation ($r = 0.558$, $p = 0.011$) is observed between stripe number and peak activation time (tp), indicating that GABA activation occurs later in more lateral regions relative to hippocampal SWRs. (iii) Sleep: A significant negative correlation ($r = -0.391$, $p = 0.040$) is observed, showing that GABA activation occurs earlier in more medial regions than hippocampal SWRs.

## Chapter 4

## GABAergic inhibition as a dynamic organizer of cortical activity

Inhibition in the cortex has long been seen as a mechanism that keeps neural activity balanced and prevents runaway excitation. Recent optical imaging studies challenge this view, revealing that GABAergic inhibition actively organizes when and how cortical circuits operate. Widefield imaging of extracellular GABA shows that inhibitory tone ramps smoothly across sleep–wake transitions, preceding and shaping changes in cortical network activity. During sensory processing, fast and spatially precise inhibitory signals define the timing and selectivity of cortical responses. Across transitions between wakefulness and sleep, slower and spatially extended inhibition coordinates widespread network reconfiguration as neuromodulatory tone changes. During internally generated activity, such as memory replay in non-REM sleep, GABAergic inhibition becomes predictive, gating when and where internal signals propagate. Thus, GABAergic inhibition may serve as a dynamic organizing principle for cortical computation across perception, sleep, and memory, challenging traditional models that define inhibition as a passive stabilizing force.

### 4.1 Reframing Cortical Inhibition

Inhibition is a fundamental principle of brain function. It allows the nervous system not only to generate activity but also to control and shape it. Early physiological studies showed **(Figure 1)** that inhibitory mechanisms help keep behaviour and neural activity selective and stable. With the discovery of inhibitory interneurons and the identification of γ-aminobutyric acid (GABA) as their main transmitter, inhibition became understood as a core biological process rather than an abstract concept (Bari & Robbins, 2013).In the cortex, excitation and inhibition constantly interact with excitatory neurons spreading information across networks, while inhibitory neurons coordinate and constrain this activity. Historically, researchers considered inhibition as a stabilizing function. It was seen as something that keeps neurons from firing too much, keeps activity balanced, and helps sharpen responses — a background control that supports brain function without changing what information is processed or when it happens (Isaacson et al., 2011). However, studies showed that inhibition is not just the opposite of excitation — it helps organize brain activity. GABAergic

networks create flexible patterns that change with brain state, behaviour, and brain region. Inhibitory signals do not remain fixed; they can modulate many temporal scales, from the fast times that control single spikes to slow GABA waves that sweep over widespread areas of the cortex (Isaacson et al., 2011; Haider et al., 2009). This flexibility allows the same cortical circuits to work in different ways depending on whether the brain is processing information from the outside world or generating its own internal activity.


**Figure 1. Historical development of the concept of inhibition in neuroscience.**

Most of what we know about cortical inhibition comes from studies of sensory systems. In visual, auditory, and somatosensory cortices, inhibitory neurons are recruited after a stimulus arrives. Parvalbumin-positive ($PV^+$) interneurons provide rapid, strong inhibition near the cell body, which helps time spikes precisely. Somatostatin-positive ($SST^+$) and layer-1 interneurons contribute slower and broader inhibition that acts on dendrites and feedback pathways (Isaacson et al., 2011; Petersen, 2019; Gentet, 2012; Urban-Ciecko et al., 2016). But the cortex does not always operate in this mode. During sleep or quiet rest, when sensory input is reduced, activity patterns arise from within the brain itself. These internally generated patterns include slow oscillations, spindles, and hippocampal sharp-wave ripples (SWRs), which are thought to support memory consolidation and planning (Isaacson et al., 2011; Haider et al., 2009; Gabernet et al., 2005; Gentet, 2012; Urban-Ciecko et al., 2016; Rudy et al., 2011; Buzsáki, 2015). In these states, inhibition cannot simply be balancing excitation, because the brain is not being driven by external input. Instead, inhibitory networks appear to control *when* and *where* these internal signals occur, organizing the flow of information between the hippocampus and the cortex.

Recent advances in optical imaging are changing how we think about cortical inhibition. Cortical inhibition is often described as a balancing mechanism that stabilizes neural activity. Yet recent imaging evidence shows that inhibition does far more—it dynamically organizes when and how cortical circuits operate. Using optical sensors for extracellular GABA (iGABASnFR2), three distinct but continuous inhibitory motifs emerge. First, during sensory processing, inhibition acts rapidly and locally to define precise windows for external input. Second, during natural transitions between wakefulness and sleep, inhibition ramps over seconds, coordinating large-scale reorganization of cortical networks. Third, during internally generated events such as hippocampal sharp-wave ripples (SWRs), inhibition becomes internally timed, predicting and constraining the flow of memory-related signals. Together, these patterns reveal that cortical inhibition is not static, but adaptive reshaping its timing, reach, and purpose across behavioural and computational states. In this Opinion, I propose that cortical inhibition acts as a flexible, state-dependent system that changes its timing and reaches across sensory, transitional, and internal modes of brain activity.

### 4.2 Fast and slow inhibitory motifs define sensory processing

When the cortex receives a sensory input, excitation is always accompanied by inhibition. Each incoming stimulus activates inhibitory neurons that target the same pyramidal cells excited by that stimulus, creating a closely linked balance between the two. Widefield imaging of extracellular GABA using iGABASnFR2 shows that sensory stimulation produces a brief and localized rise in GABA concentration in the matching sensory area (Marvin et al., 2019; Rezaei et al., 2025). **Figure 2A** shows this rise as a clear signature of sensory inhibition — spatially focused, time-locked to the stimulus, and lasting only a few hundred milliseconds. In this state, inhibition does more than stabilize activity; it defines the timing window for sensory processing, sharpening neural responses, and making excitation localized. This organization suggests that inhibition does more than keep the cortex stable: it defines the structure and timing of sensory processing itself. Fast and slow inhibitory phases create a temporal framework within which excitation can occur. The early, fast component ensures precision by confining activity to relevant circuits, while the slower, widespread component allows integration of feedback and context.

#### 4.2.1 Circuit mechanism

This form of inhibition follows a common two-step pattern across sensory systems (**Figure 2B**). The first step is a fast feedforward step driven by a thalamic input. Thalamic relays such as the ventral posteromedial nucleus (VPM) or the lateral geniculate nucleus (LGN) excite layer 4 neurons and nearby parvalbumin-positive ($PV^+$) interneurons. These $PV^+$ cells provide strong, perisomatic inhibition within tens of milliseconds, improving spike timing and keeping excitation confined to the correct cortical column (Isaacson et al., 2011; Gabernet et al., 2005). The second step is a slower feedback phase mediated by somatostatin-positive ($SST^+$) interneurons. As pyramidal neurons in layers 2/3 and 5 become active, they recruit $SST^+$ cells through facilitating synapses. These cells provide dendritic inhibition that develops over a few hundred milliseconds, gradually restoring balance and shaping the later part of the sensory response (Muñoz et al., 2017; Ferezou et al., 2007; Silberberg & Markram, 2007) A third step of control comes from inhibitory neurons in layer 1. Neurogliaform and 5-$HT3A^+$ interneurons in this layer release GABA extrasynaptically, creating slow, diffuse inhibition that spreads over larger cortical areas. These

cells integrate input from higher-order thalamus and other cortical regions, adding top-down modulation to the sensory response (Oláh et al., 2009). Together, these circuits create a layered inhibitory system: a fast PV-driven response that sets precise timing, a slower SST-driven response that regulates dendritic integration, and a widespread layer-1 response that links local sensory activity with global cortical context.

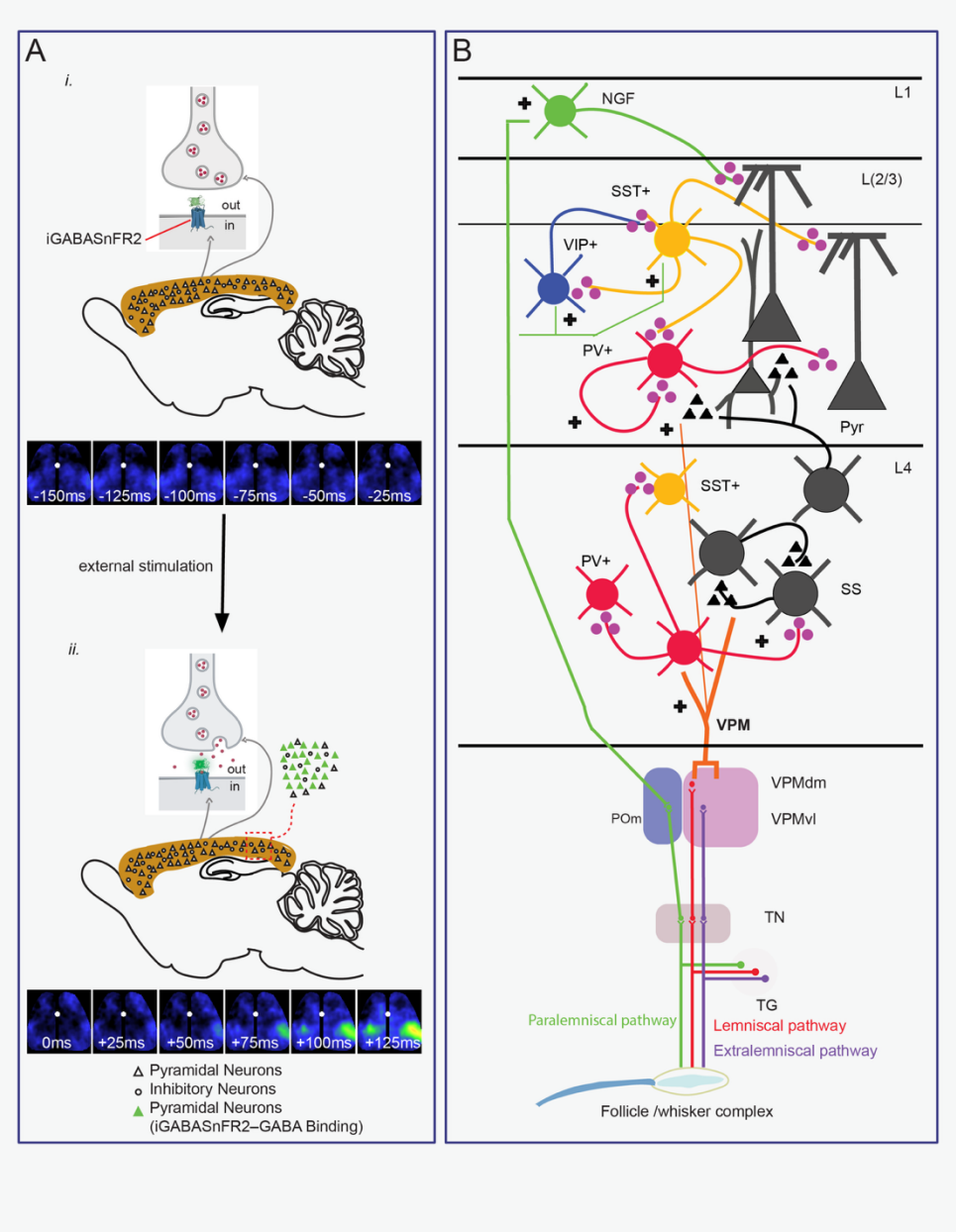


**Figure 2. External inhibition in sensory cortex: imaging and circuit anatomy.** (**Ai**) Strategy for imaging extracellular GABA using iGABASnFR2. AAV-PHP.N carrying iGABASnFR2 under a Synapsin promoter selectively labels pyramidal neurons, allowing fluorescence-based

detection of GABAergic input across the cortex. (**Aii**) Time-stamped fluorescence montages showing a stimulus-triggered increase in extracellular GABA in barrel cortex. Frames show rising inhibition on pyramidal membranes following whisker stimulation. (**B**) Canonical circuit for external inhibition in somatosensory cortex. Thalamic input activates $PV^+$ interneurons for fast feedforward inhibition in layer 4, followed by $SST^+$ and NGF cells that provide slower, spatially extended feedback and dendritic inhibition across supragranular layers.

### 4.3 Ramping inhibition coordinates cortical state transitions

Cortical state transitions don't happen suddenly—they're gradual changes in how neurons work together, which alters how the cortex processes information. As the brain is transitioning from NREM sleep to being awake or into REM sleep. But how inhibition itself changes during the transitions remains a mystery. In our wide-field imaging study **(Figure 3Ai)**, I explored how extracellular GABA changed across the mouse cortex during natural sleep and quiet wake. When the mice transitioned from NREM sleep to wakefulness, GABA levels gradually increased a few seconds before waking and peaked shortly after. This increase was strongest in the visual, retrosplenial, and somatosensory areas and was linked to stronger low-frequency activity and greater brain connectivity—signs of the brain shifting into a more synchronized waking state. While the mice transitioned from wakefulness back to NREM sleep, GABA levels slowly decreased, demonstrating more slow-wave activity and stronger local connections, marking a return to typical sleep rhythms. Transitions involving REM sleep were more complex. During NREM-to-REM, GABA increased slightly in some brain regions and then dropped, along with weaker connections between areas. During REM-to-wake transitions, extracellular GABA gradually decreased during REM sleep and then increased as the animal transitioned into wakefulness (Rezaei & Tohidi, 2025).

#### 4.3.1 Circuit mechanism

The ramping dynamics of cortical GABA across state transitions arise from shifting dominance among PV, SST, and VIP interneuron networks that redistribute inhibition across pyramidal neurons as neuromodulatory tone changes (Gentet, 2012; Pfeffer et al., 2013). During NREM-to-wake transitions, ascending monoaminergic and cholinergic inputs rapidly activate PV interneurons **(Figure 3Bii)**, generating strong perisomatic inhibition that stabilizes pyramidal spiking as thalamocortical drive resumes (Niethard et al., 2016). Simultaneous activation of VIP

neurons transiently suppresses SST-mediated dendritic inhibition, reopening corticocortical communication (Pfeffer et al., 2013). The combined effect produces the pre-arousal ramp in extracellular GABA seen in iGABASnFR2 imaging, reflecting coordinated inhibitory recruitment that synchronizes and readies the cortex for sensory engagement. However, during wake-to-NREM transitions **(Figure 3Bii)**, the reduction of ascending neuromodulators silences VIP neurons, releasing SST cells from disinhibition. Heightened SST bursting then suppresses distal dendrites, filtering long-range excitatory input and promoting locally synchronized slow oscillations (Gentet et al., 2012; Niethard et al., 2018). The observed GABA reduction therefore reflects a shift from fast PV-driven perisomatic release to slower, spatially targeted SST control, producing the synchronized slow-wave patterns characteristic of NREM sleep (Niethard et al., 2018). The NREM-to-REM transition **(Figure 3Bii)** introduces a strong cholinergic drive that selectively excites VIP interneurons. Their activation suppresses SST output, disinhibiting pyramidal dendrites, and reactivating intracortical communication while PV activity stabilizes at moderate levels (Pfeffer et al., 2013; Niethard et al., 2016). This circuit arrangement explains the transient, regionally heterogeneous GABA elevations followed by suppression during early REM: inhibition briefly reorganizes before transitioning into a decoupled, internally driven mode that supports replay and integration. However, during the REM-to-wake transition (Figure 2Bii), a brief phase of cortical disinhibition emerges as cholinergic tone collapses before PV activity rebounds. The brief dip in GABA signal observed in imaging likely indicates this timing gap—VIP-driven disinhibition fades more quickly than PV-mediated inhibition re-emerges—creating a short, disinhibited phase that re-establishes network synchrony and enables rapid re-engagement of sensory circuits upon awakening .Together, these circuit motifs suggest that ramping inhibition is not a passive reflection of state but an active control mechanism. Sequential recruitment and release among PV, SST, and VIP interneurons translate diffuse neuromodulatory signals into temporally structured inhibitory patterns that shape cortical excitability, coherence, and information flow across the sleep–wake cycle.

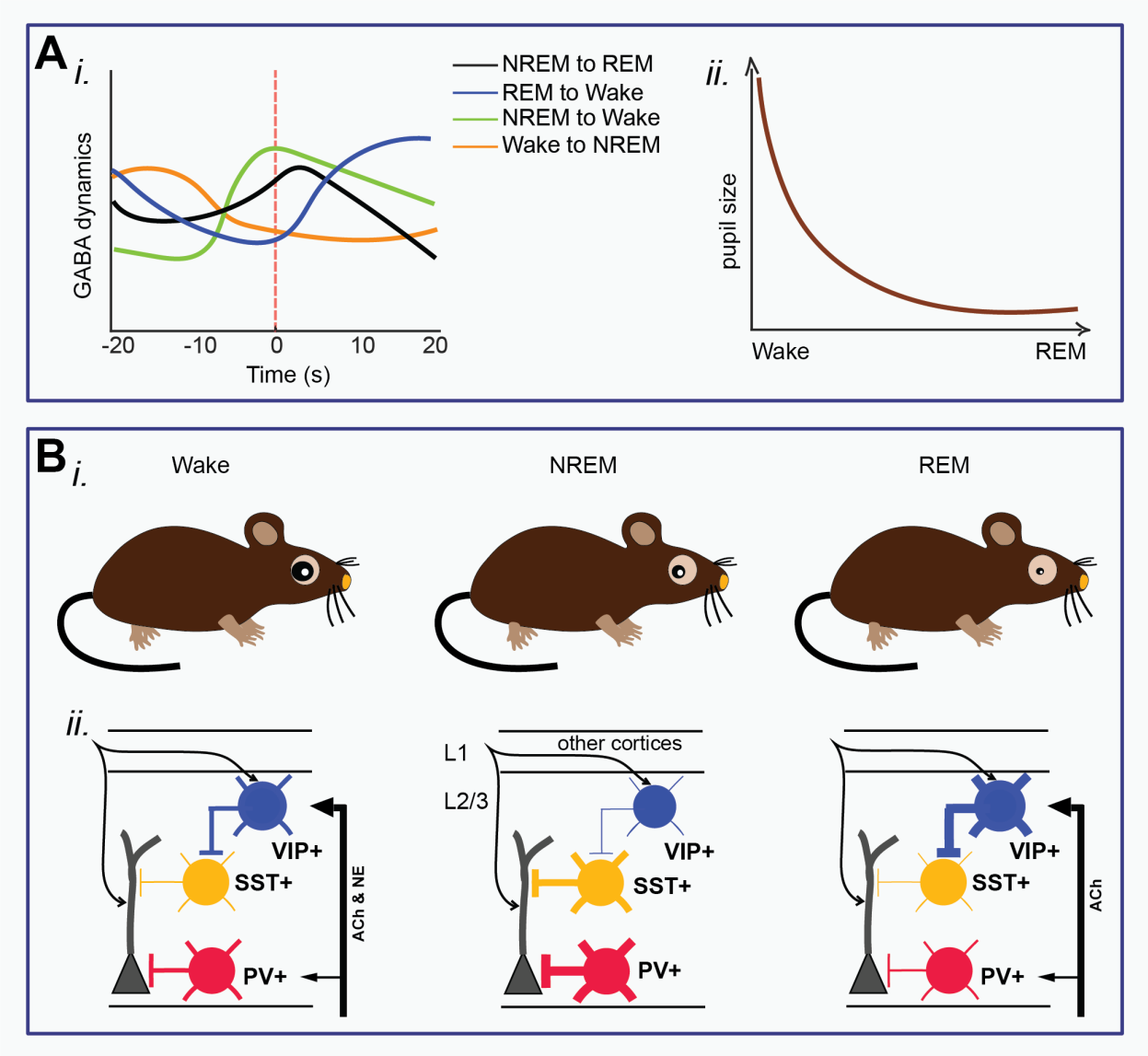


**Figure 3. Ramping inhibition and circuit reorganization across sleep–wake states.** (A) Global dynamics of cortical GABA across transitions. (i) Time series of extracellular GABA signals measured by widefield iGABASnFR2 imaging in retrosplenial cortex (RSC) during natural transitions between behavioural states. (ii) pupil size across wake, NREM, and REM states, showing progressive constriction as an independent physiological marker of arousal state. (B) behavioural correlates and circuit mechanisms. (i) Behavioural features of each state. Wakefulness is characterized by large pupils, body movement, and active whisking; NREM sleep shows immobility, reduced pupil size, and stable posture; REM sleep shows small pupils, absence of body movement, and rhythmic whisker and facial twitches. (ii) Circuit model summarizing interneuron dynamics across states. During wakefulness, $PV^+$ and $VIP^+$ interneurons co-regulate pyramidal excitability under strong cholinergic (ACh) and noradrenergic (NE) drive. During NREM sleep, $PV^+$ inhibition dominates while $SST^+$ interneurons exhibit slow bursting, and $VIP^+$ activity is minimal, producing high inhibitory tone and local synchronization. During REM sleep,

cholinergic excitation preferentially drives $VIP^+$ interneurons, suppressing $SST^+$ output and allowing dendritic disinhibition while $PV^+$ activity remains moderate.

## 4.4 Two-phase inhibition during NREM sleep: gating internal replay

During non-REM (NREM) sleep, cortical activity is dominated by slow oscillations, spindles, and hippocampal sharp-wave ripples (SWRs). Widefield imaging of extracellular GABA shows that these internally generated events are accompanied by large-scale inhibitory waves that unfold in characteristic sequences. In the retrosplenial cortex (RSC), inhibition rises twice around each hippocampal ripple: first just before the event and again immediately after. The first increase precedes hippocampal output by about 100 ms, while the second follows it by several hundred milliseconds (**Figure 4A**). This pattern suggests that cortical inhibition is not simply reactive to hippocampal input—it anticipates and shapes it. This organization implies that inhibition during sleep acts as an internal timing system. The early, pre-ripple component appears to prepare cortical circuits, setting the excitability window for when hippocampal replay will arrive. The later, post-ripple component restricts the spread of that excitation, ensuring that replay remains spatially focused and temporally precise. This pre-ripple rise in extracellular GABA reflects an internally timed inhibitory process that emerges from the intrinsic organization of NREM cortical activity rather than from direct hippocampal drive. Its consistent appearance tens of milliseconds before ripple onset indicates that cortical circuits are already engaged prior to hippocampal output. In prior glutamate and voltage imaging studies, cortical activation was likewise shown to precede hippocampal ripples, challenging a strictly hippocampus-driven model of replay initiation. Together, these findings support a framework in which internally generated cortical dynamics help set the conditions under which hippocampal replay occurs.

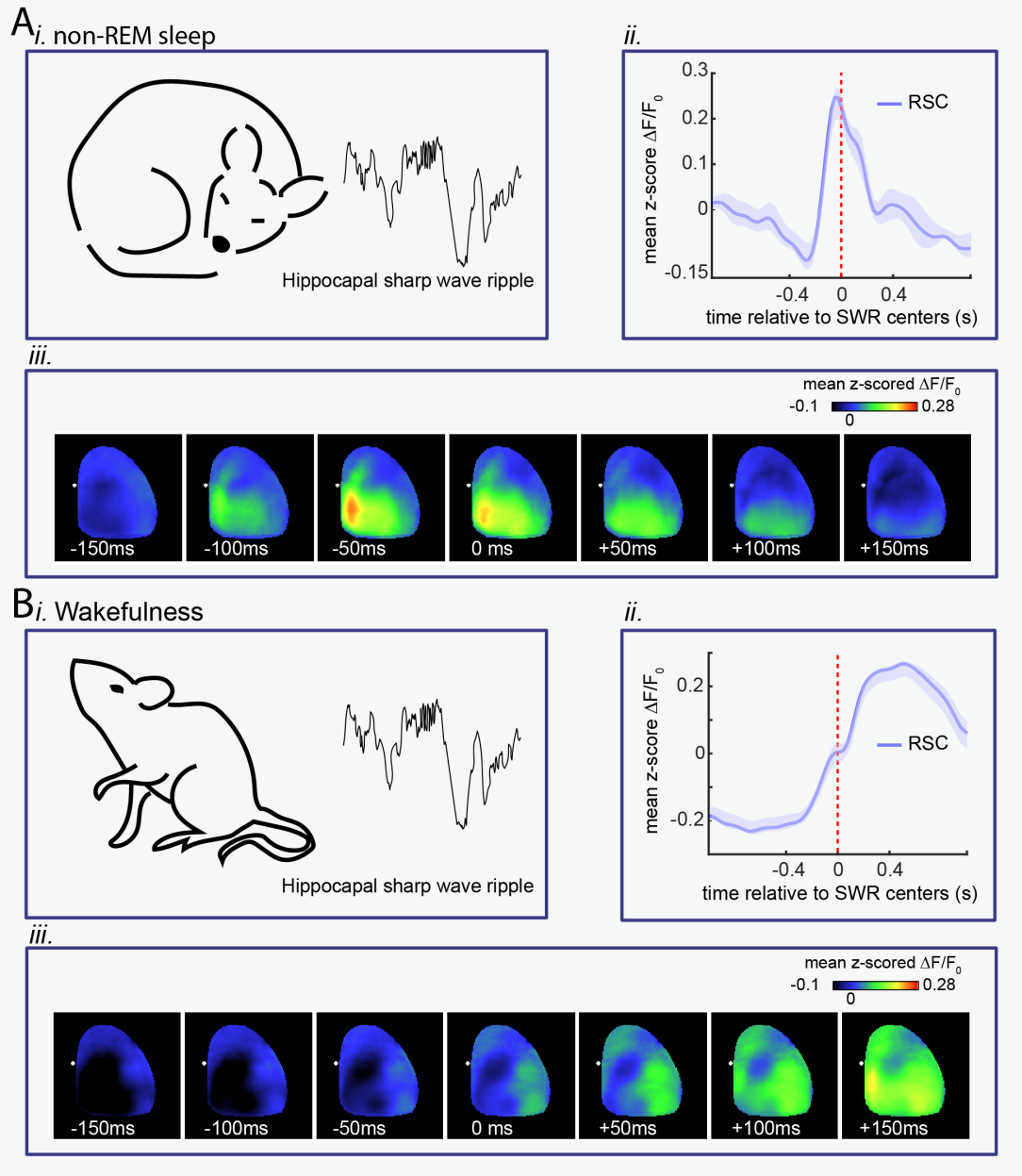


**Figure 4. State-dependent cortical inhibition during hippocampal sharp-wave ripples. (A) Non-REM sleep.** (i) Illustration of a resting mouse and a representative hippocampal SWR trace. (ii) Averaged iGABASnFR2 signal in retrosplenial cortex (RSC), aligned to SWR onset (red dotted line). (iii) Montage maps (−150 to +150 ms relative to SWR) showing z-scored GABA signals across the dorsal cortex. **(B) Wakefulness.** (i) Illustration of an awake mouse and a representative hippocampal SWR trace. (ii) Averaged iGABASnFR2 signal in RSC, aligned to SWR onset. (iii) Montage maps (−150 to +150 ms relative to SWR) showing z-scored GABA signals across the dorsal cortex.

### 4.4.1 Circuit mechanism

#### 4.4.1.1 The pre-ripple gate

During NREM sleep (**Figure 5Ai)**, slow oscillations alternate cortical neurons between down- and (Cruikshank et al., 2007) up-states, with pyramidal neurons becoming most excitable near the peak of each up-state (Steriade et al., 1993 ).When this up-state coincides with corticothalamic output, thalamic relay cells and the reticular nucleus engage in a spindle loop (**Figure 5Aii)** at ~10–15 Hz (Halassa & Acsády, 2016). These thalamocortical volleys reach the cortex while it is excitable but before pyramidal activity peaks. During this window (**Figure 5Aiii-iv)**, fast-spiking $PV^+$ interneurons are recruited first, providing perisomatic feedforward inhibition, whereas $SST^+$ cells remain mostly silent (Gentet et al., 2012; Cruikshank et al., 2007). The summed PV output elevates extracellular GABA at pyramidal membranes, producing the early fluorescence rise observed in RSC 50–100 ms before ripple onset (**Figure 4Aii-iii)**. This pre-ripple increase represents an internally timed inhibitory gate, generated by the natural sequence of cortical and thalamic rhythms rather than by external input. Spindles often precede ripples in both rodents and humans, helping to align cortical readiness with upcoming replay.

#### 4.4.1.2 The ripple-timed inhibition

When a sharp-wave ripple arises in the hippocampus, excitatory output from CA1 and subiculum is transmitted to retrosplenial cortex (RSC) through long-range glutamatergic projections (Figure 5Bi). This hippocampal–cortical input is well positioned to engage local inhibitory circuitry in RSC, giving rise to the rapid post-ripple increase in extracellular GABA observed in our wide-field imaging data. Such a transformation of hippocampal excitation into cortical inhibition is consistent with prior reports of ripple-linked recruitment of retrosplenial inhibitory neurons and feedforward inhibitory motifs in hippocampal–cortical pathways. The timing and spatial profile of this inhibitory response indicate that hippocampal output is followed by a rapid rise in cortical extracellular GABA that limits the spread of ripple-associated activation. In our data, this post-ripple inhibition emerges first in medial cortex and then propagates laterally, defining a restricted temporal window during which hippocampal output can influence cortical

targets. This organization suggests that hippocampal excitation is translated into a spatially structured inhibitory response in cortex, consistent with prior reports of ripple-linked recruitment of retrosplenial inhibitory neurons.

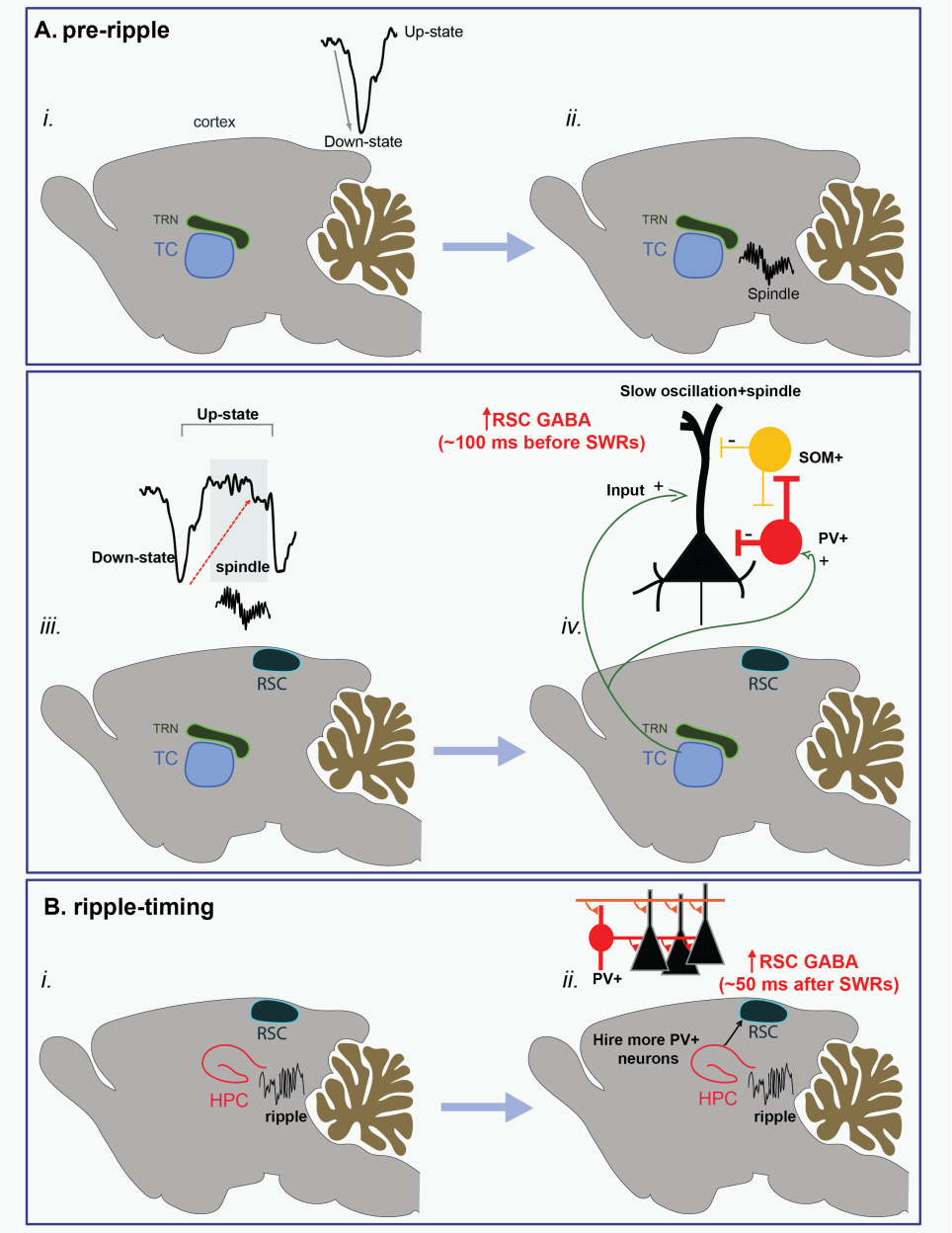

**Figure 5. Circuit mechanisms of cortical inhibition during NREM sleep. (A) Pre-ripple dynamics.** (i) During NREM, the slow oscillation flips retrosplenial cortex (RSC) from a down-state to an up-state, increasing pyramidal excitability. (ii) This depolarized state drives corticothalamic neurons that activate thalamic relay cells (TC) and the thalamic reticular nucleus (TRN), initiating a ~10–15 Hz spindle loop. (iii) Thalamocortical volleys from TC cells return to cortex during the up-state and recruit fast-spiking $PV^+$ interneurons in RSC. $SST^+$ interneurons remain suppressed. (iv) $PV^+$ cell activity produces strong perisomatic inhibition, raising extracellular GABA and generating a fluorescence increase in iGABASnFR2 signals ~-50 ms before hippocampal sharp-wave ripples (SWRs).**(B) Ripple-timed inhibition. (**i) At ripple onset (t = 0), output from hippocampal CA1 and subiculum projects to RSC via excitatory long-range axons. (ii) These inputs further drive local feedforward inhibition in RSC, primarily through $PV^+$ interneurons.

### 4.5 Internal cortical inhibition during wakefulness: suppressed pre-ripple and time-locked post-ripple dynamics

During wakefulness, cortical activity shifts to a tonic, desynchronized state maintained by ascending neuromodulators such as acetylcholine from the basal forebrain and brainstem, and noradrenaline from the locus coeruleus (Poulet & Crochet, 2018; Lee & Dan, 2012). These modulators (**Figure 6A**) depolarize both pyramidal neurons and interneurons, increasing membrane conductance and firing variability while preventing large-scale synchronized rhythms. Thalamic relay cells also switch from burst to tonic firing, disrupting rhythmic activity in the thalamic reticular nucleus and eliminating spindle generation (Poulet & Crochet, 2018; Lee & Dan, 2012; McGinley et al., 2015). As a result, cortical local field potentials (LFPs) display low-amplitude, broadband activity without slow oscillations or spindles (Reimer et al., 2014). Within this background, cholinergic input engages vasoactive intestinal peptide (VIP) interneurons, which suppress somatostatin-positive ($SST^+$) cells and thereby disinhibit pyramidal dendrites. Parvalbumin-positive ($PV^+$) interneurons remain poised to deliver fast perisomatic inhibition but are recruited only by salient inputs (Pfeffer et al., 2013) These physiological conditions transform the logic of cortical inhibition. Without rhythmic slow oscillations or spindles, the cortex lacks a shared excitability phase for anticipatory inhibitory recruitment. iGABASnFR2 imaging shows no pre-ripple increase in extracellular GABA, and $PV^+$ interneurons remain inactive until excitatory drive arrives. This suggests that unlike in NREM sleep, inhibition in wakefulness is not predictive but reactive (**Figure 5B**).

In this state, the cortex does not prepare for hippocampal input—it responds only once it occurs. The absence of a pre-ripple inhibitory gate reflects the functional shift from internally coordinated computation to externally driven processing. Inhibition remains essential, but its temporal organization adapts to the demands of the awake brain.

### 4.5.1 Circuit mechanism

#### 4.5.1.1 Pre-ripple phase: loss of anticipatory inhibition

In the desynchronized waking cortex, neuromodulator input flattens membrane potentials and breaks rhythmic coordination among interneurons. With no slow-wave or spindle-coupled up-states, $PV^+$ and $SST^+$ interneurons cannot build coordinated activity before hippocampal sharp-wave ripples (SWRs). The resulting flat baseline in iGABASnFR2 signals indicates the absence of an anticipatory inhibitory rise. In some cases, a small reduction in inhibition occurs just before ripple onset, possibly reflecting dis-facilitation of thalamocortical input or superficial-layer disinhibition (**Figure 6A**).

#### 4.5.1.2 Ripple-timed phase: localized, propagating inhibition

At ripple onset (**Figure 6B**), excitatory projections from hippocampal CA1 and subiculum reach retrosplenial cortex (RSC), recruiting local interneurons within milliseconds. This produces a fast feed-forward inhibitory response onto pyramidal neurons, captured as a transient, time-locked GABA increase. Widefield imaging reveals that GABA levels first rise in lateral cortical regions and later in RSC, peaking about 300 ms after ripple onset. This delay suggests lateral-to-medial propagation of inhibition. Lateral cortices—especially sensory and associative areas—maintain stronger coupling to thalamocortical and motor drives, enabling more synchronized inhibitory output. Hippocampal signals may reach these regions through subicular or para-hippocampal routes, activating $PV^+$ interneurons that initiate a lateral inhibitory wave. This wave then spreads medially through cortico-cortical pathways, reaching RSC after a short delay.

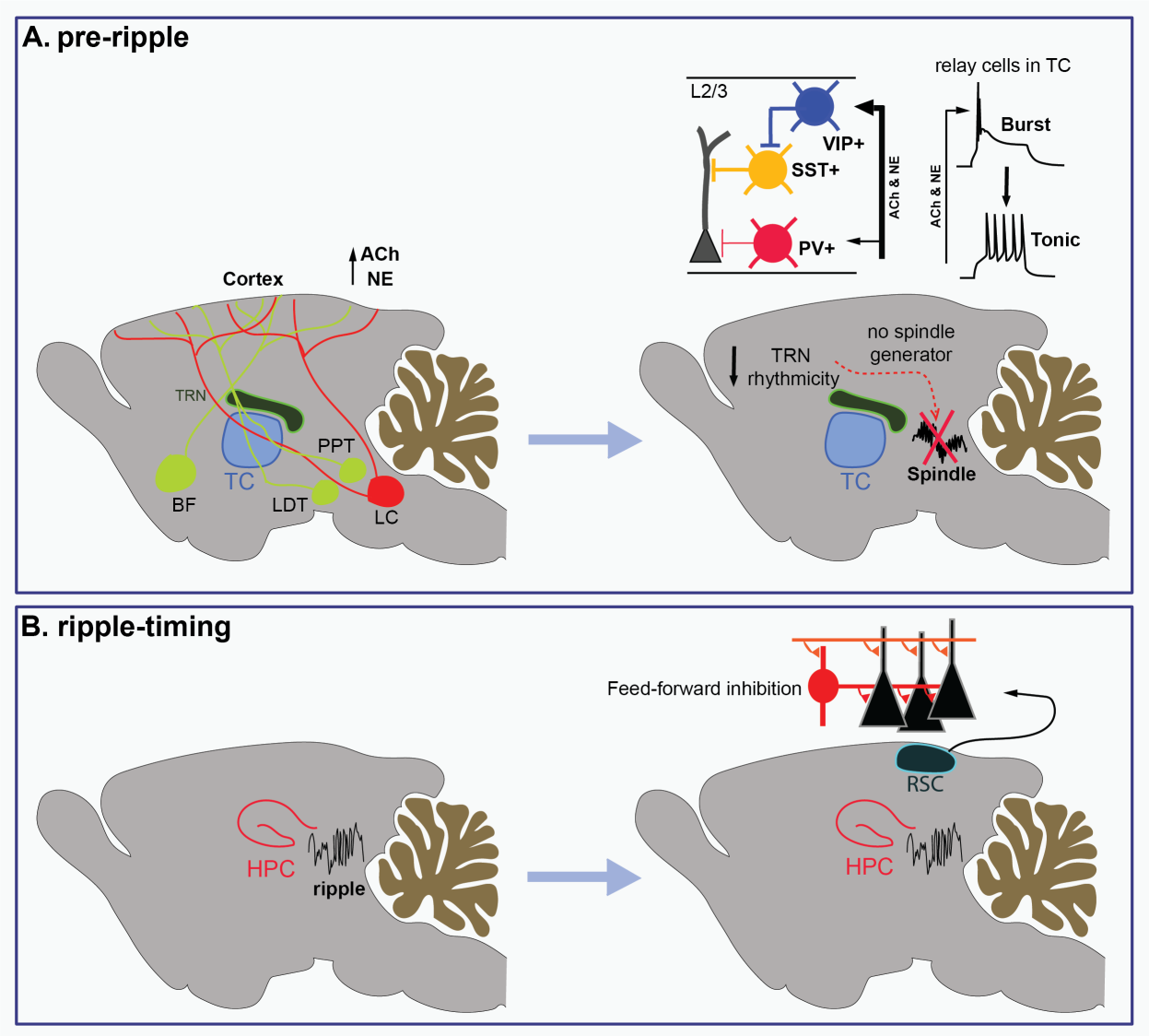


**Figure 6. Mechanisms of cortical inhibition during wakefulness.** (Ai) Schematic of ascending arousal systems. During wake, basal forebrain (BF) acetylcholine (ACh) and locus-coeruleus (LC) noradrenaline (NE) levels rise, depolarizing cortical and thalamic neurons. (Aii) Thalamic consequences. ACh/NE drive thalamo-cortical (TC) relay cells from burst to tonic mode and suppresses rhythmic inhibition in the thalamic reticular nucleus (TRN), preventing spindle generation and removing slow oscillatory synchrony. (Bi) Circuit model of ripple-timed inhibition. Hippocampal (HPC) sharp-wave ripples send excitatory projections to retrosplenial cortex (RSC), recruiting local interneurons through feed-forward connections. (Bii) Functional outcome. In the absence of slow oscillations or spindles, there is no pre-ripple cortical priming; RSC GABA levels remain flat.

## 4.6 Concluding remarks and future perspectives

Cortical inhibition has evolved from being viewed as a balancing force to being recognized as a dynamic organizer of brain function. Across sensory, transitional, and internal states, GABAergic networks continuously reshape the temporal and spatial structure of cortical activity. Rather than simply stabilizing excitation, inhibition defines when, where, and how neurons communicate—switching flexibly between modes optimized for perception, state coordination, and memory integration. Widefield imaging of extracellular GABA now reveals this organization at mesoscale resolution, linking inhibitory tone to behavioural and network dynamics in real time. These findings highlight inhibition as a unifying mechanism that bridges moment-to-moment computation with large-scale state transitions. Understanding how interneuron subtypes and neuromodulators systems interact to generate these inhibitory motifs remains a key challenge. The sequential engagement of PV, SST, and VIP interneurons provides a framework for how inhibition translates diffuse neuromodulators signals into structured patterns of network coordination. Yet precise timing, laminar pathways, and cell-type–specific contributions during natural behaviour are only beginning to be resolved. Using cell-type–specific calcium two-photon imaging of PV, SST, and VIP interneurons during natural behaviour will be essential to dissect how local inhibitory circuits coordinate across cortical and subcortical networks. Furthermore, closed-loop manipulations using optogenetic or chemogenetic control of defined interneuron classes can test how modulation of inhibition influences transitions between sensory, sleep, and memory states. Looking forward, viewing inhibition as an organizing principle rather than a stabilizing constraint invites a new framework for cortical computation. By regulating the balance between external and internal processing across multiple timescales, GABAergic inhibition may serve as the common language that unites sensory encoding, memory replay, and behavioural state control. In this light, inhibition is not merely the brain brake—but its conductor, orchestrating the transitions that make cognition possible.

**References**


Aggarwal, A., Liu, R., Chen, Y., Ralowicz, A. J., Bergerson, S. J., Tomaska, F., Mohar, B., Hanson, T. L., Hasseman, J. P., Reep, D., Tsegaye, G., Yao, P., Ji, X., Kloos, M., Walpita, D., Patel, R., Mohr, M. A., Tillberg, P. W., The GENIE Project Team, Looger, L. L., Marvin, J. S., Hoppa, M. B., Konnerth, A., Kleinfeld, D., Schreiter, E. R., & Podgorski, K. (2023). Glutamate indicators with improved activation kinetics and localization for imaging synaptic transmission. *Nature Methods, 20*, 925–934.

Albert, P. R., & Vahid-Ansari, F. (2019). The 5-HT1A receptor: Signaling to behavior. *Biochimie, 161*, 34–45.

Alexander, A. S., Rangel, L. M., Tingley, D., & Nitz, D. A. (2018). Neurophysiological signatures of temporal coordination between retrosplenial cortex and the hippocampal formation. *Behavioral Neuroscience, 132*(5), 453–468.

Alfonsa, H., Burman, R. J., Brodersen, P. J. N., Newey, S. E., Mahfooz, K., Yamagata, T., Panayi, M. C., Bannerman, D. M., Vyazovskiy, V. V., & Akerman, C. J. (2023). Intracellular chloride regulation mediates local sleep pressure in the cortex. *Nature Neuroscience, 26*, 64–78.

Andersen, P., Eccles, J. C., & Løyning, Y. (1963). Recurrent inhibition in the hippocampus with identification of the inhibitory cell and its synapses. *Nature, 198*, 540–542.

Aprison, M. H., & Werman, R. (1965). The distribution of glycine in cat spinal cord and roots. *Life Sciences, 4*(21), 2075–2083.

Atallah, B. V., Bruns, W., Carandini, M., & Scanziani, M. (2012). Parvalbumin-expressing interneurons linearly transform cortical responses to visual stimuli. *Neuron, 73*(1), 159–170.

Atallah, B. V., & Scanziani, M. (2009). Instantaneous modulation of gamma oscillation frequency by balancing excitation with inhibition. *Neuron, 62*(4), 566–577.

Aston-Jones, G., & Cohen, J. D. (2005). An integrative theory of locus coeruleus–norepinephrine function: Adaptive gain and optimal performance. *Annual Review of Neuroscience, 28*, 403–450.

Awapara, J. (1950). Occurrence of free gamma-aminobutyric acid in brain and its formation from L-glutamic acid. *Texas Reports on Biology and Medicine, 8*(4), 443–447.

Bari, A., & Robbins, T. W. (2013). Inhibition and impulsivity: Behavioral and neural basis of response control. *Progress in Neurobiology, 108*, 44–79.

Bazemore, A. W., Elliott, K. A. C., & Florey, E. (1957). Isolation of factor I. *Journal of Neurochemistry, 1*, 334–339.

Beaulieu, J.-M., & Gainetdinov, R. R. (2011). The physiology, signaling, and pharmacology of dopamine receptors. *Pharmacological Reviews, 63*(1), 182–217.

Ben-Ari, Y., Gaiarsa, J.-L., Tyzio, R., & Khazipov, R. (2007). GABA: A pioneer transmitter that excites immature neurons and generates primitive oscillations. *Physiological Reviews, 87*(4), 1215–1284.

Bettler, B., Kaupmann, K., Mosbacher, J., & Gassmann, M. (2004). Molecular structure and physiological functions of GABA(B) receptors. *Physiological Reviews, 84*(3), 835–867.

Bormann, J. (2000). The "ABC" of GABA receptors. *Trends in Pharmacological Sciences, 21*(1), 16–19.

Breathnach, C. S. (2004). Charles Scott Sherrington's *Integrative Action*: A centenary notice. *Journal of the Royal Society of Medicine, 97*(1), 34–36.

Buzsáki, G. (1989). Two-stage model of memory trace formation: A role for "noisy" brain states. *Neuroscience, 31*(3), 551–570.

Buzsáki, G. (2015). Hippocampal sharp wave-ripple: A cognitive biomarker for episodic memory and planning. *Hippocampus, 25*(10), 1073–1188.

Bell, C. (1824). *An exposition of the natural system of the nerves of the human body: With a republication of the papers delivered to the Royal Society on the subject of the nerves*. A. & R. Spottiswoode.

Chan, K. Y., Jang, M. J., Yoo, B. B., Greenbaum, A., Ravi, N., Wu, W.-L., Sánchez-Guardado, L., Lois, C., Mazmanian, S. K., Deverman, B. E., & Gradinaru, V. (2017). Engineered AAVs for efficient noninvasive gene delivery to the central and peripheral nervous systems. *Nature Neuroscience, 20*(8), 1172–1179.

Chen, Q., Cichon, J., Wang, W., Qiu, L., Lee, S.-J. R., Campbell, N. R., Destefino, M. J., Goard, M. J., Fu, Z., Yasuda, R., Looger, L. L., Arenkiel, B. R., Gan, W.-B., & Feng, G. (2012). Imaging neural activity using Thy1-GCaMP transgenic mice. *Neuron, 76*(2), 297–308.

Urban-Ciecko, J., & Barth, A. L. (2016). Somatostatin-expressing neurons in cortical networks. *Nature Reviews Neuroscience, 17*(7), 401–409.

Cruikshank, S. J., Lewis, T. J., & Connors, B. W. (2007). Synaptic basis for intense thalamocortical activation of feedforward inhibitory cells in neocortex. *Nature Neuroscience, 10*(4), 462–468.

Curley, A. A., & Lewis, D. A. (2012). Cortical basket cell dysfunction in schizophrenia. *The Journal of Physiology, 590*(4), 715–724.

Curtis, D. R., & Watkins, J. C. (1960). The excitation and depression of spinal neurones by structurally related amino acids. *Journal of Neurochemistry, 6*, 117–141.

Dalby, N. O. (2000). GABA-level increasing and anticonvulsant effects of three different GABA uptake inhibitors. *Neuropharmacology, 39*(12), 2399–2407.

Dash, M. B., Douglas, C. L., Vyazovskiy, V. V., Cirelli, C., & Tononi, G. (2009). Long-term homeostasis of extracellular glutamate in the rat cerebral cortex across sleep and waking states. *The Journal of Neuroscience, 29*(3), 620–629.

De Lanerolle, N. C., Kim, J. H., Robbins, R. J., & Spencer, D. D. (1989). Hippocampal interneuron loss and plasticity in human temporal lobe epilepsy. *Brain Research, 495*(2), 387–395.

Desrosiers, J., & Basha, D. (2023). Cortical inhibition, plasticity, and sleep. *The Journal of Neuroscience, 43*(4), 523–525.

Douglas, R. (1967). The Hippocampus and Behavior. *Psychological Bulletin*, 416–442.

Dutertre, S., Becker, C.-M., & Betz, H. (2012). Inhibitory glycine receptors: An update. *The Journal of Biological Chemistry, 287*(48), 40216–40223.

Eccles, J. C., Fatt, P., & Koketsu, K. (1954). Cholinergic and inhibitory synapses in a pathway from motor-axon collaterals to motoneurones. *The Journal of Physiology, 126*(3), 524–562.

Ego-Stengel, V., & Wilson, M. A. (2010). Disruption of ripple-associated hippocampal activity during rest impairs spatial learning in the rat. *Hippocampus, 20*(1), 1–10.

Farrant, M., & Nusser, Z. (2005). Variations on an inhibitory theme: Phasic and tonic activation of GABA_A receptors. *Nature Reviews Neuroscience, 6*(3), 215–229.

Ferezou, I., Haiss, F., Gentet, L. J., Aronoff, R., Weber, B., & Petersen, C. C. H. (2007). Spatiotemporal dynamics of cortical sensorimotor integration in behaving mice. *Neuron, 56*(5), 907–923.

Ferguson, B. R., & Gao, W.-J. (2018). PV interneurons: Critical regulators of E/I balance for prefrontal cortex-dependent behavior and psychiatric disorders. *Frontiers in Neural Circuits, 12*, Article 37.

Fink-Jensen, A., Suzdak, P. D., Swedberg, M. D., Judge, M. E., Hansen, L., & Nielsen, P. G. (1992). The gamma-aminobutyric acid (GABA) uptake inhibitor, tiagabine, increases

extracellular brain levels of GABA in awake rats. *European Journal of Pharmacology, 220*(2–3), 197–201.

Florey, E., & McLennan, H. (1959). The effects of factor I and of gamma-aminobutyric acid on smooth muscle preparations. *The Journal of Physiology, 145*(1), 66–76.

Froemke, R. C. (2015). Plasticity of cortical excitatory–inhibitory balance. *Annual Review of Neuroscience, 38*, 195–219.

Gabernet, L., Jadhav, S. P., Feldman, D. E., Carandini, M., & Scanziani, M. (2005). Somatosensory integration controlled by dynamic thalamocortical feed-forward inhibition. *Neuron, 48*(2), 315–327.

Gentet, L. J., Avermann, M., Matyas, F., Staiger, J. F., & Petersen, C. C. H. (2010). Membrane potential dynamics of GABAergic neurons in the barrel cortex of behaving mice. *Neuron, 65*(3), 422–435.

Gentet, L. J., Kremer, Y., Taniguchi, H., Huang, Z. J., Staiger, J. F., & Petersen, C. C. H. (2012). Unique functional properties of somatostatin-expressing GABAergic neurons in mouse barrel cortex. *Nature Neuroscience, 15*(4), 607–612.

Girardeau, G., Benchenane, K., Wiener, S. I., Buzsáki, G., & Zugaro, M. B. (2009). Selective suppression of hippocampal ripples impairs spatial memory. *Nature Neuroscience, 12*(10), 1222–1223.

Glykys, J., & Mody, I. (2007). The main source of ambient GABA responsible for tonic inhibition in the mouse hippocampus. *The Journal of Physiology, 582*(3), 1163–1178.

Haider, B., & McCormick, D. A. (2009). Rapid neocortical dynamics: Cellular and network mechanisms. *Neuron, 62*(2), 171–189.

Halassa, M. M., & Acsády, L. (2016). Thalamic inhibition: Diverse sources, diverse scales. *Trends in Neurosciences, 39*(10), 680–693.

Horovitz, S. G., Braun, A. R., Carr, W. S., Picchioni, D., Balkin, T. J., Fukunaga, M., & Duyn, J. H. (2009). Decoupling of the brain's default mode network during deep sleep. *Proceedings of the National Academy of Sciences of the United States of America, 106*(27), 11376–11381.

Huang, L., Zhu, W., Li, N., Zhang, B., Dai, W., Li, S., & Xu, H. (2024). Functions and mechanisms of adenosine and its receptors in sleep regulation. *Sleep Medicine, 115*, 210–217.

Isaacson, J. S., & Scanziani, M. (2011). How inhibition shapes cortical activity. *Neuron, 72*(2), 231–243.

Kandel, E. R., Spencer, W. A., & Brinley, F. J., Jr. (1961). Electrophysiology of hippocampal neurons: I. Sequential invasion and synaptic organization. *Journal of Neurophysiology, 24*(3), 225–258.

Karimi Abadchi, J., Rezaei, Z., Knöpfel, T., McNaughton, B. L., & Mohajerani, M. H. (2023). Inhibition is a prevalent mode of activity in the neocortex around awake hippocampal ripples in mice. *eLife, 12*, Article e79513.

Karimi Abadchi, J., Nazari-Ahangarkolaee, M., Gattas, S., Bermudez-Contreras, E., Luczak, A., McNaughton, B. L., & Mohajerani, M. H. (2020). Spatiotemporal patterns of neocortical activity around hippocampal sharp-wave ripples. *eLife, 9*, Article e51972.

Keller, G. B., & Mrsic-Flogel, T. D. (2018). Predictive processing: A canonical cortical computation. *Neuron, 100*(2), 424–435.

Kepecs, A., & Fishell, G. (2014). Interneuron cell types are fit to function. *Nature, 505*(7483), 318–326.

Kimble, D. (1968). Hippocampus and Internal Inhibition. *Psychological Bulletin*, 285–295.

Kozlov, A. S., Angulo, M. C., Audinat, E., & Charpak, S. (2006). Target cell-specific modulation of neuronal activity by astrocytes. *Proceedings of the National Academy of Sciences of the United States of America, 103*(26), 10058–10063.

Kramer, R. S., & Pearlstein, R. D. (1979). Cerebral cortical microfluorometry at isosbestic wavelengths for correction of vascular artifact. *Science, 205*(4407), 693–696.

Lancel, M., Faulhaber, J., & Deisz, R. A. (1998). Effect of the GABA uptake inhibitor tiagabine on sleep and EEG power spectra in the rat. *British Journal of Pharmacology, 123*(7), 1471–1477.

Lang, R., Gundlach, A. L., Holmes, F. E., Hobson, S. A., Wynick, D., Hökfelt, T., & Kofler, B. (2015). Physiology, signaling, and pharmacology of galanin peptides and receptors: Three decades of emerging diversity. *Pharmacological Reviews, 67*(1), 118–175.

Larson-Prior, L. J., Zempel, J. M., Nolan, T. S., Prior, F. W., & Raichle, M. E. (2009). Cortical network functional connectivity in the descent to sleep. *Proceedings of the National Academy of Sciences of the United States of America, 106*(11), 4489–4494.

Lee, S.-H., & Dan, Y. (2012). Neuromodulation of brain states. *Neuron, 76*(1), 209–222.

Lewis, D. A., & Moghaddam, B. (2006). Cognitive dysfunction in schizophrenia: Convergence of γ-aminobutyric acid and glutamate alterations. *Archives of Neurology, 63*(10), 1372–1376.

Ma, Y., Shaik, M. A., Kim, S. H., Kozberg, M. G., Thibodeaux, D. N., Zhao, H. T., Yu, H., & Hillman, E. M. C. (2016). Wide-field optical mapping of neural activity and brain haemodynamics: Considerations and novel approaches. *Philosophical Transactions of the Royal Society B: Biological Sciences, 371*(1705), Article 20150360.

Marín, O. (2012). Interneuron dysfunction in psychiatric disorders. *Nature Reviews Neuroscience, 13*(2), 107–120.

Markram, H., Toledo-Rodriguez, M., Wang, Y., Gupta, A., Silberberg, G., & Wu, C. (2004). Interneurons of the neocortical inhibitory system. *Nature Reviews Neuroscience, 5*(10), 793–807.

Marvin, J. S., Shimoda, Y., Magloire, V., Leite, M., Kawashima, T., Jensen, T. P., Kolb, I., Knott, E. L., Novak, O., Podgorski, K., Leidenheimer, N. J., Rusakov, D. A., Ahrens, M. B., Kullmann, D. M., & Looger, L. L. (2019). A genetically encoded fluorescent sensor for in vivo imaging of GABA. *Nature Methods, 16*(8), 763–770.

Marvin, J. S., Borghuis, B. G., Tian, L., Cichon, J., Harnett, M. T., Akerboom, J., Gordus, A., Renninger, S. L., Chen, T.-W., Bargmann, C. I., Orger, M. B., Schreiter, E. R., Demb, J. B., Gan, W.-B., Hires, S. A., & Looger, L. L. (2013). An optimized fluorescent probe for visualizing glutamate neurotransmission. *Nature Methods, 10*(2), 162–170.

McGinley, M. J., Vinck, M., Reimer, J., Batista-Brito, R., Zagha, E., Cadwell, C. R., Tolias, A. S., Cardin, J. A., & McCormick, D. A. (2015). Waking state: Rapid variations modulate neural and behavioral responses. *Neuron, 87*(6), 1143–1161.

Minamisawa, G., Kwon, S. E., Chevée, M., Brown, S. P., & O'Connor, D. H. (2018). A non-canonical feedback circuit for rapid interactions between somatosensory cortices. *Cell Reports, 23*(9), 2718–2731.e6.

Mohajerani, M. H., McVea, D. A., Fingas, M., & Murphy, T. H. (2010). Mirrored bilateral slow-wave cortical activity within local circuits revealed by fast bihemispheric voltage-sensitive dye imaging in anesthetized and awake mice. *The Journal of Neuroscience, 30*(10), 3745–3751.

Mohajerani, M. H., Chan, A. W., Mohsenvand, M., LeDue, J., Liu, R., McVea, D. A., Boyd, J. D., Wang, Y. T., Reimers, M., & Murphy, T. H. (2013). Spontaneous cortical activity alternates between motifs defined by regional axonal projections. *Nature Neuroscience, 16*(10), 1426–1435.

Muñoz, W., Tremblay, R., Levenstein, D., & Rudy, B. (2017). Layer-specific modulation of neocortical dendritic inhibition during active wakefulness. *Science, 355*(6328), 954–959.

Nazari, M., Karimi Abadchi, J., Naghizadeh, M., Bermudez-Contreras, E. J., McNaughton, B. L., Tatsuno, M., & Mohajerani, M. H. (2023). Regional variation in cholinergic terminal

activity determines the non-uniform occurrence of cortical slow waves during REM sleep in mice. *Cell Reports, 42*(5), Article 112450.

Neumahr, S., Hapfelmeier, G., Scheller, M., Schneck, H., Franke, C., & Kochs, E. (2000). Dual action of isoflurane on the gamma-aminobutyric acid (GABA)-mediated currents through recombinant α1β2γ2L GABA $_A$ receptor channels. *Anesthesia & Analgesia, 90*(5), 1184–1190.

Niethard, N., Hasegawa, M., Itokazu, T., Oyanedel, C. N., Born, J., & Sato, T. R. (2016). Sleep-stage-specific regulation of cortical excitation and inhibition. *Current Biology, 26*(20), 2739–2749.

Niethard, N., Ngo, H.-V. V., Ehrlich, I., & Born, J. (2018). Cortical circuit activity underlying sleep slow oscillations and spindles. *Proceedings of the National Academy of Sciences of the United States of America, 115*(39), E9220–E9229.

Niethard, N., Burgalossi, A., & Born, J. (2017). Plasticity during sleep is linked to specific regulation of cortical circuit activity. *Frontiers in Neural Circuits, 11*, Article 65.

Okun, M., & Lampl, I. (2008). Instantaneous correlation of excitation and inhibition during ongoing and sensory-evoked activities. *Nature Neuroscience, 11*(5), 535–537.

Opalka, A. N., Huang, W.-Q., Liu, J., Liang, H., & Wang, D. V. (2020). Hippocampal ripple coordinates retrosplenial inhibitory neurons during slow-wave sleep. *Cell Reports, 30*(2), 432–441.e3.

Pakan, J. M. P., Lowe, S. C., Dylda, E., Keemink, S. W., Currie, S. P., Coutts, C. A., & Rochefort, N. L. (2016). Behavioral-state modulation of inhibition is context-dependent and cell type specific in mouse visual cortex. *eLife, 5*, Article e14985.

Petersen, C. C. H. (2007). The functional organization of the barrel cortex. *Neuron, 56*(2), 339–355.

Peyrache, A., Khamassi, M., Benchenane, K., Wiener, S. I., & Battaglia, F. P. (2009). Replay of rule-learning related neural patterns in the prefrontal cortex during sleep. *Nature Neuroscience, 12*(7), 919–926.

Pfeffer, C. K., Xue, M., He, M., Huang, Z. J., & Scanziani, M. (2013). Inhibition of inhibition in visual cortex: The logic of connections between molecularly distinct interneurons. *Nature Neuroscience, 16*(8), 1068–1076.

Poulet, J. F. A., & Crochet, S. (2019). The cortical states of wakefulness. *Frontiers in Systems Neuroscience, 12*, Article 64.

Qiu, J., Yang, Y., Liu, J., Zhao, W., Li, Q., Zhu, T., Liang, P., & Zhou, C. (2023). The volatile anesthetic isoflurane differentially inhibits voltage-gated sodium channel currents between pyramidal and parvalbumin neurons in the prefrontal cortex. *Frontiers in Neural Circuits, 17*, Article 1185095.

Reimer, J., Froudarakis, E., Cadwell, C. R., Yatsenko, D., Denfield, G. H., & Tolias, A. S. (2014). Pupil fluctuations track fast switching of cortical states during quiet wakefulness. *Neuron, 84*(2), 355–362.

Renshaw, B. (1946). Central effects of centripetal impulses in axons of spinal ventral roots. *Journal of Neurophysiology, 9*(3), 191–204.

Rezaei, E., Tohidi, S., Nazari, M., & Karimi Abadchi, J. (2025). Characterization of iGABASnFR2 for in vivo mesoscale imaging of intracortical GABA dynamics. *Neurophotonics, 12*(3), 035006.

Rezaei, E., & Tohidi, S. (2025). Cortical GABAergic inhibition dynamics around hippocampal sharp-wave ripples. *biorxiv*.

Ridder, W. H., III, & Nusinowitz, S. (2006). The visual evoked potential in the mouse—Origins and response characteristics. *Vision Research, 46*(6–7), 902–913.

Roberts, E., & Frankel, S. (1950). γ-Aminobutyric acid in brain: Its formation from glutamic acid. *Journal of Biological Chemistry, 187*(1), 55–63.

Rubenstein, J. L. R., & Merzenich, M. M. (2003). Model of autism: Increased ratio of excitation/inhibition in key neural systems. *Genes, Brain and Behavior, 2*(5), 255–267.

Rudy, B., Fishell, G., Lee, S., & Hjerling-Leffler, J. (2011). Three groups of interneurons account for nearly 100% of neocortical GABAergic neurons. *Developmental Neurobiology, 71*(1), 45–61.

Rysztak, L. G., & Jutkiewicz, E. M. (2022). The role of enkephalinergic systems in substance use disorders. *Frontiers in Systems Neuroscience, 16*, Article 932546.

Scimemi, A. (2014). Plasticity of GABA transporters: An unconventional route to shape inhibitory synaptic transmission. *Frontiers in Cellular Neuroscience, 8*, Article 128.

Scott, B. B., Thiberge, S. Y., Guo, C., Tervo, D. G. R., Brody, C. D., Karpova, A. Y., & Tank, D. W. (2018). Imaging cortical dynamics in GCaMP transgenic rats with a head-mounted widefield macroscope. *Neuron, 100*(5), 1045–1058.e5.

Semyanov, A., Walker, M. C., Kullmann, D. M., & Silver, R. A. (2004). Tonically active GABA_A receptors: Modulating gain and maintaining the tone. *Trends in Neurosciences, 27*(5), 262–269.

Silasi, G., Xiao, D., Vanni, M. P., Chen, A. C. N., & Murphy, T. H. (2016). Intact skull chronic windows for mesoscopic wide-field imaging in awake mice. *Journal of Neuroscience Methods, 267*, 141–149.

Silberberg, G., & Markram, H. (2007). Disynaptic inhibition between neocortical pyramidal cells mediated by Martinotti cells. *Neuron, 53*(5), 735–746.

Steriade, M., McCormick, D. A., & Sejnowski, T. J. (1993). Thalamocortical oscillations in the sleeping and aroused brain. *Science, 262*(5134), 679–685.

Stuart, D. G., Schaefer, A. T., Massion, J., Graham, B. A., & Callister, R. J. (2014). Pioneers in CNS inhibition: 1. Ivan M. Sechenov, the first to clearly demonstrate inhibition arising in the brain. *Brain Research, 1548*, 20–48.

Syeda, A., Zhong, L., Tung, R., Long, W., Pachitariu, M., & Stringer, C. (2024). Facemap: A framework for modeling neural activity based on orofacial tracking. *Nature Neuroscience, 27*, 187–195.

Tagliazucchi, E., & Laufs, H. (2014). Decoding wakefulness levels from typical fMRI resting-state data reveals reliable drifts between wakefulness and sleep. *Neuron, 82*(3), 695–708.

Tatti, R., Haley, M. S., Swanson, O. K., Tselha, T., & Maffei, A. (2017). Neurophysiology and regulation of the balance between excitation and inhibition in neocortical circuits. *Biological Psychiatry, 81*(10), 821–831.

Topf, N., Jenkins, A., Baron, N., & Harrison, N. L. (2003). Effects of isoflurane on gamma-aminobutyric acid type A receptors activated by full and partial agonists. *Anesthesiology, 98*(2), 306–311.

Tossell, K., Yu, X., Giannos, P., Anuncibay Soto, B., Nollet, M., Yustos, R., Miracca, G., Vicente, M., Miao, A., Hsieh, B., Ma, Y., Vyssotski, A. L., Constandinou, T., Franks, N. P., & Wisden, W. (2023). Somatostatin neurons in prefrontal cortex initiate sleep-preparatory behavior and sleep via the preoptic and lateral hypothalamus. *Nature Neuroscience, 26*, 1805–1819.

Tremblay, R., Lee, S., & Rudy, B. (2016). GABAergic interneurons in the neocortex: From cellular properties to circuits. *Neuron, 91*(2), 260–292.

Urban-Ciecko, J., & Barth, A. L. (2016). Somatostatin-expressing neurons in cortical networks. *Nature Reviews Neuroscience, 17*(7), 401–409.

Vanni, M. P., & Murphy, T. H. (2014). Mesoscale transcranial spontaneous activity mapping in GCaMP3 transgenic mice reveals extensive reciprocal connections between areas of somatomotor cortex. *The Journal of Neuroscience, 34*(48), 15931–15946.

Vyazovskiy, V. V., Cirelli, C., Pfister-Genskow, M., Faraguna, U., & Tononi, G. (2008). Molecular and electrophysiological evidence for net synaptic potentiation in wake and depression in sleep. *Nature Neuroscience, 11*(2), 200–208.

Wang, D. V., & Ikemoto, S. (2016). Coordinated interaction between hippocampal sharp-wave ripples and anterior cingulate unit activity. *The Journal of Neuroscience, 36*(41), 10663–10672.

Wilson, N. R., Runyan, C. A., Wang, F. L., & Sur, M. (2012). Division and subtraction by distinct cortical inhibitory networks in vivo. *Nature, 488*(7411), 343–348.

Wilson, M. A., & McNaughton, B. L. (1994). Reactivation of hippocampal ensemble memories during sleep. *Science, 265*(5172), 676–679.

Wu, J., Abdelfattah, A. S., Zhou, H., Ruangkittisakul, A., Qian, Y., Ballanyi, K., & Campbell, R. E. (2018). Genetically encoded glutamate indicators with altered color and topology. *ACS Chemical Biology, 13*(7), 1832–1837.

Wu, F.-S., Gibbs, T. T., & Farb, D. H. (1993). Dual activation of $GABA_A$ and glycine receptors by β-alanine: Inverse modulation by progesterone and 5α-pregnan-3α-ol-20-one. *European Journal of Pharmacology, 246*(3), 239–246.

Wu, J.-Y., & Prentice, H. (2010). Role of taurine in the central nervous system. *Journal of Biomedical Science, 17*(Suppl 1), Article S1.

Wu, Y., Wang, W., & Richerson, G. B. (2001). GABA transaminase inhibition induces spontaneous and enhances depolarization-evoked GABA efflux via reversal of the GABA transporter. *The Journal of Neuroscience, 21*(8), 2630–2639.

Xiao, D., Forys, B. J., Vanni, M. P., & Murphy, T. H. (2021). MesoNet allows automated scaling and segmentation of mouse mesoscale cortical maps using machine learning. *Nature Communications, 12*(1), Article 5992.

Xie, Y., Chan, A. W., McGirr, A., Xue, S., Xiao, D., Zeng, H., & Murphy, T. H. (2016). Resolution of high-frequency mesoscale intracortical maps using the genetically encoded glutamate sensor iGluSnFR. *The Journal of Neuroscience, 36*(4), 1261–1272.

Yüzgeç, Ö., Prsa, M., Zimmermann, R., & Huber, D. (2018). Pupil size coupling to cortical states protects the stability of deep sleep via parasympathetic modulation. *Current Biology, 28*(3), 392–400.e3.

Yardeni, T., Eckhaus, M., Morris, H. D., Huizing, M., & Hoogstraten-Miller, S. (2011). Retro-orbital injections in mice. *Lab Animal, 40*(5), 155–160.

Yuste, R. (2005). Origin and classification of neocortical interneurons. *Neuron, 48*(4), 524–527.

Zhou, Y., & Danbolt, N. C. (2014). Glutamate as a neurotransmitter in the healthy brain. *Journal of Neural Transmission, 121*(8), 799–817.

Zielinski, M. R., Atochin, D. N., McNally, J. M., McKenna, J. T., Huang, P. L., Strecker, R. E., & Gerashchenko, D. (2019). Somatostatin+/nNOS+ neurons are involved in delta electroencephalogram activity and cortical-dependent recognition memory. *Sleep, 42*(10), Article zsz143.